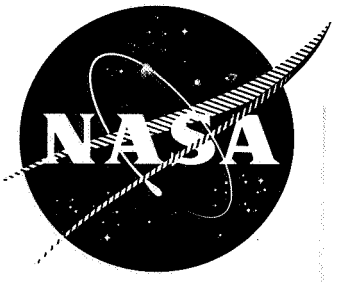

GPO PRICE $ _____

CSFTI PRICE(S) $ _____

Hard copy (HC) 3.00

Microfiche (MF) .65

ff 653 July 65

FINAL REPORT

CHARACTERIZATION OF RECOMBINATION AND CONTROL ELECTRODES FOR SPACECRAFT NICKEL-CADMIUM CELLS

by

W. N. Carson, Jr., G. Rampel and I. B. Weinstock

prepared for

NATIONAL AERONAUTICS AND SPACE ADMINISTRATION

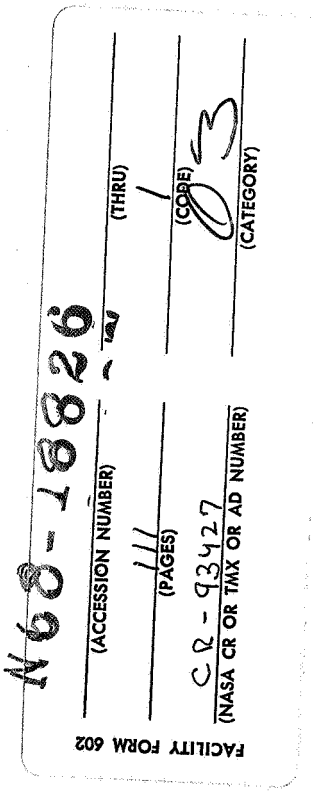

January 1968

CONTRACT NAS 5-10261

Goddard Space Flight Center
Greenbelt, Maryland

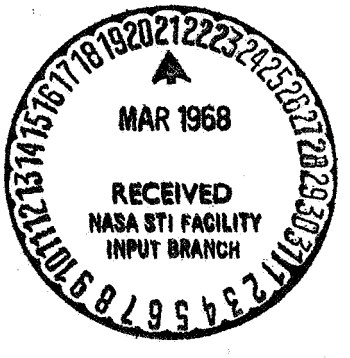

GENERAL ELECTRIC

Battery Business Section
Gainesville, Florida

FINAL REPORT

CHARACTERIZATION OF RECOMBINATION AND CONTROL ELECTRODES FOR SPACECRAFT NICKEL-CADMIUM CELLS

by

W.N. Carson, Jr., G. Rampel and I.B. Weinstock

prepared for

NATIONAL AERONAUTICS AND SPACE ADMINISTRATION

January 1968

CONTRACT NAS 5-10261

Goddard Space Flight Center
Greenbelt, Maryland

General Electric Company
Battery Business Section
Gainesville, Florida

ABSTRACT

Oxygen signal and recombination electrodes were developed to provide reliable charge control for spacecraft nickel-cadmium cells operable over a -20°C to +40°C temperature range in near-earth orbits to cycle depths of 75%.

The signal electrode voltage output was essentially proportional to oxygen pressure in the range of 5 to 30 PSIA. Performance was constant during the test program.

The rate of oxygen recombination provided by the recombination electrode was greater than required to reduce pressure between charge cycles. The electrode is also active in recombining any hydrogen formed in the cell. Utilizing these features it was possible to operate cells with the negative electrodes nearly fully charged. The cycle capability of these cells was greater by a factor of more than 10 at 40°C to 50% DOD and more than 8 at 25°C to 75% DOD. The cells were still cycling at the conclusion of the contract so that the full capability was not obtained. It was also possible to alter the cycle regime of cells without a reconditioning procedure, indicating that the "memory effect" has been greatly reduced.

TABLE OF CONTENTS

TABLE OF CONTENTS
(continued)

LIST OF ILLUSTRATIONS

LIST OF TABLES

1.0 INTRODUCTION AND SUMMARY

1.1 Background and Objective

The ampere-hour utilization of conventional spacecraft nickel-cadmium cells, especially in short, near-earth orbits is low, due in part to the inability to safely recharge these cells at high rates. High rate charging may be safely used, however, if adequate control of the charge can be provided. This charge control must permit adequate recharge of the cell, but carefully limit the overcharge in order to prevent excessive pressure build up and heat generation. Various auxiliary electrodes capable of detecting the oxygen generated at the end of the charge period have been developed and incorporated into sealed nickel-cadmium cells to provide this control function.

The oxygen fuel cell (recombination) electrode is capable of maintaining low cell pressures under conditions of high rate charging. When used as a charge control electrode, however, its extreme sensitivity to oxygen results in essentially "on-off" control. The signal from such an electrode saturates whenever a small amount of oxygen is generated in the cell, causing the charge to be terminated prematurely. Complicated time delay circuitry and/or trickle charge modes must then be employed to insure full charge.

Electrodes with output voltages which are proportional to oxygen pressure (oxygen sensing) have also been developed. These are good for control purposes since the pressure corresponding to a given amount of overcharge can be determined and the charging cut off by a signal from the auxiliary electrode. This approach has been somewhat unattractive for short orbits, however, since the decay of the oxygen pressure, and hence the signal, is slow. As a consequence, the signal voltage at the beginning of the charge is very near the cut-off value.

A system designed to eliminate the weaknesses of these individual electrodes would combine the best features of both in a single cell. The objective of this program, then, is to produce aerospace cells which contain electrodes of both types.

The oxygen sensing electrode is used as the charge control electrode because of its near linear response to oxygen pressure. The recombination electrode is employed to maintain the cell pressure within safe limits and also to return the pressure to a low level during open circuit and discharge periods. This is especially advantageous during short orbits, as it insures that the subsequent charge will not be terminated by a premature signal from the control electrode on account of residual oxygen pressure.

To provide program visibility for reporting and monitoring purposes, and to schedule, the program was broken down into five tasks, as follows:

1.2 Task I - Oxygen Sensing Electrode

The objective of this task was to develop an oxygen sensing electrode that will give a linear (or a reasonably close to linear) response to oxygen partial pressure in the range 5 to 30 PSIA. The appraoch tested and found satisfactory was the use of an electode in which oxygen reaction rate is under diffusion control. Several materials were found satisfactory; the material of choice is a sintered nickel substrate covered with 0.001" Teflon film serving as the diffusion barrier. This electrode shows good linearity over the desired pressure range, is mechanically rugged, and has very rapid response to changes in oxygen pressure. The optimum location for this electrode within the cell was found to be on one broad face of the pack..

1.3 Task II - Oxygen Recombination Electrode

The objective of this task was to develop an oxygen recombination electrode capable of recombining the oxygen generated by the positive plates during charging. This electrode must be able to function over the temperature range of -20°C to +40°C. Selection of electrodes was based upon their polarization behavior.

During the course of this investigation, a number of electrode types were evaluated. These included electrodes from the American Cyanamid Company, Teflon-bonded electrodes from the General Electric Company Research and Development Center, and plaque based electrodes fabricated locally. The electrode selected was a version of the plaque-based electrodes, and consists of a Platinum catalysed sintered nickel structure with a Teflon film on the gas face.

The stability of electrode performance over long periods of time was demonstrated. In addition, it was demonstrated that the techniques used in preparing these electrodes are capable of producing electrodes of consistent quality.

1.4 Task III - Negative Plate Evaluation

The use of carefully selected negative plates minimizes changes in cell characteristics during cycling. The objective of this task was, therefore, to select suitable lots of negative plates for use in prototype and final cells. Three lots of negative plates were received from manufacturing and subjected to evaluation. The lot with the highest recombination ability and ampere hour stability was retained for use in prototype and final cells.

1.5 Task IV - Prototype Cell Design

The objective of this task was to bring together the results of the previous tasks and arrive at a final cell electrode configuration. A design was proposed, and one pre-prototype cell was assembled to demonstrate the feasibility of the design. The cell was subjected to over 100 cycles of operation at rates corresponding to 25%, 50%, and 75% depth-of-discharge over the temperature range of -20°C to +40°C. The performance of the cell demonstrated the adequacy of the proposed design.

1.6 Task V - Prototype Cell Tests

The objective of this task was to confirm the results obtained previously and to provide a basis for designing the final cells. Prototype cells were assembled according to the design developed in Task IV and were subjected to cycling throughout the temperature range of -20°C to +40°C. Cells cycled at low temperatures and depths, i.e., to 50% DOD at -20°C and 25% DOD at both -20°C and 25°C, completed nearly 1000 cycles of operation with no decline in the performance of the cells or the auxiliary electrodes. The initial cycle tests involving greater depths-of-discharge and/or elevated temperatures, i.e., to 75% DOD at all temperatures and to 50% DOD at 40°C and 25°C, showed that the cells had a tendency to lose capacity during cycling. It was possible, however, to

greatly reduce this tendency by proper processing of the cells prior to cycling. This processing has made it possible to increase cycle capability of cells cycled to 50% DOD at 40°C in excess of 10 fold.

2.0 TECHNICAL DISCUSSION

2.1 Task I - Oxygen Sensing Electrode

2.1.1 Theoretical Approach

Oxygen can be reduced at low, but useful, rates on a variety of metal surfaces, such as nickel, platinum, gold, and cobalt, without substantial oxidation of the metal. Because the exchange current for oxygen reduction is very small, such electrodes show a mixed potential response very much lower than the thermodynamic value of 1.23 volts. Although these electrodes are useless for power generation due to their low current and voltage capability, they can serve as the basis of a simple oxygen pressure sensing system when operated in the diffusion-limited region.

The principle of diffusion-limited operation is simple: The surface of the electrode is covered by a barrier through which oxygen is transported by diffusion. The rate of oxygen diffusion is governed by the area, thickness of the film, nature of the film, temperature, and pressure differential:

$$r_{O_2} = k \frac{A}{d} (P - P_o) = \text{moles of oxygen/sec.}$$

where k is the diffusion constant for the barrier material

A is the area

d is the thickness of the barrier

P is the pressure of the gas side of the barrier

P_o is the pressure of the electrode side of the barrier.

If the electrode is operated in the limiting current region, i.e., the electrode is driven by an external power source against a suitable counter-electrode such that P_o is reduced to a very low value, the current is linear with pressure P, and is given by an expression:

$$i_c = nF\, r_{O_2} = k\, n\, F \frac{A}{d} P = KP = \text{amperes}$$

In a nickel-cadmium cell, the electrode cannot be readily driven by an external power source, and so that voltage required to drive the electrode must be obtained from the electrode itself. This is accomplished by coupling the electrode, through an external resistance, to the cadmium electrode.

The general equation for the voltage of the oxygen sensor -

Cd couple can be derived by considering its current, internal cell resistance, polarizations due to the kinetics of oxygen reduction, and polarizations due to mass transport impedances. For the O_2-Cd couple voltage at current i, we have the general equation:

$$V = iX = E - \frac{RT}{nF} \ln i/i_o - \frac{RT}{nF} \ln i_c/(i_c - i) - ix$$

where V = O_2-Cd couple voltage at current i

X = external impedance

x = internal impedance

E = O_2-Cd voltage in absence of polarization or current drain

i = current

i_o = exchange current

i_c = limiting current = KP

R = gas constant, 8.314 watt-sec/mole - °K

T = absolute temperature, °K

n = number of electrodes transferred, 4 equiv./mole

F = Faraday's constant, 96,484 amp-sec/equiv

The expression $\frac{RT}{nF} \ln i/i_o$ is the polarization due to slowness of the reaction of oxygen at the electrode. For oxygen, i_o is very small, and high polarization occurs with low currents.

The expression $\frac{RT}{nF}$ ln $i_c/(i_c - i)$ represents the polarization due to mass transport impedances. Both the oxygen and cadmium electrodes contribute to this term, and i_c is the current that could be obtained from the cell if the electrical impedances were made zero.

The effect of changing the external impedance is readily predictable from the general equation in a qualitative manner. For low values of the impedance, the voltage is controlled in large part by the logarithmic terms, and tends to be non-linear with oxygen pressure. At medium values of the impedance, the RT/nF ln i/i_o term becomes small, and the RT/nF in $i_c/(i_c - i)$ term governs. This is, for a first approximation with i a constant fraction of i_c, linear with i_c. At larger values of the impedance, the voltage becomes constant with change in pressure, since the cell voltage approaches E as i decreases and the current cannot exceed the value of E/X. These predictions are borne out experimentally.

Teflon film was selected as the diffusion barrier because:

1. Teflon is non-wettable, and thus the diffusion barrier will remain constant during operation since a film of electrolyte cannot form on the gas side of the barrier. Films of electrolyte are also substantial diffusion barriers and must be prevented from forming, or be made constant in value.
2. Teflon has a high diffusivity constant for oxygen, and thus thicker films can be used for a given transport value. This contributes to greater mechanical strength and lessens the chance of deleterious pinholes.
3. Teflon film is available in a wide range of thicknesses and widths, which permits an optimization of film dimensions without procurement problems.

2.1.2 Sensing Electrode Fabrication

The electrodes are fabricated by pressing the substrate and film together under controlled temperature and pressure for 45-60 minutes. In some cases, times as short as 6-10 minutes can be used. Table I gives the details of substrates tested, and pressing conditions.

For pressing, a sandwich made of a Ferrotype disk, substrate disc, Teflon film, aluminum foil, and a second Ferrotype disc was placed in a steel die and pressed. The Ferrotype discs are used to protect the die surface

TABLE I

SENSING ELECTRODE MATERIALS

NO.	SUBSTRATE MATERIAL	FILM THICKNESS (1,2)	SUBSTRATE DESCRIPTION
1	Nickel Sinter	1 mil	0.020" porous nickel (nominal) 4-7 micron pores, 80% total porosity. Support: Exmet 5 Ni 10-1/0. General Electric, Gainesville, Florida
2	"	0.5 mil	DO
3	"	0.25 mil	DO
4	Nickel Screen	1 mil	Exmet nickel mesh 5 Ni 10-3/0. Exmet Corporation, Tuckahoe, N. Y.
5		0.5 mil	DO
6		0.25 mil	DO
7	Gold Mesh	1 mil	100 X 100 screen 0.003" pure gold wire. Cole Roscoe Mfg. Co., So. Norwalk, Conn.
8	"	0.5 mil	DO
9	"	0.25 mil	DO
10	Platinum-coated Tantalum Mesh (3)	1 mil	0.010" expanded tantulum mesh one face covered with 0.00025"bright platinum. Anode stock, Metal and Controls, Inc., Attleboro, Mass.
11	Platinum Coated Tantalum Screen (4)	1 mil	0.010" expanded tantalum mesh, two faces with 0.00025" bright platinum. Anode stock, Metal and Controls, Inc., Attleboro, Mass.

NOTES TO TABLE I

1. Films were Teflon skived films, Dilectrix Corp., Farmingdale, N.Y.
2. Films were applied as follows:
   1 mil 12,000 PSI at 672°F for ca. 45 min.
   0.5 mil 8,000 PSI at 672°F for ca. 60 min.
   0.25 mil 6,000-8,000 PSI at 672°F for ca. 60 min.
   All electrodes are air cooled under pressure to room temperature.
3. Mesh approximates Exmet 3/10 style. No designation given by manufacturer.
4. Mesh approximates Exmet 3/10 style, but is ribbed so that adjacent strands are not in same plane.

from the irregular substrate, and were replaced as necessary in order to assure a smooth outer surface on the film. The aluminum foil was used to prevent the Teflon from bonding to the Ferrotype; it is removed by dissolution in a 25% KOH solution.

After pressing, the sandwich is removed from the die and carefully separated. The electrode is quenched in warm alkali to remove the aluminum foil, and after being washed and dried is ready for use.

2.1.3 Screening Tests

The results of a study made of the response of the various electrode materials listed in Table I to oxygen pressure at various temperatures and with various external load resistances are summarized in Table II. The remarks are based on the visual analysis of the curves of signal current (milliamperes flowing between the sensing and cadmium electrodes) vs. oxygen pressure (0 to 30 PSIA) at various temperatures and with various load resistances. A current was always obtained at zero oxygen pressure, due probably to traces of oxygen adsorbed on the electrode or dissolved in the electrolyte.

The test data were obtained using dual cells containing

TABLE II

SUMMARY OF RESPONSE STUDIES
ON SENSING ELECTRODES

ELECTRODE		TEST		
NO (1)	SIZE cm^2	TEMP ^oC	LOAD OHMS	REMARKS
1	0.86	-10	20-200	Linear
		0	do.	Linear
		10	do.	Curves upward (3)
		25	do.	Curves upward (3)
		35	do.	Linear to 25 PSIA (4)
1	9.8	-10	10-200	Linear to 25 PSIA
		0	do.	Linear
		10	do.	Linear
		25	do.	Curves upward (4)
		35	do.	Linear
2	0.86	-10	20-200	Curves upward (5)
		0	do.	Curves upward (5)
		10	do.	Linear
		25	do.	Linear
		35	do.	Linear
2	9.8	-10	10-200	Curves upward (3)
		0	do.	Curves upward (3)
		10	do.	Linear
		25	do.	Curves upward (3)
		35	do.	Curves upward (3)
3	0.86	25	20-200	Sigmoid curve (6)
	9.8	25	10-200	Sigmoid curve (6)
4	9.2	10	do.	Test cell failed (7)
		25	do.	Linear
		35	do.	Linear
4	0.86	25	20-200	Linear
		35	do.	Linear
5	0.86	-10	do.	Linear to 25 PSIA (4)
		0	do.	Linear to 25 PSIA (4)
		10	do.	Curves upwards (3)
		25	do.	Sigmoid curve (6)
		35	do.	Sigmoid curve (6)
5	9.8	-10	10-200	Curves upwards (3)
		0	do.	Curves upwards (3)
		10	do.	Curves upwards (3)
		25	do.	Curves upwards (3)
		35	do.	Linear
6	0.86	25	20-200	Sigmoid curve (6)
	9.8	25	10-200	Sigmoid curve (6)
7	0.86	25	20-200	Erratic behavior on load
	9.8	25	10-200	Erratic behavior on load
8	0.86	-10	20-200	Curves upwards (3)
		0	do.	Linear to 25 PSIA (3)
		10	do.	Linear to 20 PSIA (3)
		25	do.	Sigmoid curve (6)
		35	do.	Sigmoid curve (6)
8	9.8	-10	10-200	Linear
		0	do.	Linear

TABLE II
Cont'd

ELECTRODE NO	ELECTRODE SIZE cm^2	TEST TEMP ^oC	TEST LOAD OHMS	REMARKS
8		10	do.	Linear
		25	do.	Curve saturates (8)
		35	do.	Curve saturates (8)
9	0.86	25	20-200	Curve upwards (3)
	9.8	25	10-200	Erratic behavior on load
10	0.86	25	20-200	Curves upward (3)
	9.8	25	10-200	Curves upward (3)
11	0.86	25	20-200	Curves upward (3)
	9.8	25	10-200	Curves upward (3)

Remarks Table II

1. Refer to Table I for details of electrode.
2. Curves plotted ma of signal electrode to cadmium electrode vs. PSIA oxygen 0-30 PSIA for various loads.
3. Curve increases with increase in oxygen pressure.
4. Curve flattens at higher oxygen pressures.
5. Curve linear 0-20 PSIA of oxygen, then curves upward
6. Sigmoid curve, not suitable for indicator use over desired range of 0 to 25+ PSIA. Curve is flat on ends with sharp rise in middle.
7. Short in nickel-cadmium section of test cell.
8. Curve flattens in higher resistance ranges, showing that not all oxygen is being reacted upon arrival at electrode surface.

sensing electrodes of 0.86 cm^2 and 9.8 cm^2 area. These were mounted in a Lucite frame, and placed against a cadmium electrode with a non-woven nylon separator saturated with 31% KOH placed in between. Before each series of tests, the cadmium electrode was charged against a nickel mesh counter electrode. The oxygen pressure was adjusted manually, using tank oxygen and a mechanical vacuum pump. Tests at various temperatures were made in appropriate cold boxes or ovens.

A typical plot of electrode current vs oxygen pressure for a fixed temperature at various loads is presented in Figure 1. Data of this type are closely related to cell behavior of the electrodes, since they are used to detect variations in pressure. Plots of this type were analyzed in the preparation of Table II.

A three dimensional model would be required to depict the electrode response for variations in oxygen pressure, temperature and load resistance. Some idea of the rather complex behavior can be obtained by using two dimensional plots of electrode current vs temperature for a fixed oxygen pressure and various loads (Figures 2 through 9), and plots of electrode signal vs oxygen pressure for a fixed load at various temperatures (Figures 10 and 11).

FIGURE 1

Typical Sensing Electrode Behavior

10°C

Electrode Mat'l #1

Ni Sinter 0.001" Film

9.8 cm^2

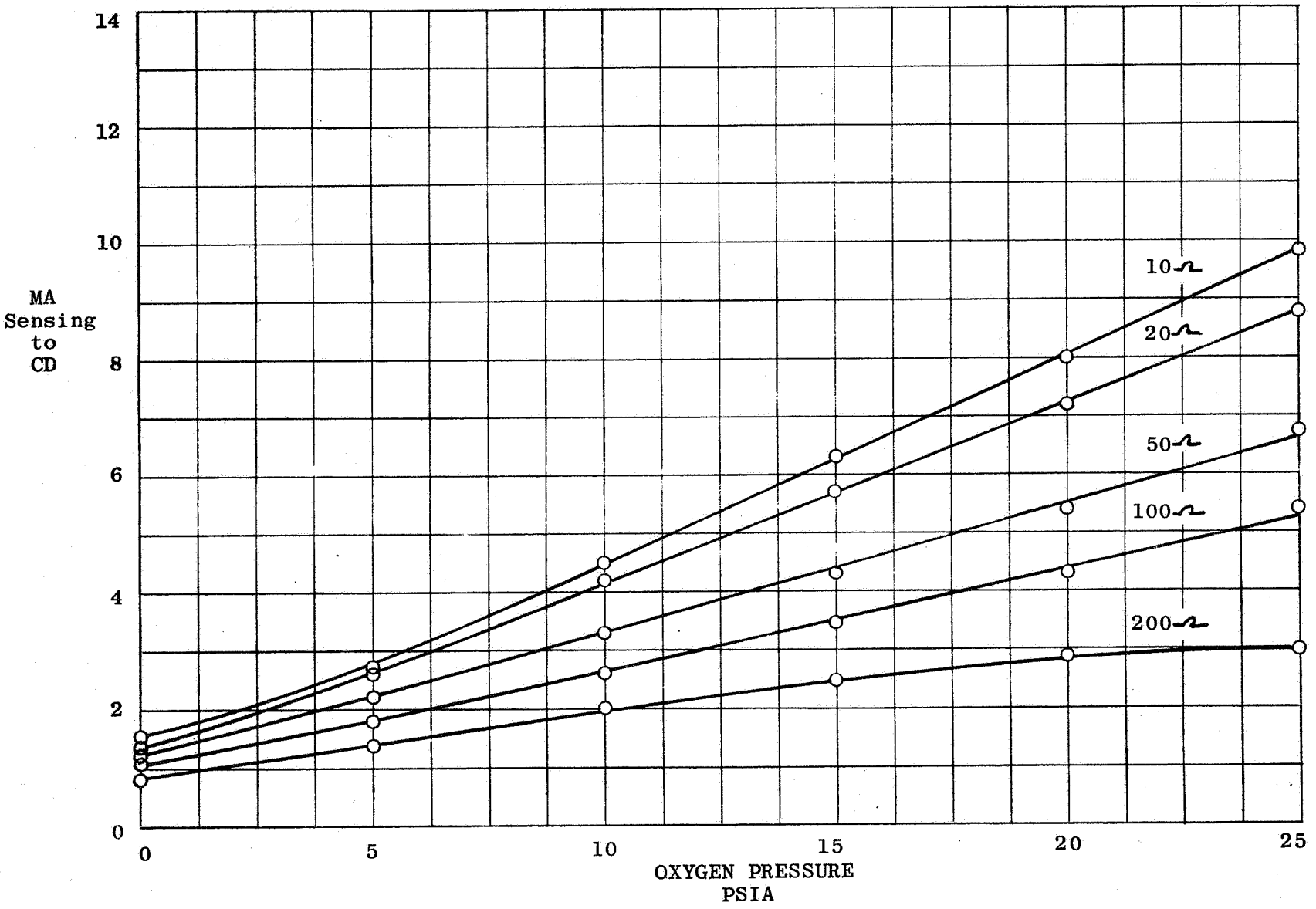

FIGURE 2

Sensing Electrode Behavior

30 PSIA

Electrode Mat'l. #1

Ni Sinter 0.001"Film

9.8 cm^2

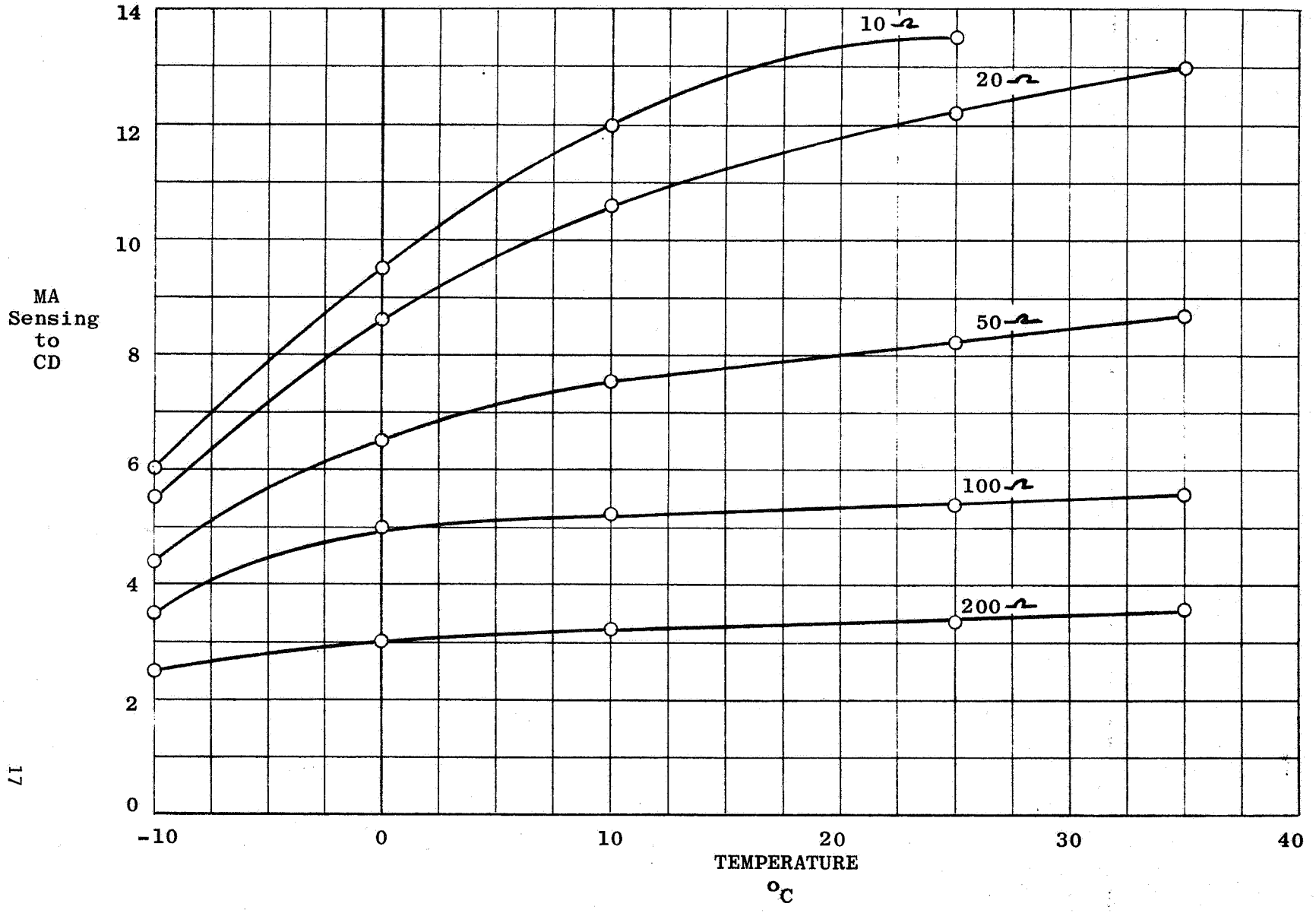

FIGURE 3

Sensing Electrode Behavior

25 PSIA

Electrode Mat'l. #1

Nickel Sinter 0.001" Film

9.8 cm^2

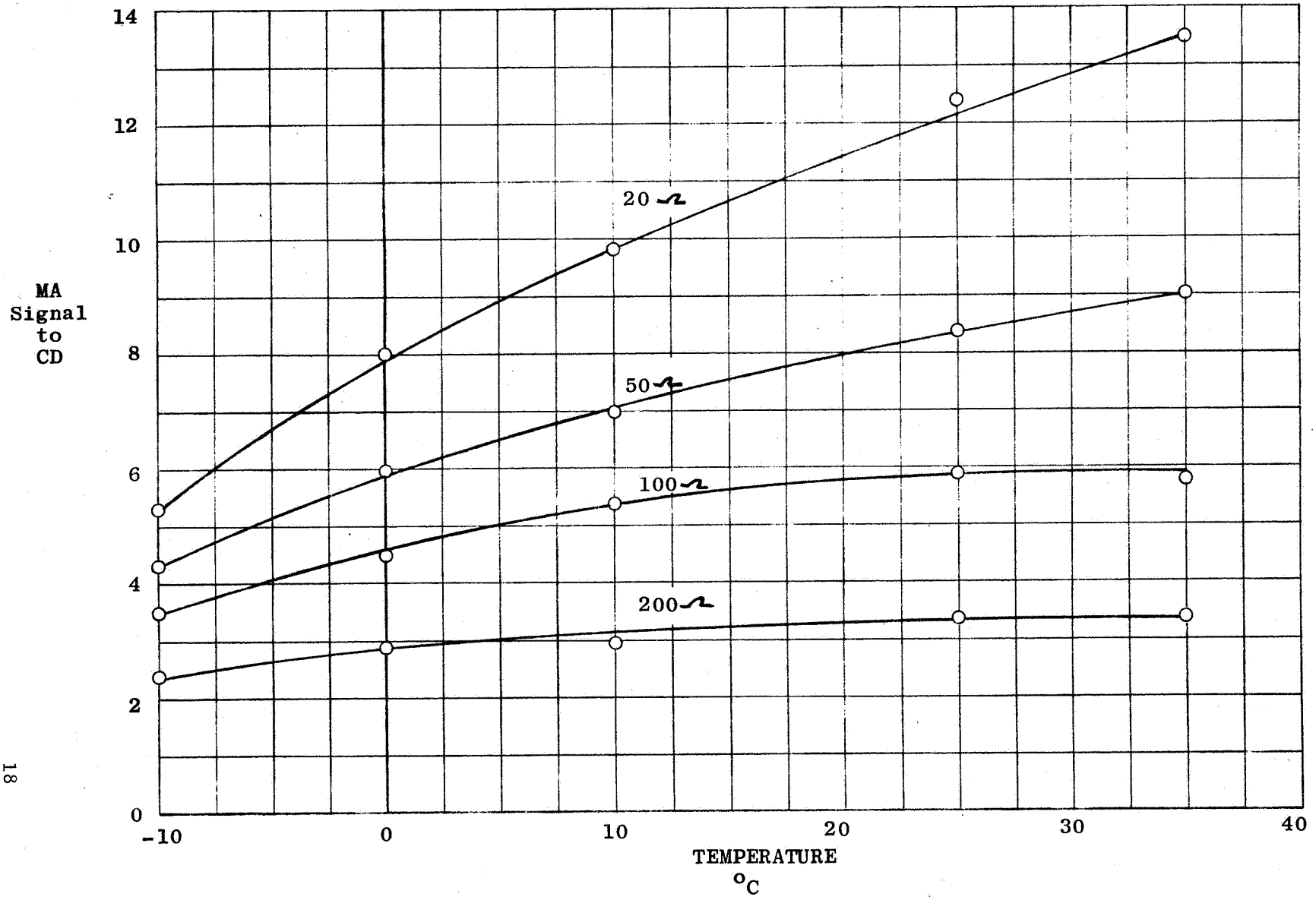

FIGURE 4

Sensing Electrode Behavior

20 PSIA

Electrode Mat'l. #1

Nickel Sinter 0.001" Film

9.8 cm^2

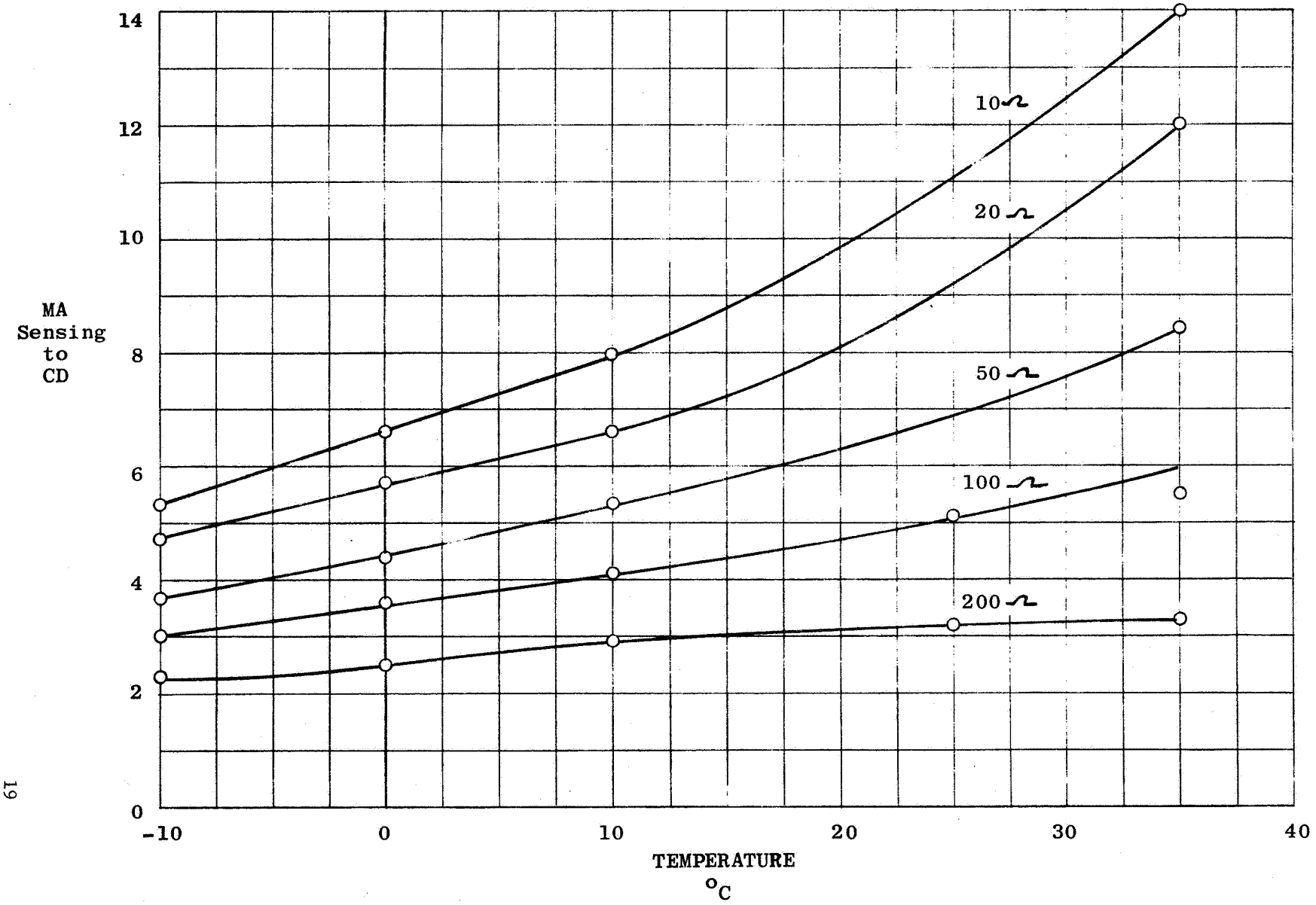

FIGURE 5

Sensing Electrode Behavior

10 PSIA

ELECTRODE MAT'L. #1

Nickel Sinter 0.001" Film

9.8 cm^2

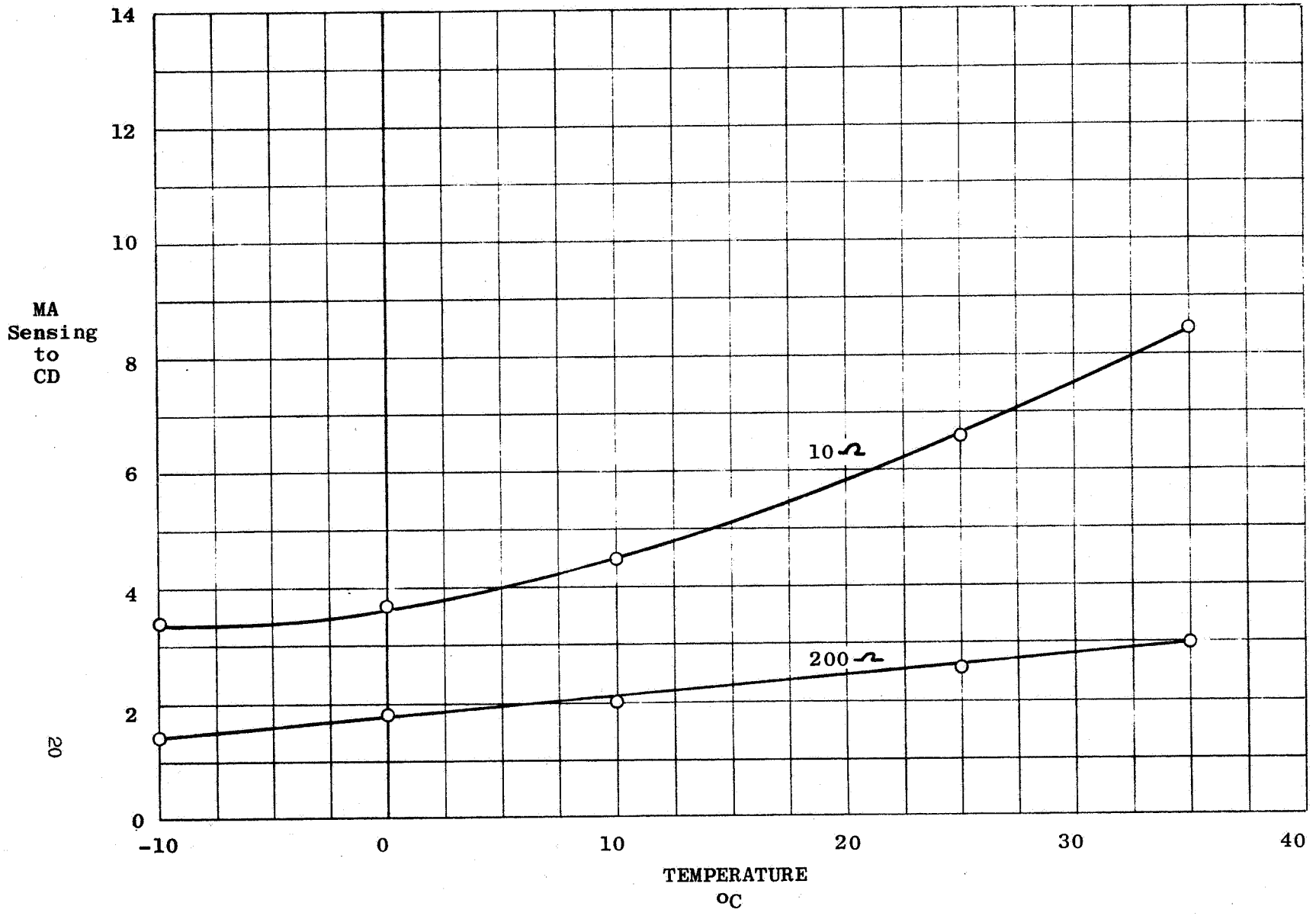

FIGURE 6

Sensing Electrode Behavior

30 PSIA

Electrode Mat'l. #8

Gold Mesh, 0.0005" Film

9.8 cm^2

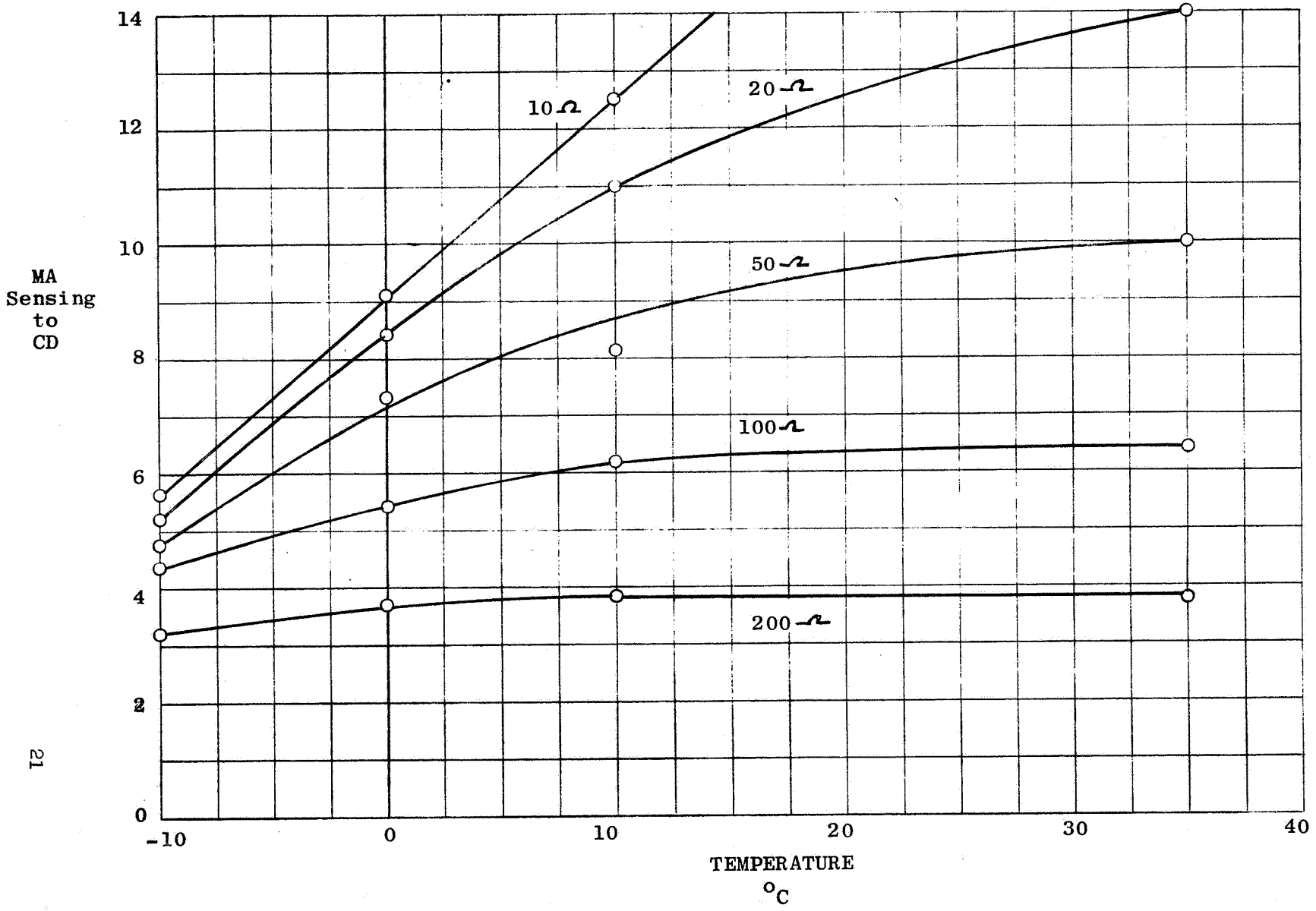

FIGURE 7

Sensing Electrode Behavior

25 PSIA

Electrode Mat'l. #8

Gold Mesh, 0.0005" Film

9.8 cm^2

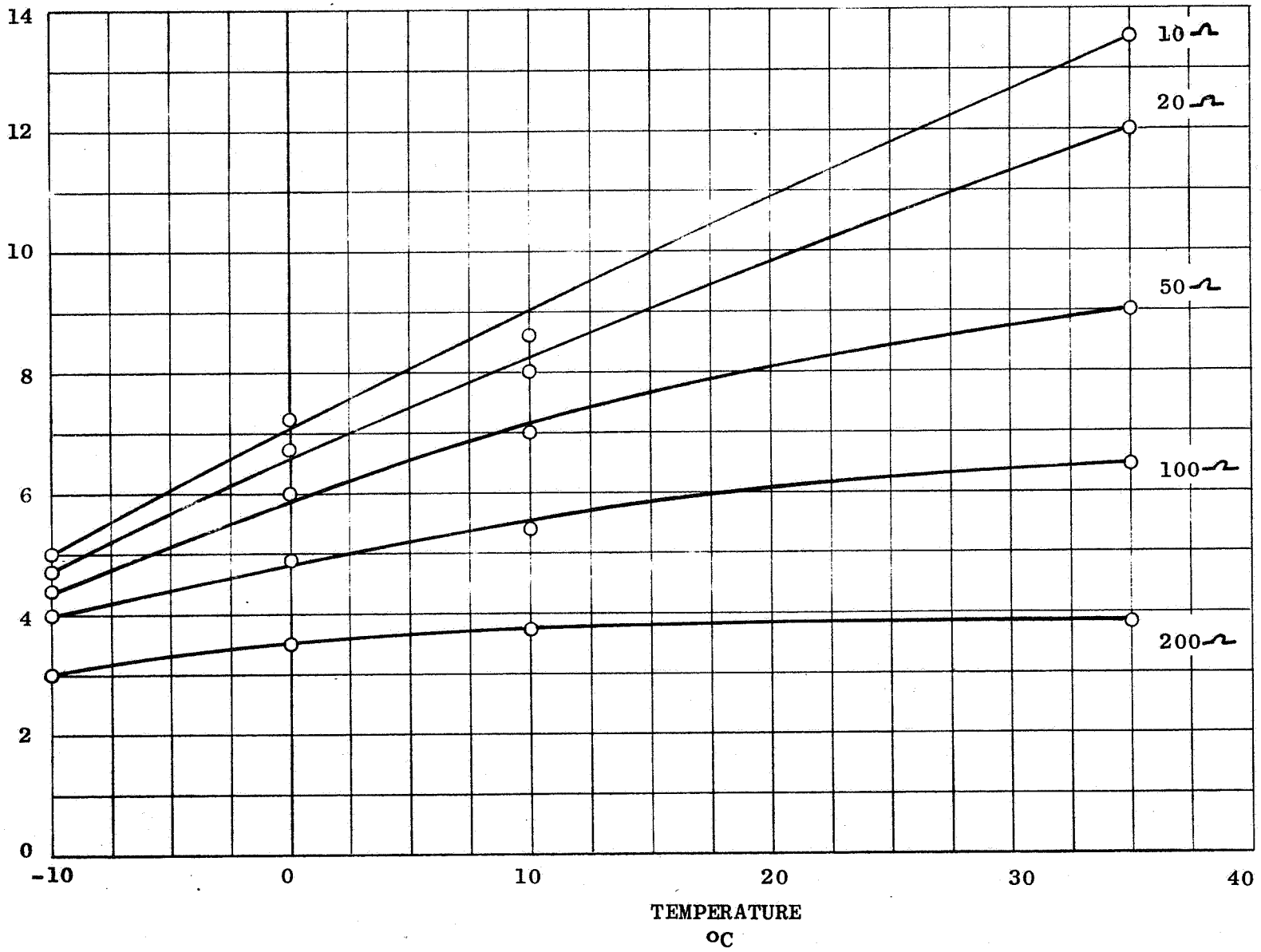

FIGURE 8

Sensing Electrode Behavior

20 PSIA

Electrode Mat'l. #8

Gold Mesh, 0.0005" Film

9.8 cm^2

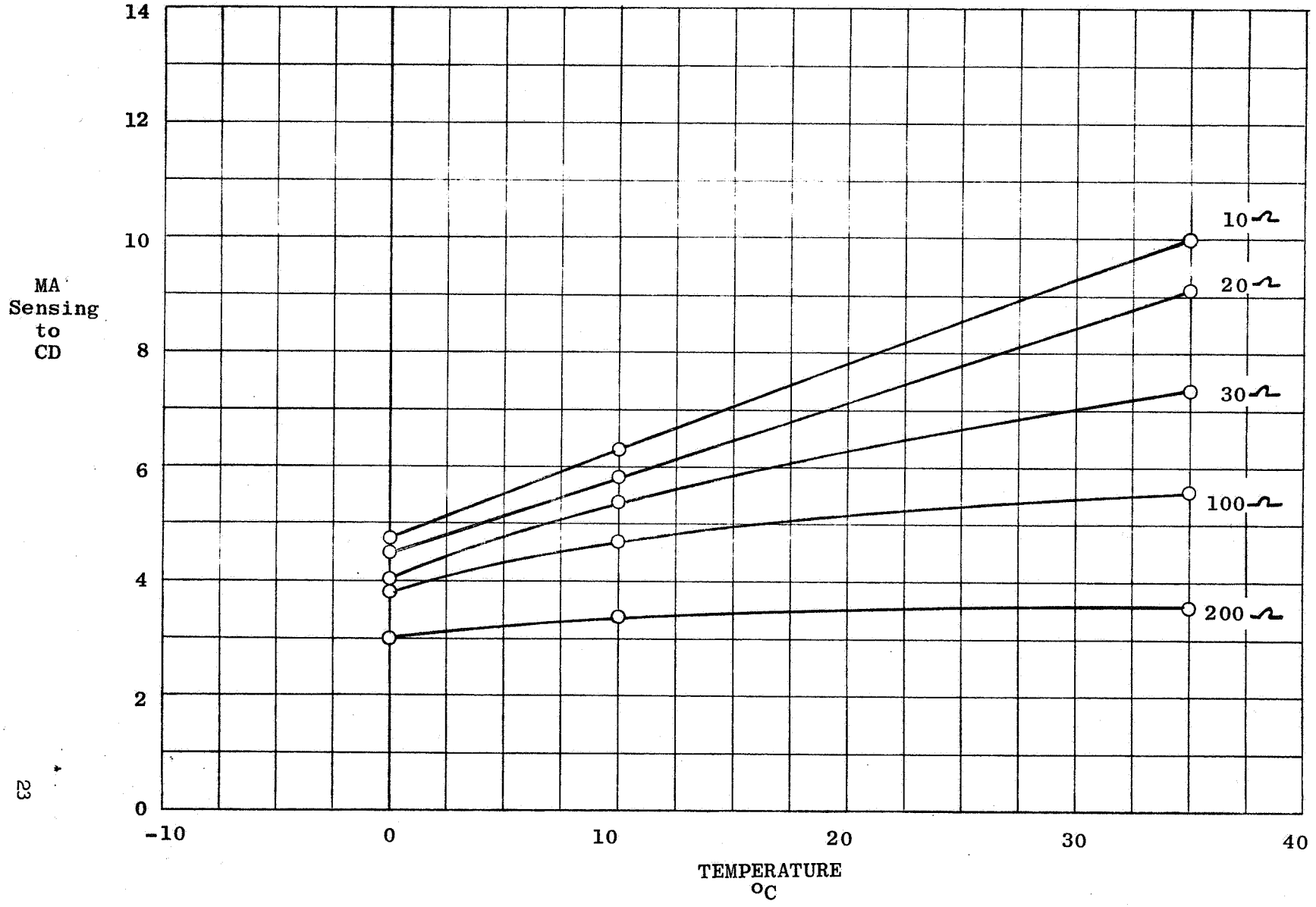

FIGURE 9

Sensing Electrode Behavior

10 PSIA

Electrode Mat'l. #8
Gold Mesh, 0.0005" Film

9.8 cm^2

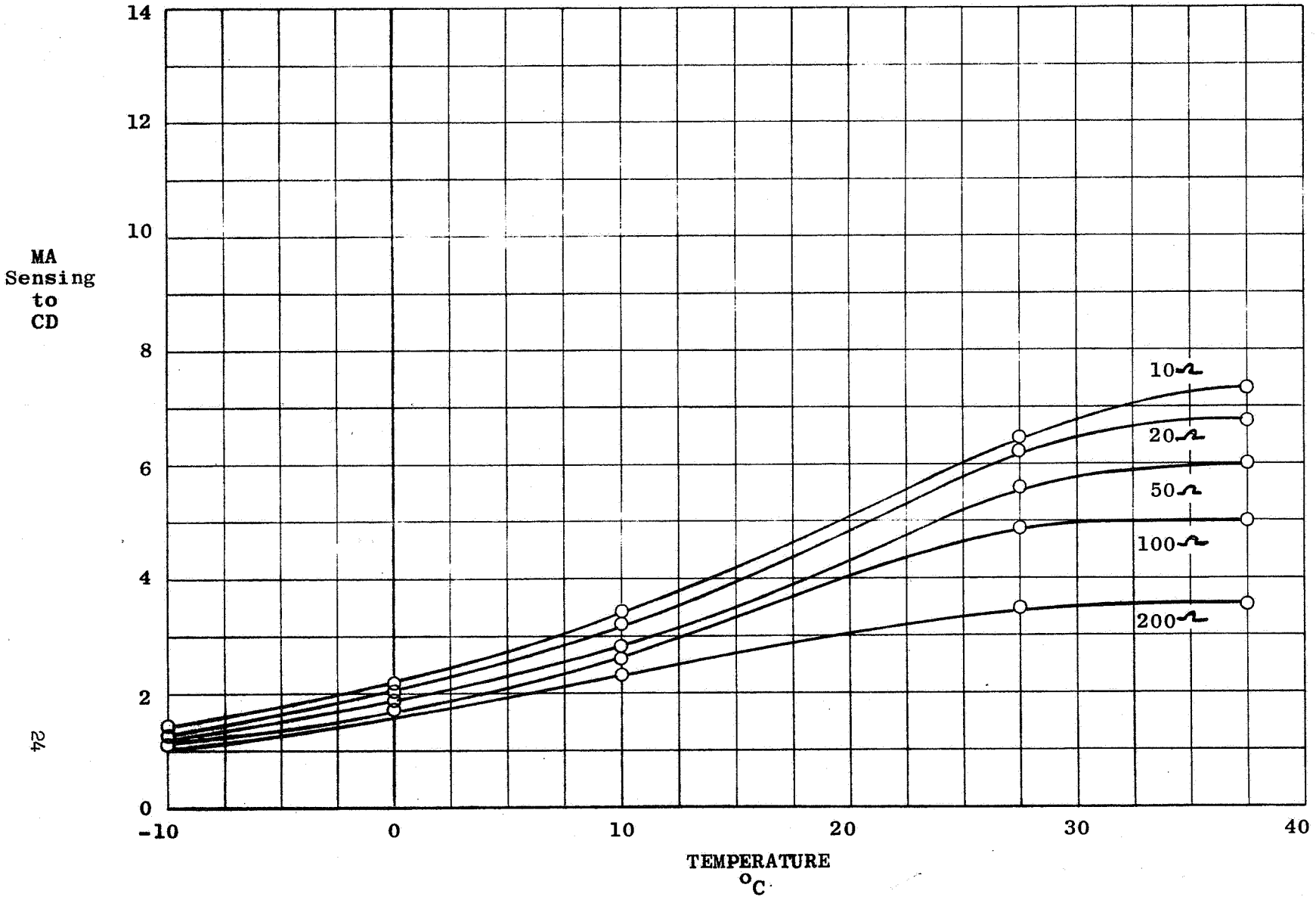

FIGURE 10

Sensing Electrode Behavior

50Ω Load

Electrode Mat'l. #1

Nickel Sinter 0.001" Film

9.8 cm^2

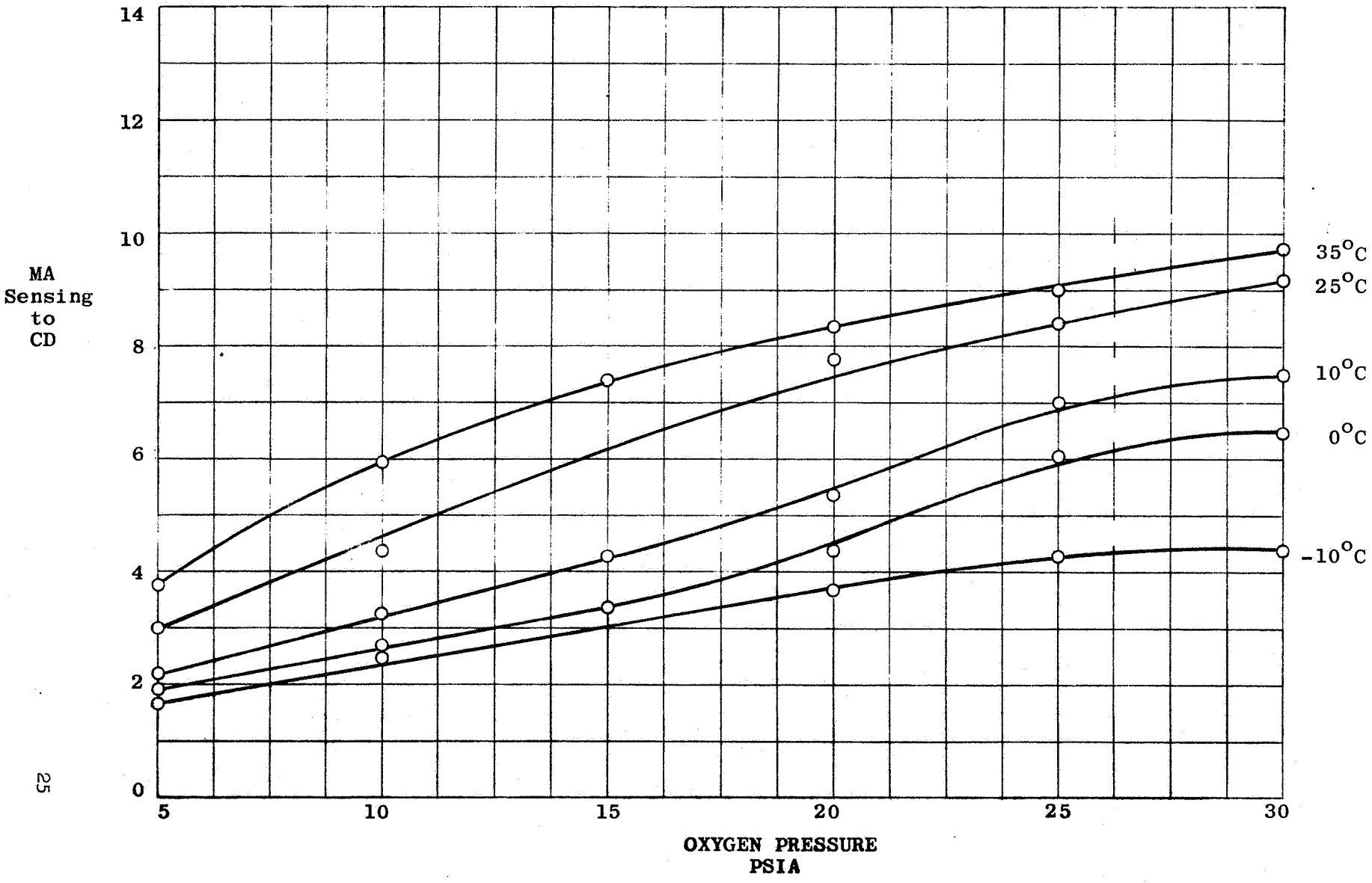

FIGURE 11.
Sensing Electrode Behavior
50Ω Load

Electrode Mat'l. #8
Gold Mesh, 0.0005" Film
9.8 cm^2

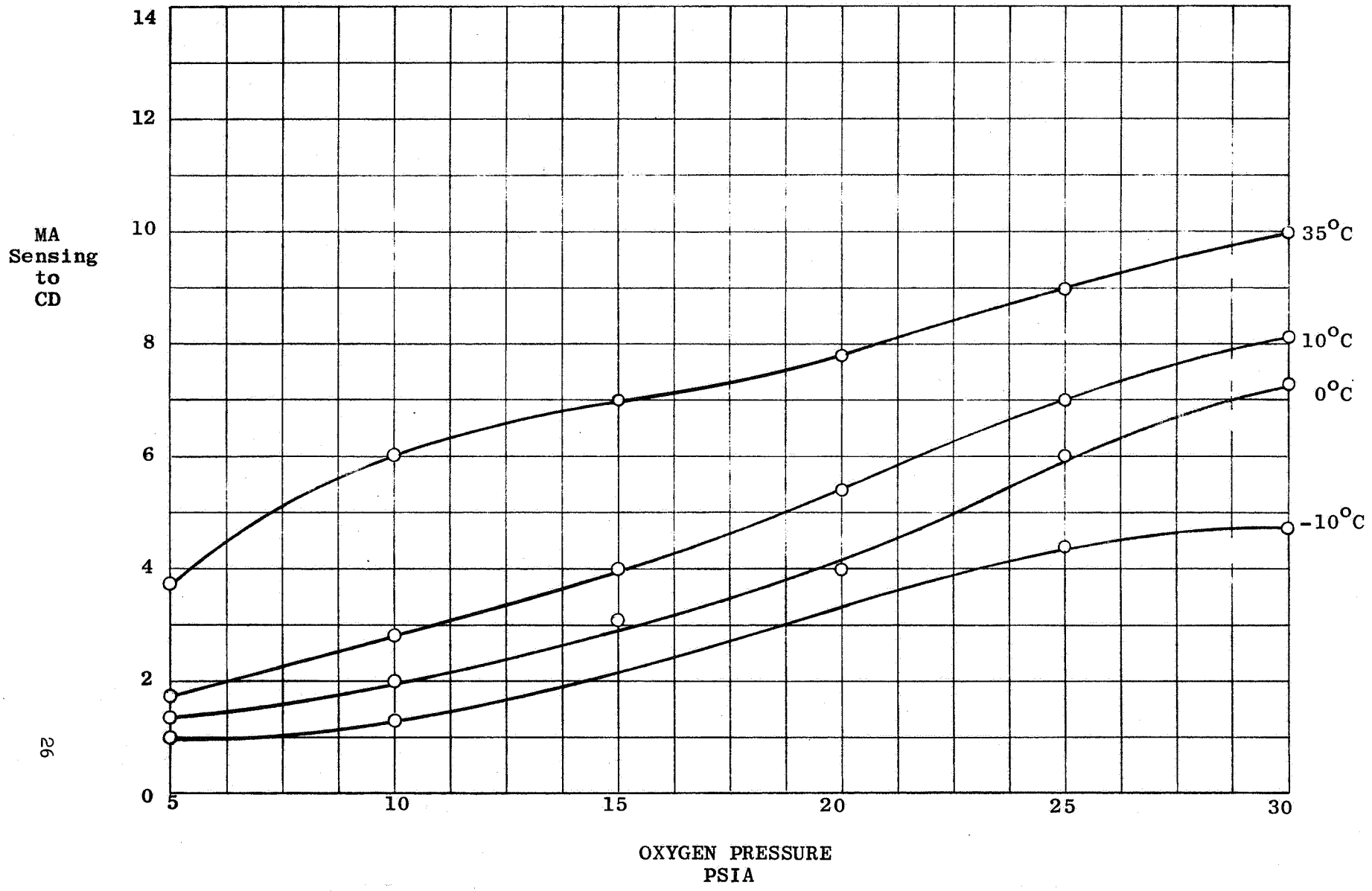

The figures give the response of nickel sinter and gold mesh electrodes.

The response of both the nickel sinter and gold mesh electrodes, with 0.001" or 0.0005" Teflon films, are essentially linear with respect to oxygen partial pressure. In addition, the magnitudes of the signals generated by both types of electrodes are essentially the same. It was concluded, therefore, that either type of electrode would be satisfactory. Nickel sinter was chosen for further study on account of its lower cost. Larger area electrodes appear more suitable than smaller, based primarily upon current carrying ability.

The output of the sensing electrodes was also found to be highly temperature dependent, as would be expected from the general response equation and the fact that the diffusion of a gas through a barrier is also highly dependent upon temperature. The observed dependence, in the linear regions, is about 2% per degree centigrade. This is about the same order of magnitude as for the diffusion of a gas through a barrier.

2.1.4 Evaluation of Signal Electrodes

A key factor in the use of an oxygen sensing electrode is

the reproducibility of the signal with respect to oxygen pressure under fixed conditions of temperature and external load. This was tested for nickel sinter electrodes in special test cells.

In the cell, the 9.8 cm^2 test electrode was separated from the cadmium electrode by non-woven nylon saturated with 31% KOH. The cadmium electrode was continuously trickle charged during the test at 20 mA. The signal (sensing to cadmium) current was passed through a 0-1 mA meter relay which had high-low contacts. The range of the meter was adjusted with external fixed resistors. The operation of the control for cycling was as follows: Tank oxygen was admitted to the cell via a shut off solenoid, operated by the control circuit, and a manually set flow control valve. When the upper pressure signal was reached on the meter relay, the oxygen solenoid was closed and the cell evacuated via a second shut off solenoid and flow control valve. Evacuation continued until the lower pressure signal was reached, at which time the vacuum was cut off and oxygen readmitted. Cell pressures were monitored with 0-40 PSIA pressure transducers. Cells were cycled over the temperature range of

-20°C to +40°C.

Typical results for a test conducted at 25°C are shown in Figure 12. The pressure recordings show a series of regular waves whose period is controlled by the gas flow rates. The wave crests represent the cut off pressures sensed by the electrodes at high pressures, and the troughs for the low pressures. For a given temperature and load (meter plus shunts), the wave crests were within 1-2% of each other throughout the period of the test. This indicates good reproducibility and rapid response to changes in oxygen pressure. A response time of about one second is estimated from the tests. These results demonstrate that the sensitivity and reproducibility of the sintered nickel electrode are more than adequate for use in cells.

In order to complete the evaluation of the sensing electrode, and determine the proper position for the electrode in the cell, full scale cells were constructed. Component parts of these cells are shown in Figure 13. The sensing electrode is the circular piece in the middle of the bottom row. Electrode holders to the left and right are used for positioning the electrode on the pack face and top, respectively.

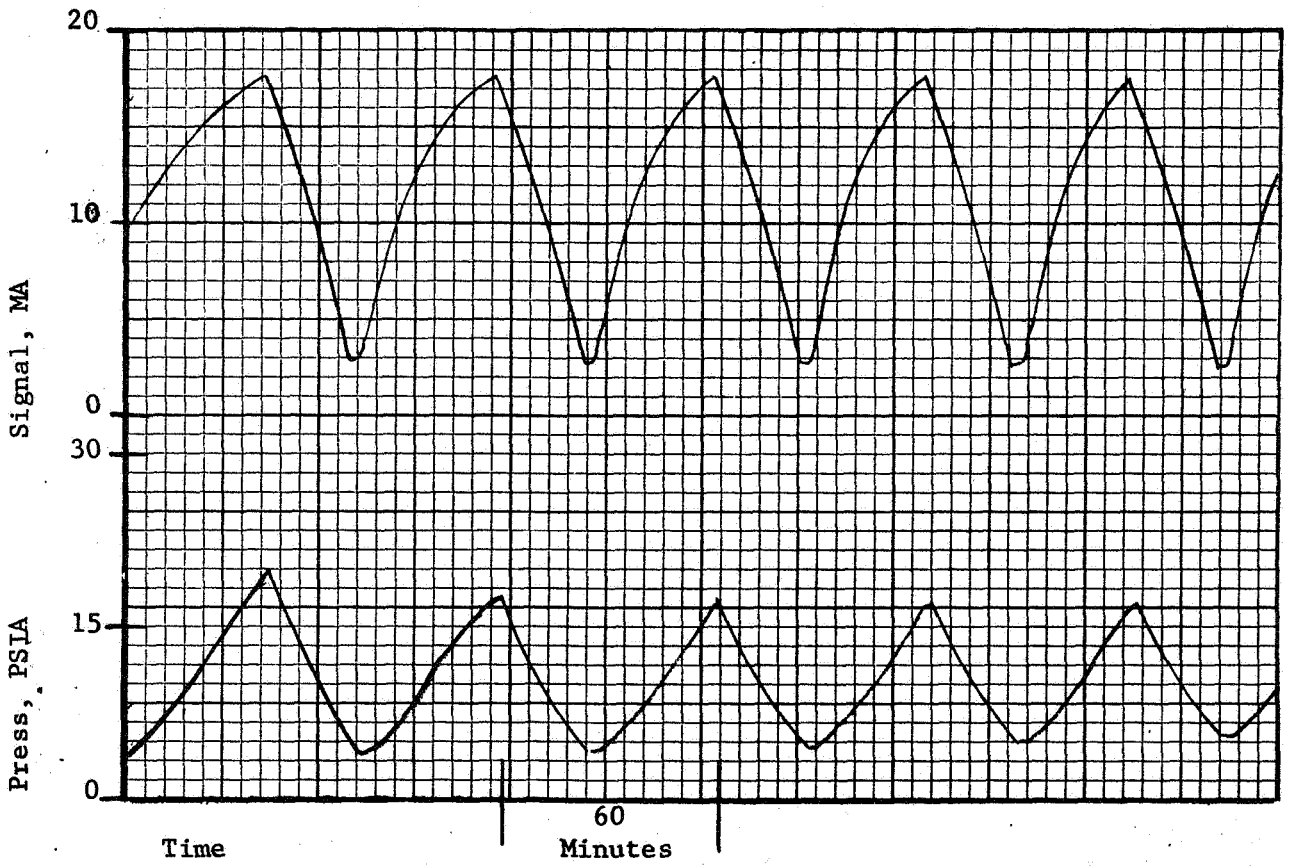

Figure 12

SIGNAL ELECTRODE CYCLE TEST

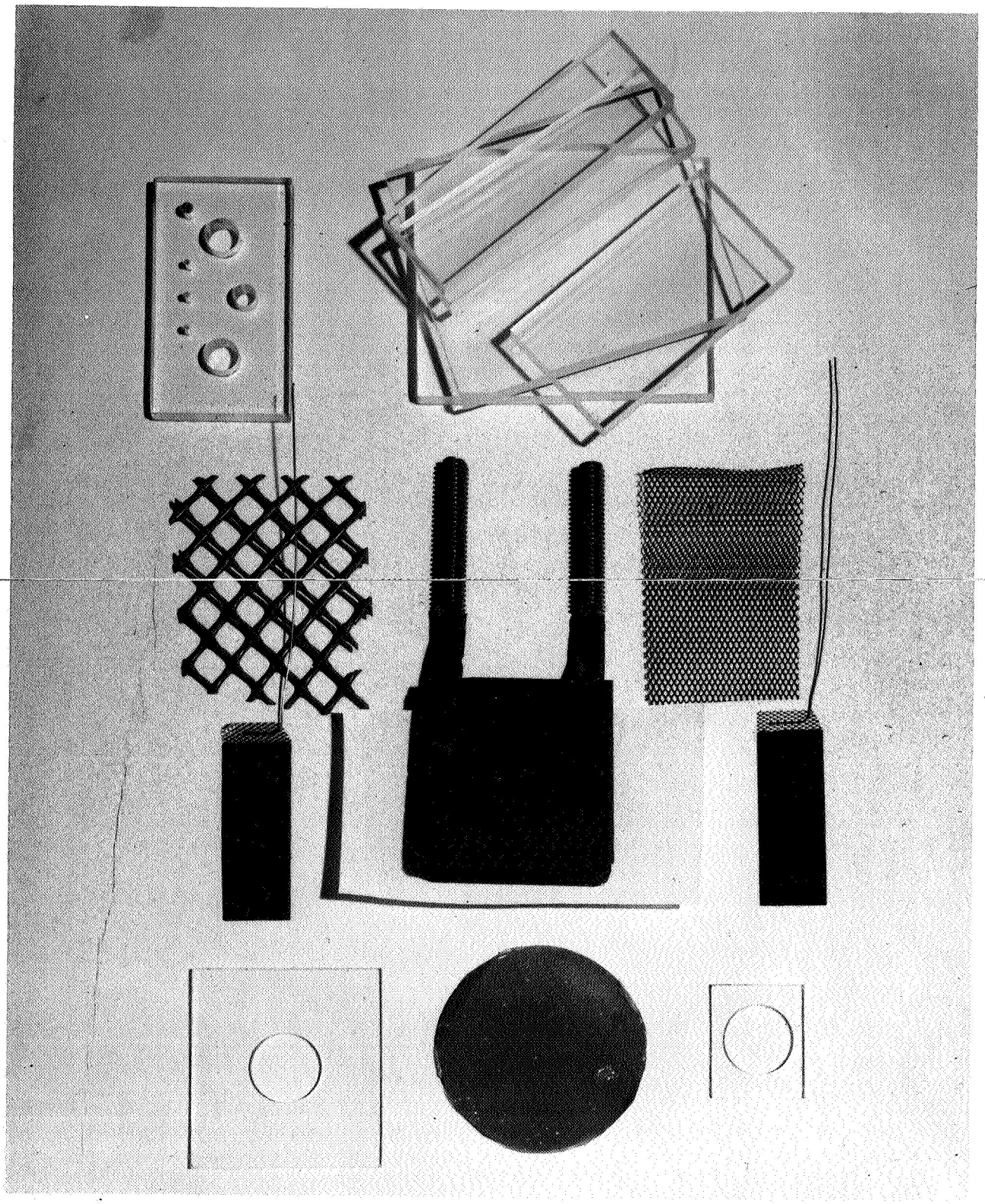

Figure 13

Sensing Electrode Test Cell
Components

Dummy solid pieces were used as appropriate to maintain equal free volumes in the cells. The recombination electrodes are shown at either extreme of the middle row; these were located on the sides of the pack and were connected in parallel. The total area of the recombination electrodes is 17.5 cm^2. The nickel-cadmium cell pack is shown in the center, and consists of 10 negative and 9 positive plates, with a nominal capacity of six ampere hours.

Figure 14 shows the completed cell, and the case in which it is potted. This photograph shows a dummy electrode holder piece on the top of the cell pack; the sensing electrode is on the back side (not shown). A thermocouple is seen on the left hand side. Electrical connections to the recombination and sensing electrodes are the wire leads; the bolts provide connection to the nickel and cadmium electrodes.

The cells were cycled at various rates and temperatures with various load resistances in the recombination and sensing electrode circuits. Tests were carried out using the control equipment shown in Figure 15. The equipment

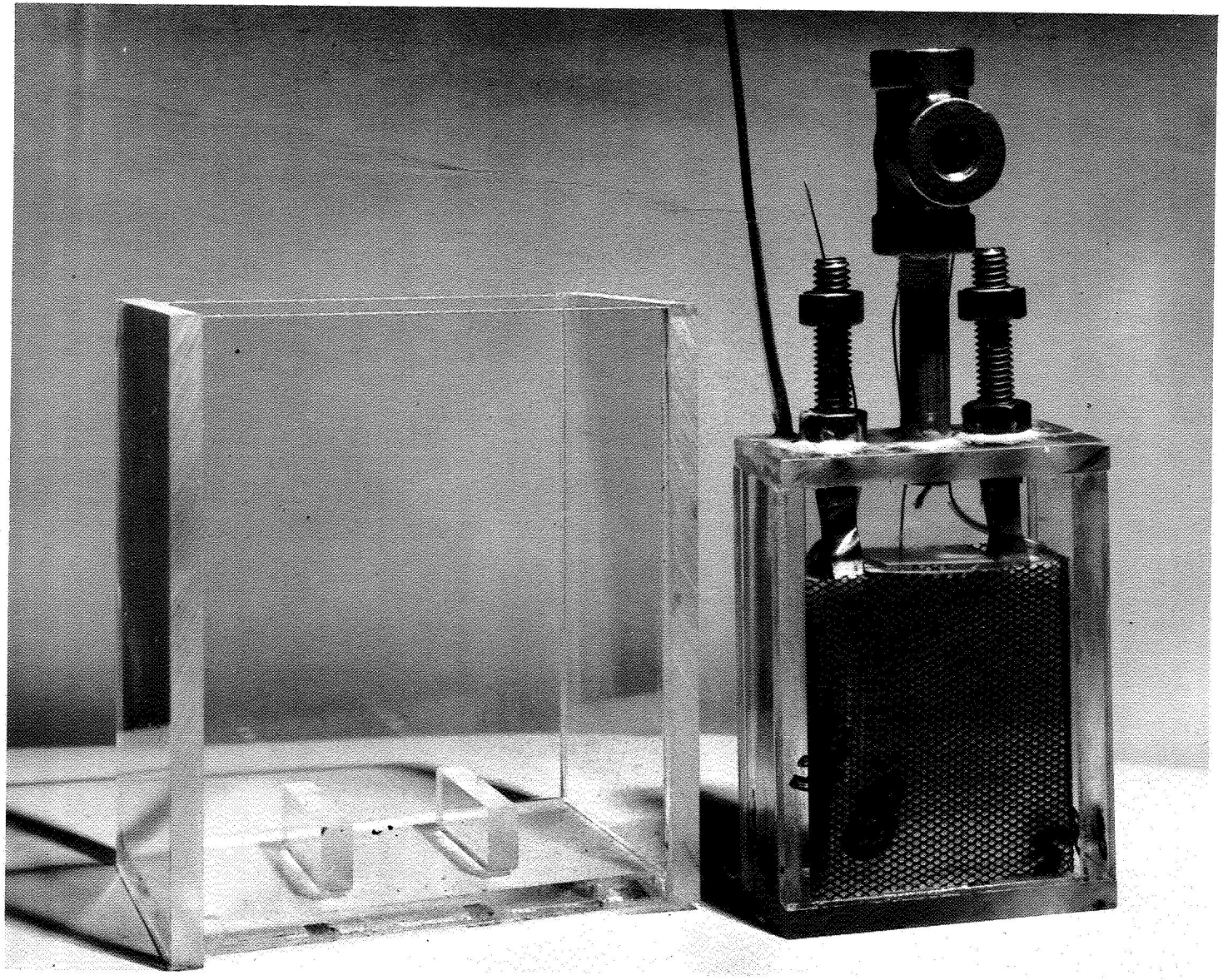

Figure 14

Sensing Electrode Test Cell

Assembly

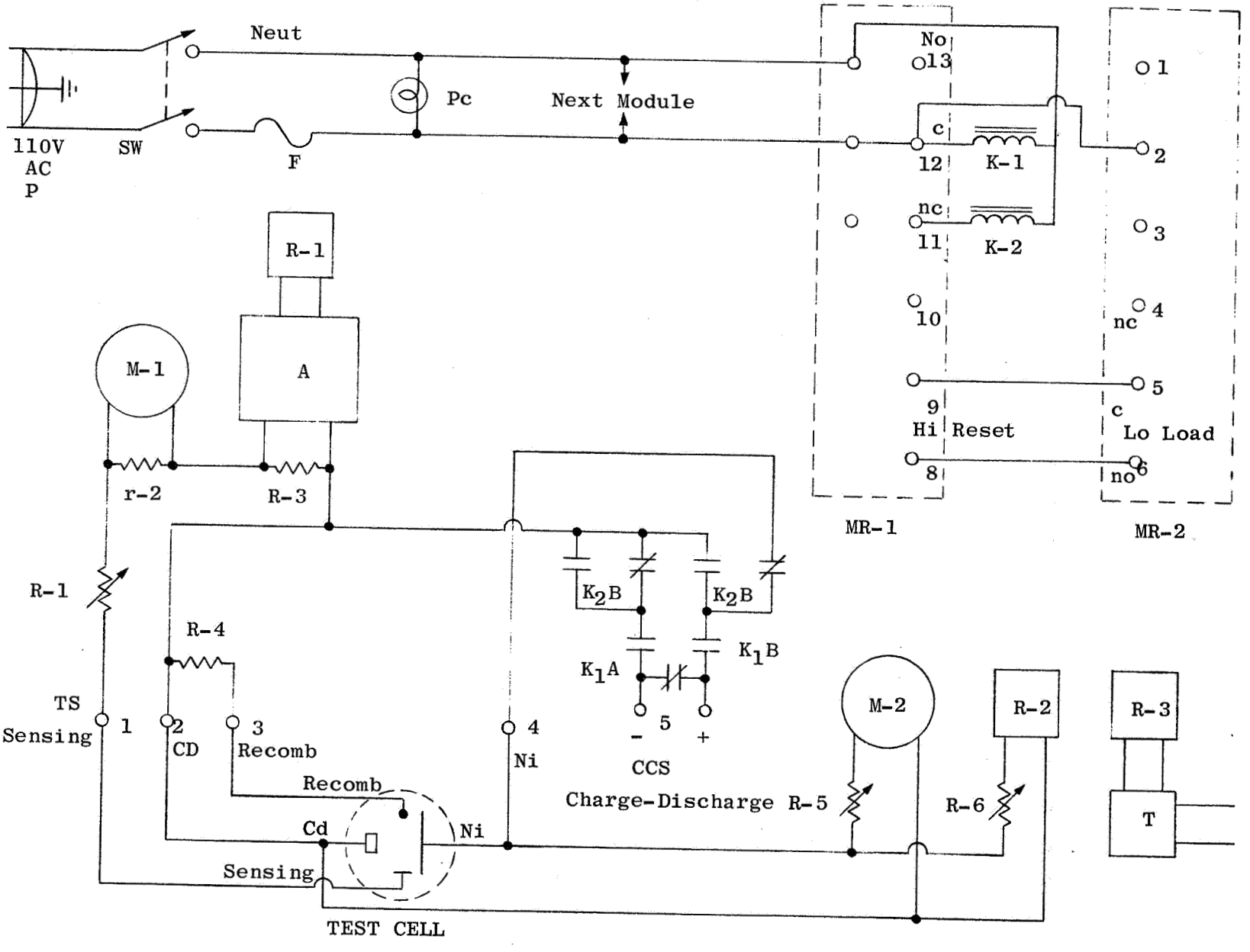

Figure 15 Test Cell Circuits

allows charging to a sensing electrode signal, followed by discharge to a fixed cell voltage. Meter relays are used for sensing the end of cycle conditions.

Table III gives the pertinent identification of the cells. Table IV gives the outline of the cycling tests made on the various test cells. The program was designed so that each temperature was covered for all electrode samples and sensor locations. Each series of tests was run at three current levels: C/6, C/2, and C, as indicated.

The signal electrode to cadmium electrode load was held constant; the meter relay trip point was adjusted for each temperature to a value corresponding to an oxygen pressure of 20 PSIA, in accordance with the signal electrode calibration curve at that temperature. The latter was obtained for each cell at each temperature at the beginning of the series by manually adjusting the oxygen pressure in the cell over the range 0 to 30 PSIA, and observing the signal current. This was a convenient method of selecting the trip point for this test, but was not used in later test programs.

TABLE III

TEST CELL CONSTRUCTION

Cell	Recombination Electrode Number	O_2 Sensor Location
1	RE08-1	Top
2	RE08-1	Top
3	RE08-2	Top
4	RE08-2	Top
5	RE08-1	Face
6	RE08-1	Face
7	RE08-2	Face
8	RE08-2	Face

All cells have two recombination electrodes 2" x 3/4" located on edge of cell packs. Oxygen sensor electrode is circle 1-1/16" diameter and located either on top of the cell pack ("top" position) or on face of cell pack ("face" position). The sensor electrode is nickel sinter with 0.001" Teflon film. Cell pack is nominal 6 AH capacity.

TABLE IV

TEST CELL CYCLE PROGRAM

Cell	Temperature, °C			
	Series 1	Series 2	Series 3	Series 4
1	25	+10	-10	-20
2	25	0	-20	+40
3	25	+10	-10	+40
4	25	0	-20	+40
5	25	0	-20	+40
6	25	-10	+10	+40
7	25	0	-20	-20
8	25	-10	+10	+40

In each series, the tests were as follows:

Test	Charge Current Amps	Recombination-Cd Load, Ohms (1)	Time Days	O_2 Sensor-Cd Load Ohms (2)
A	1	3	2	20
B	3	1	2	20
C	6	0.5	2	20

(1) Including leads; selected to give 0.6 volt drop at 20% of charging current.

(2) Including leads; cut-off on meter set to operate at signal corresponding to 20-25 PSIA as determined from calibration made on cell at temperature of series.

The effect of top vs face position was mainly on signal level. The signal for face position electrodes was usually 35-50% greater than for those in top position. The signal for top position electrodes varied during cycling, decreasing to about 80% of the initial value for a given oxygen pressure and temperature after 15-30 cycles. This decline was due to poor electrolyte wicking resulting in drying out of the separator in contact with the electrode. This decreased signal led to severe overcharging of cell #4 during series 3, with damage to the pressure gauge and recorder. This cell recovered satisfactorily on cycling at 25°C and was used at 40°C to complete the tests. Signals of face position electrodes were stable, within 5%, during the entire test program, indicating that drying of the separator did not occur.

Each series required about one week to complete, with 3 low rate, 9 medium rate and 18 high rate cycles in each. A total of 120 cycles was thus acquired for each cell. For the cells which charged to a cutoff, the charge returned, to a 20 PSIA signal, was about 120% of the capacity delivered. This varied from cell to cell, but never was less than 110% or more than 135%. Discharge capacities were all greater than 6 A-Hr.

2.2 Task II - Oxygen Recombination Electrodes

2.2.1 Electrode Fabrication

Recombination electrodes were fabricated by application of a Pt catalyst to a substrate consisting of nickel powder sintered to an expanded nickel strip. The electrodes are wet-proofed by application of a Teflon suspenpension to the gas face of the electrode and subsequently curing at an elevated temperature.

A number of changes in the structure of these electrodes were made in order to optimize performance, especially at the extremely low temperatures. These changes included varying the porosity and thickness of the sintered nickel structure, varying the catalyst loading, and adjusting the thickness of the Teflon film on the gas face. Details of the electrodes fabricated during this program are presented in Table V.

2.2.2 Experimental Details

The performance of recombination electrodes was evaluated by obtaining current density-voltage (polarization) curves for the various electrodes as a function of operating temperature and oxygen pressure. The cell and components used in this evaluation are shown in Figure 16.

Table V

DETAILS OF RECOMBINATION ELECTRODE FABRICATION

Electrode		Sintered Ni Plaque			Catalyst	Teflon
Group	Number	Lot	Thickness mils	Porosity %	mg/cm^2	mg/cm^2
1	183	5-C	10	74.5	1.23	1.96
	184	5-C	10	74.5	1.25	1.84
2	192	8	14	81.2	2.69	1.77
	193	8	14	81.2	2.59	1.24
	195	8	14	81.2	2.67	1.55
3	R-1	5	11	85.4	2.62	0.96
	R-2	5	11	85.4	2.70	1.23
	R-3	5	11	85.4	5.00	1.12
4	500-1	5	11	85.4	5.16	1.19
	500-2	5	11	85.4	5.08	1.17
	500-3	5	11	85.4	10.29	1.23
5	R-4 thru R-7	5	11	85.4	5.00*	1.20*

*Design values. Tolerances held were ±0.10 on catalyst, ±0.05 on Teflon.

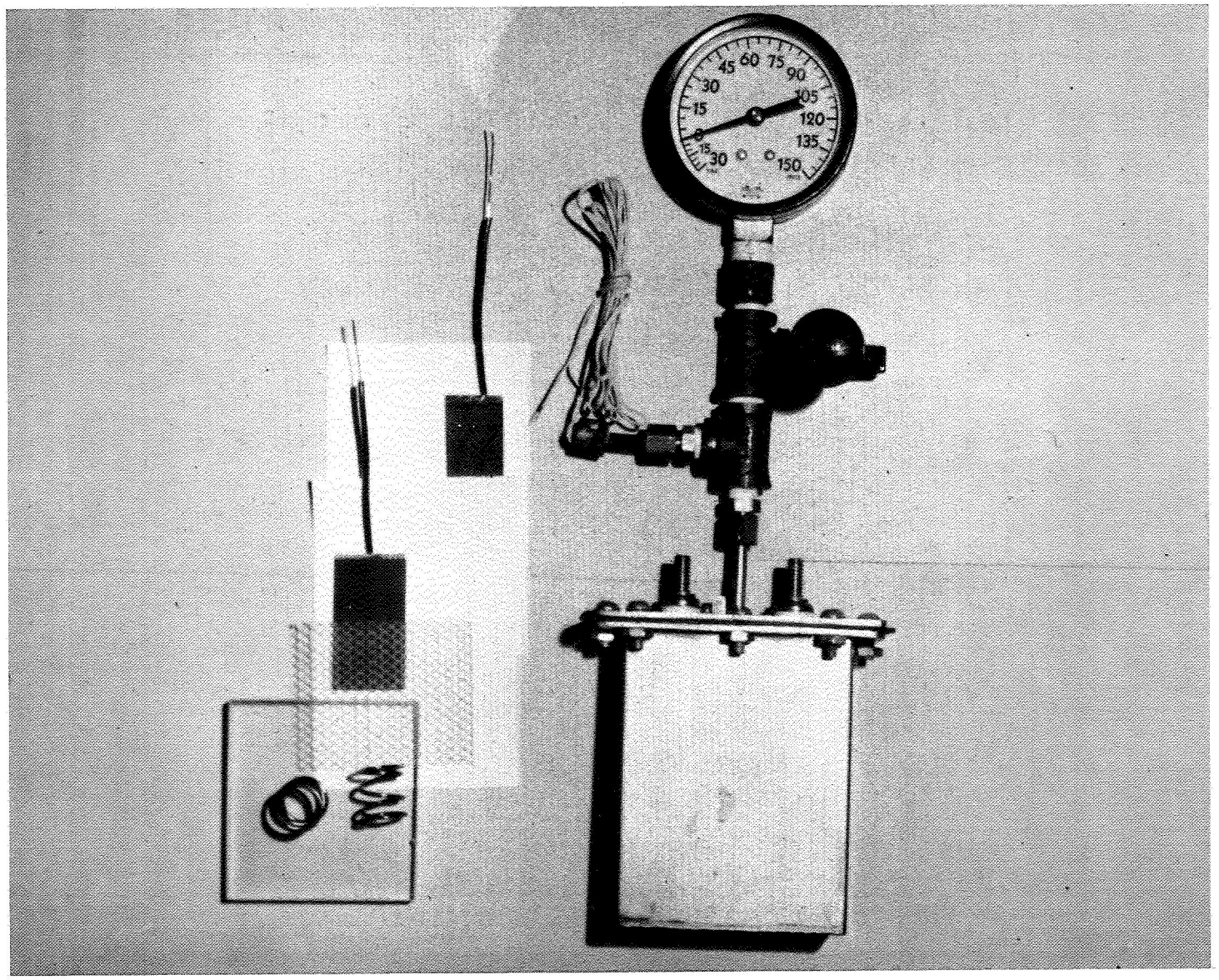

Figure 16

Recombination Electrode Test Cell
Components

The stainless steel can is fitted with a removeable cover which has provision for evacuating and/or pressurizing the cell, a pressure gauge, a thermocouple for measuring the temperature of the test electrode, and terminals for electrical connection to the various electrodes.

The cell assembly is shown in Figure 17. The counter electrode is a piece of sintered nickel plaque, and is welded directly to the can in order to improve heat transfer and minimize non-uniform temperature effects. The reference electrode is a piece of well-aged, partially charged positive plate. The separator is non-woven nylon, and dips into a pool of electrolyte, 34% KOH, in the bottom of the cell, thus insuring a uniform degree of saturation in all tests. The perforated, corrugated PVC provides access of O_2 to the gas face of the test electrode. Uniform compression of the components is provided by the two nickel-plated springs between the lucite face plate and the can wall. For operation, the test cells, after final assembly and pressure test, were evacuated to 30 inches of Hg vacuum and back filled with O_2 to the desired pressure. They were then equilibrated for 16 hours at the test temperature. Following this temperature stabilization, current was passed

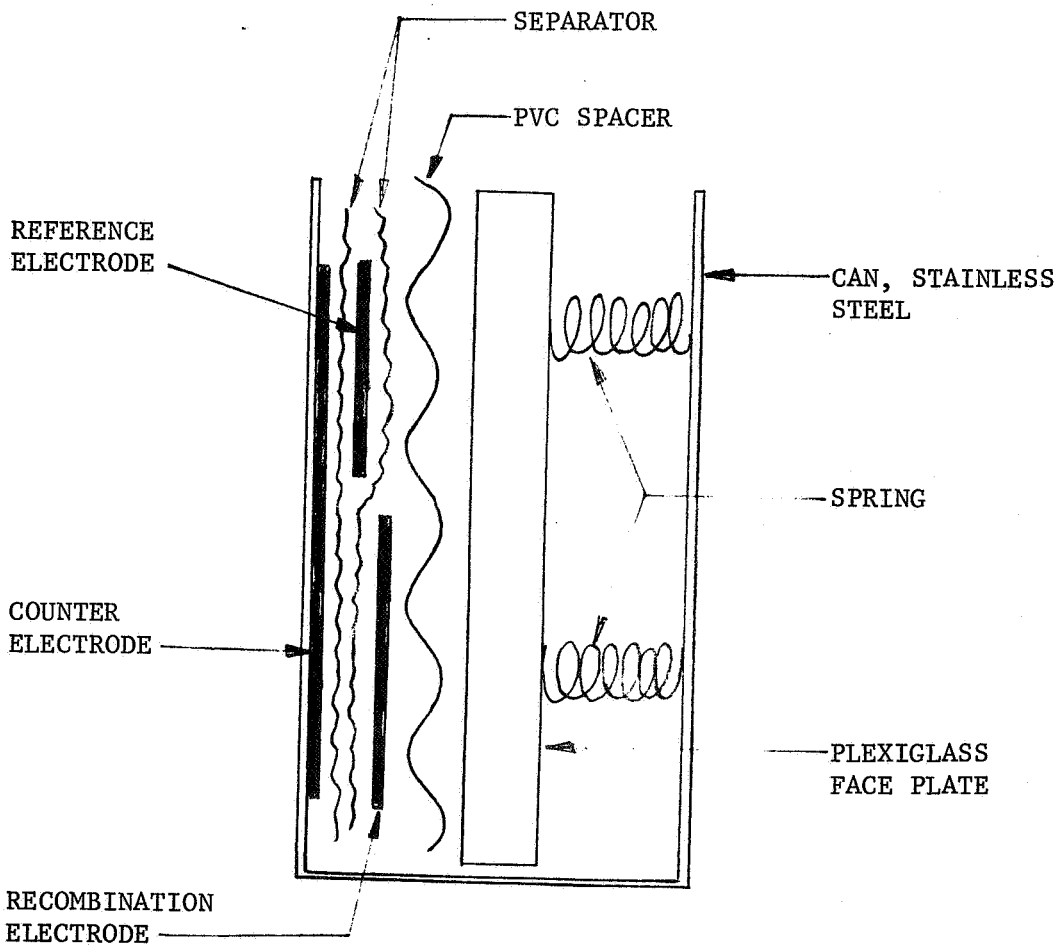

Figure 17

Recombination Electrode Test Cell Assembly

between the counter and test electrodes, causing O_2 to be generated on the former and recombined on the latter. The voltage between the test and reference electrodes was then measured at each current level.

2.2.3 Results of Polarization Tests

The performance of Group 1 electrodes is presented in Figure 18. As can be seen, the electrodes were capable of recombining oxygen at substantial rates, at moderate temperatures and pressures, with only slight polarization. Also it was observed that there was only a slight decrease in performance when the oxygen pressure was reduced from 20 to 10 PSIA. At -20°C, however, the electrodes polarized severely. In addition, the effect of varying oxygen pressure is more pronounced at -20°C. This pronounced pressure dependence led to the conclusion that accessibility of oxygen to the active sites within the electrode was limiting the low temperature performance.

A number of alterations in electrode structure were made, as outlined in Section 2.2.1, to improve the low temperature performance. The use of thinner, higher porosity plaque resulted in improved performance at -20°C, as did increased

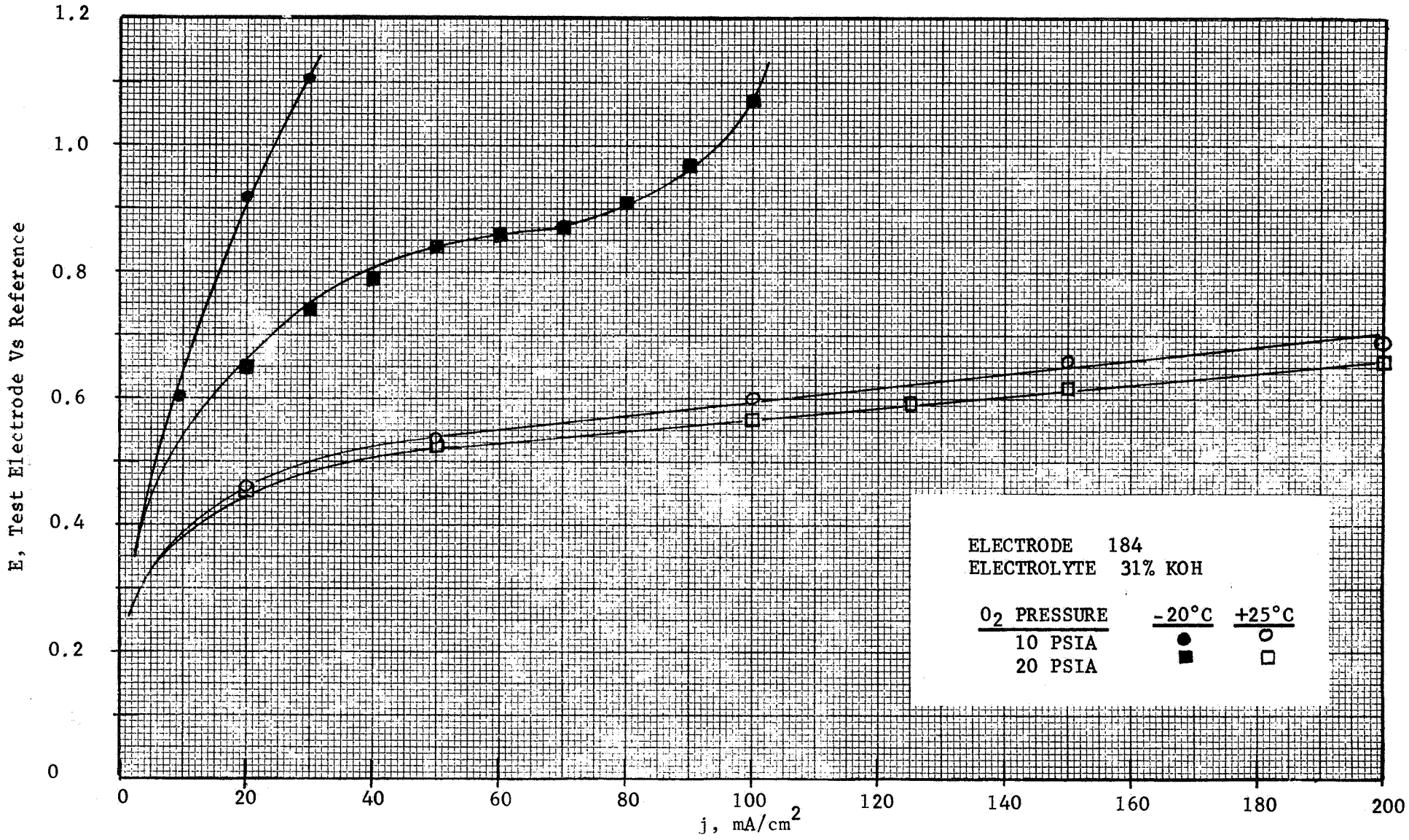

Figure 18 Performance of Recombination Electrode No. 184 at Various Temperatures and Pressures

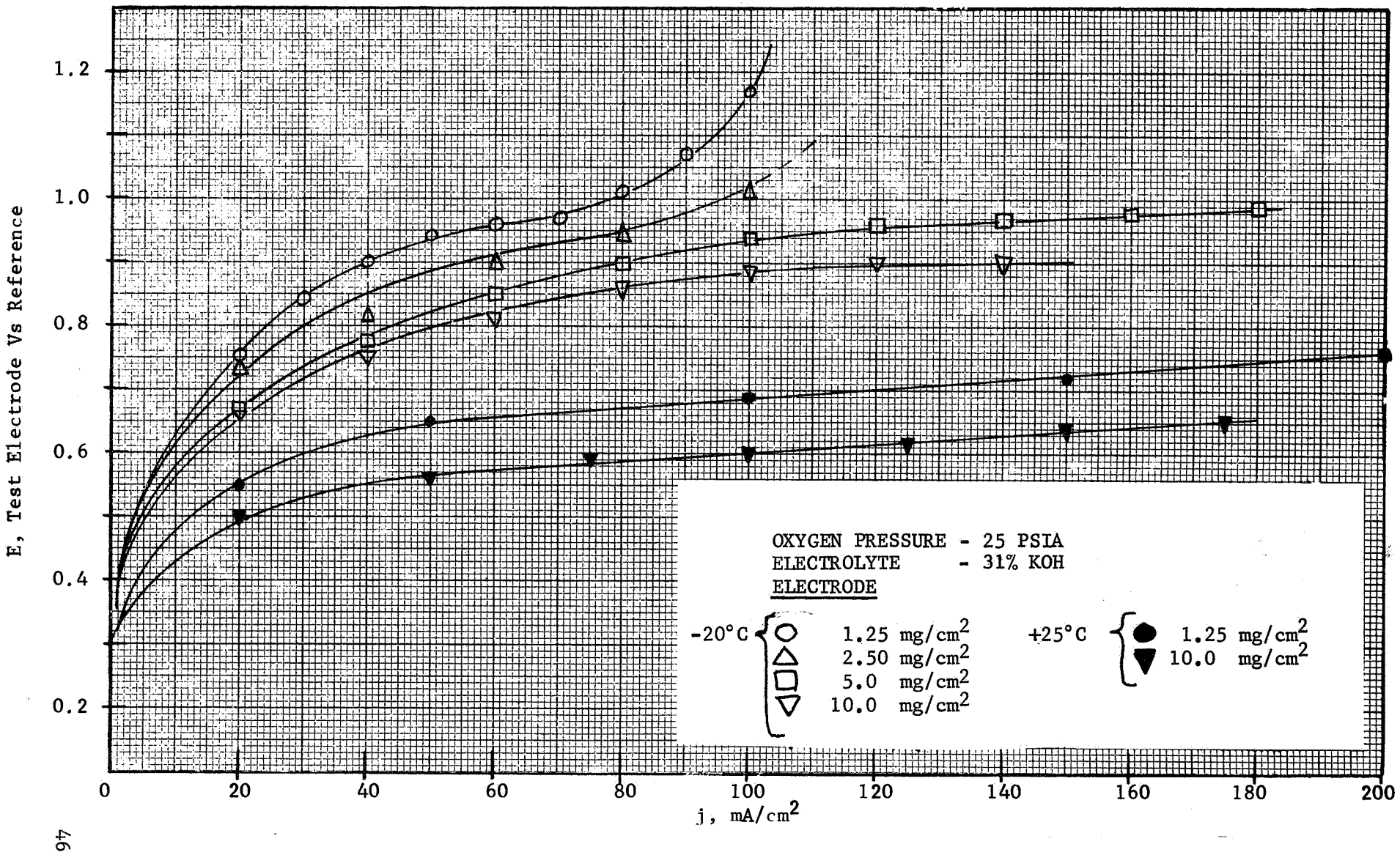

Figure 19 Effect of Catalyst Loading on Electrode Performance

catalyst loadings. The effect of catalyst loading is shown in Figure 19.

These improved electrodes are fabricated on a thin (0.011 inch thick), high porosity (85%) sintered nickel structure, and have a catalyst loading of 5.0 mg/cm^2 and a Teflon surface film of 1.20 mg/cm^2. Performance of these electrodes is typified by electrode number 500-2.

The performance of these electrodes was compared to that obtained with a variety of oxygen fuel cell electrodes. Comparisons were made at 25°C and -20°C. The fuel cell electrodes evaluated included the General Electric Research and Development Center Type 511 and American Cyanamid Company Types E and LBB-3CG. Polarization curves for these electrodes are presented in Figures 20 and 21. As can be seen, the 25°C performance of all the electrodes evaluated are comparable. At the low temperature, however, the improved electrodes developed in this program offer the lowest polarization, and so were selected for further study.

2.2.4 Electrode Reproducibility and Stability

Two series of tests were performed in order to determine whether the improved electrode described above could be

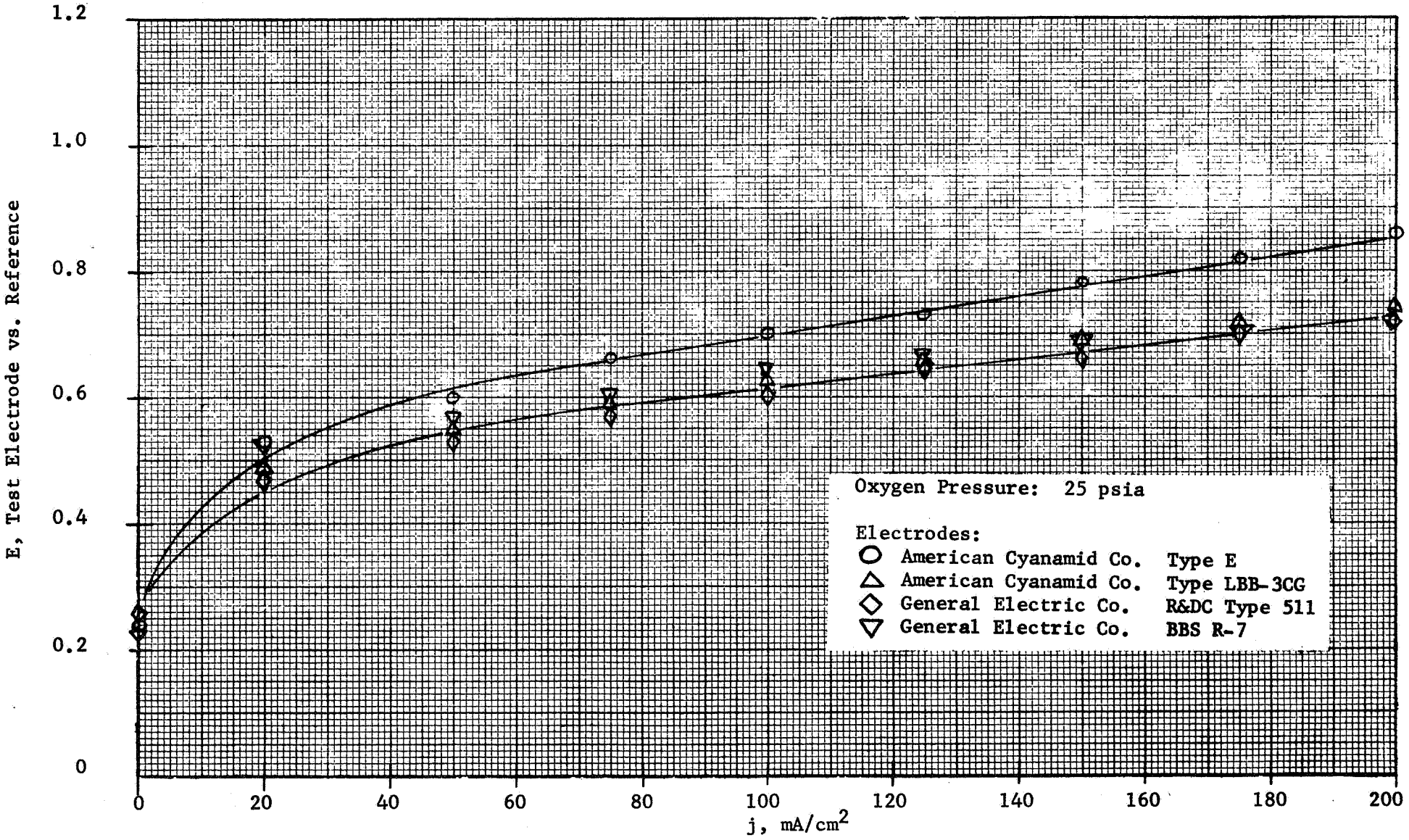

Figure 20 Performance of Various Fuel Cell Electrodes at 25°C

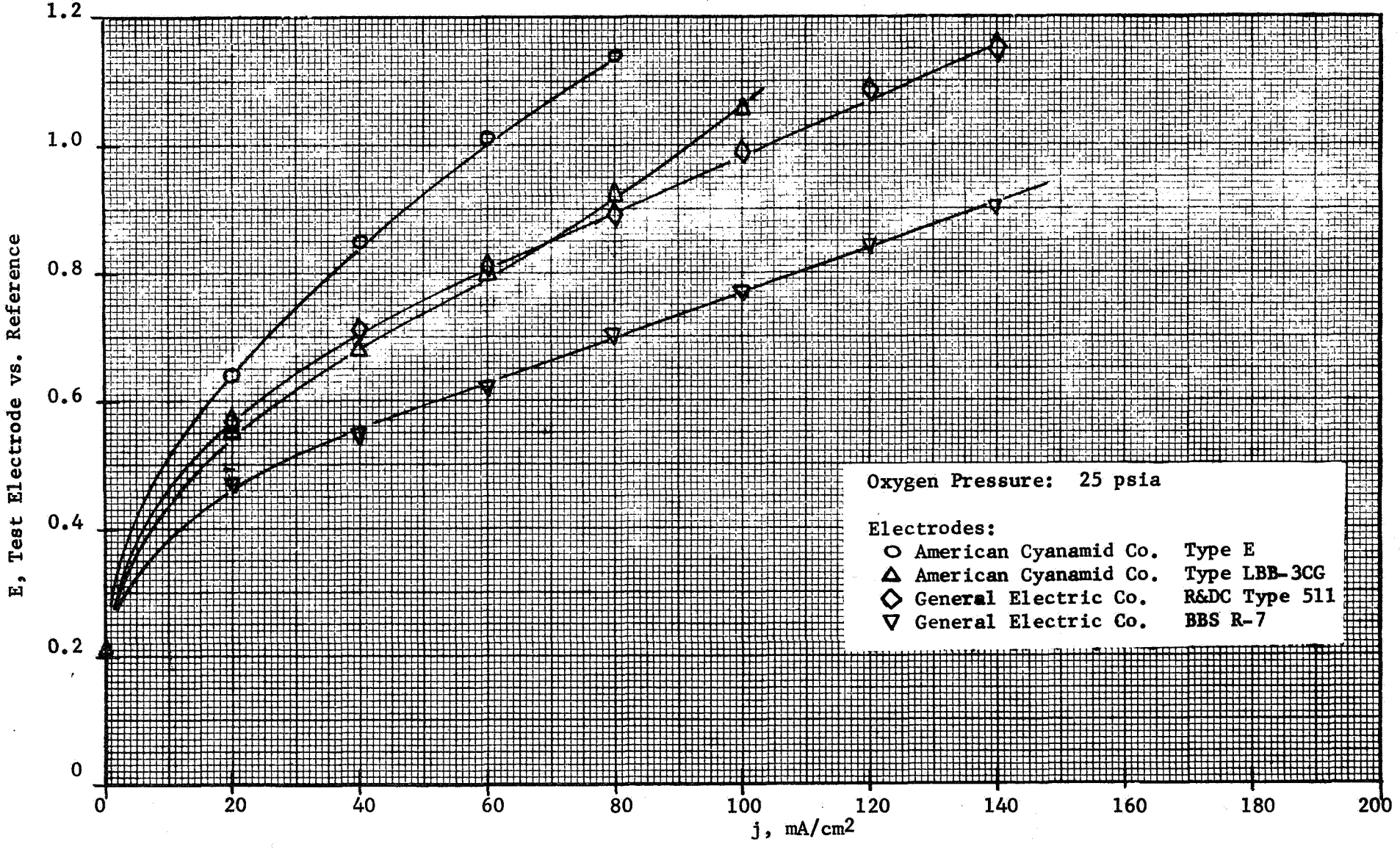

Figure 21 Performance of Various Fuel Cell Electrodes at -20°C

reproducibly made. The first test series was performed using three electrodes from the same lot. Polarization curves indicating the range in performance observed at both 25°C and -20°C are presented in Figure 22.

The second series compared the performance of electrodes from lots prepared two months apart. The ranges in performance observed at both 25°C and -20°C were similar to those shown in Figure 22. These results indicated that electrodes of consistent quality could be prepared by the techniques employed.

An investigation of the stability of recombination electrodes was also carried out. This program consisted of determining the initial performance of the electrode at both 25°C and -20°C with 25 PSIA oxygen pressure. The electrodes were then subjected to storage at 40°C under 25 PSIA oxygen and the -20°C polarization checked at regular intervals. The high temperature storage should have accelerated any degradation processes, and the extent to which these processes affected performance should have readily been seen at -20°C.

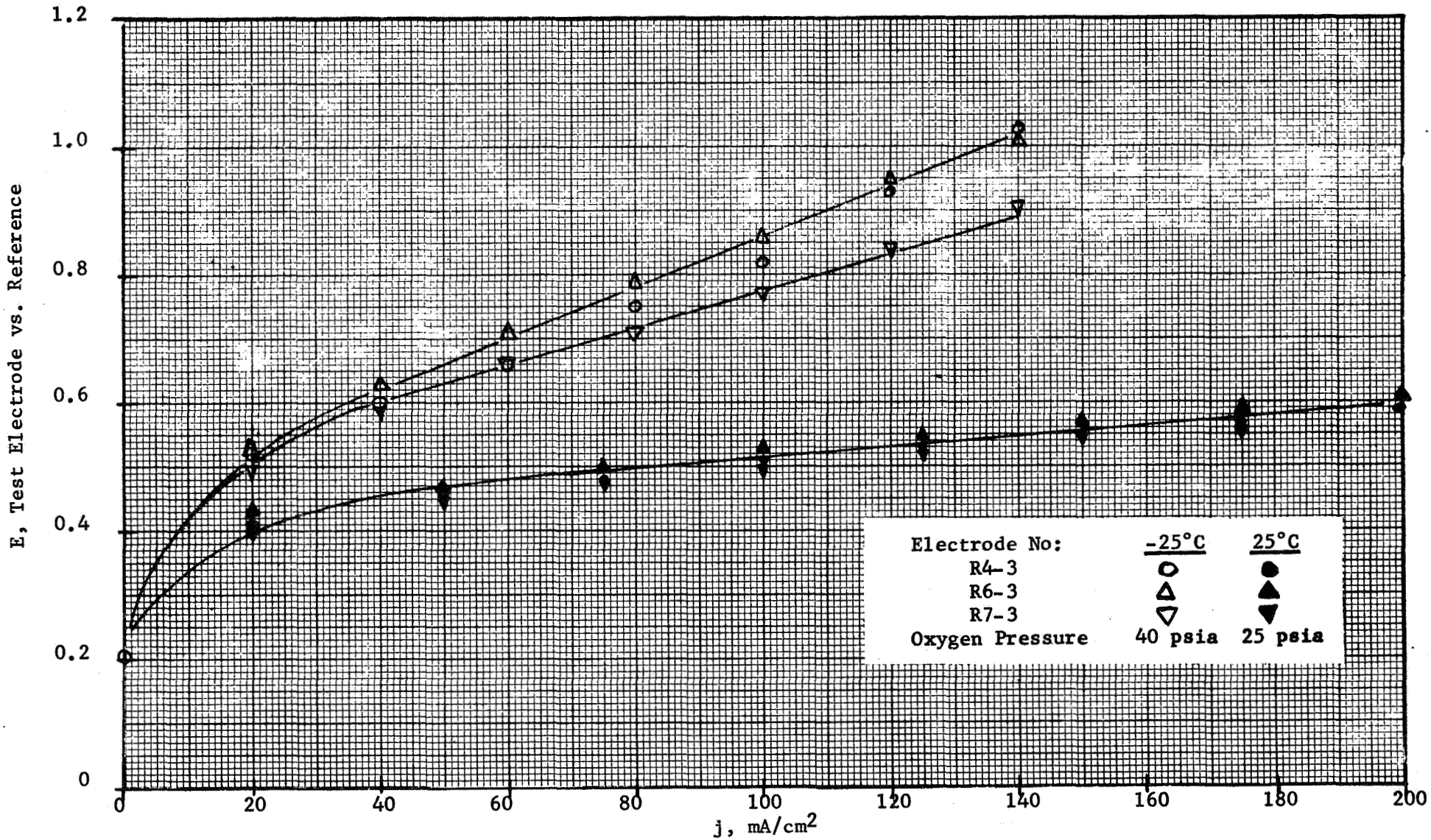

Figure 22 Reproducibility of Improved Recombination Electrodes

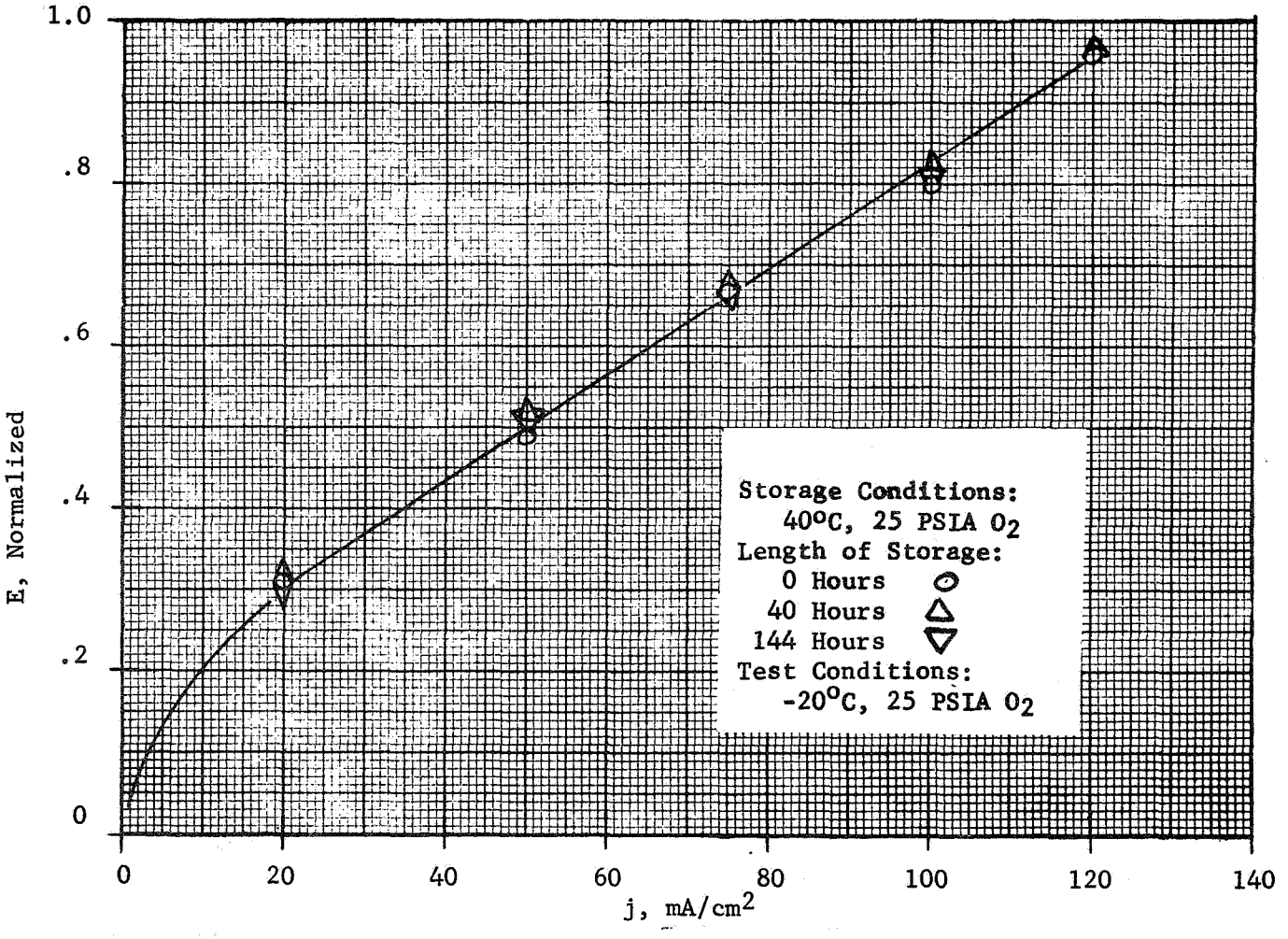

Figure 23 Normalized Polarization Curves for Electrode Before and after 40°C Storage

The results of one such test, involving a total of 144 hours of high temperature storage are presented in Figure 23. The polarization data presented in this figure were "Normalized" by subtracting the open circuit test electrode - reference electrode voltage from the voltage measured at each current. This mormalization procedure eliminates any errors due to shifts in the potential of the reference electrode as a result of the high temperature storage. The fact that the polarization curves are essentially superimposed indicates that the high temperature storage did not effect the electrodes.

2.3 Task III - Negative Plate Evaluation

2.3.1 Experimental Details

Three lots of negative plates were received from manufacturing for evaluation of ampere-hour stability and oxygen recombination ability. Twelve cells, of nominal 4AH configuration, were assembled from each lot, using a common lot of positive plate for all cells. Sufficient 34% KOH electrolyte was added to produce semi-starved cells. The cells were fitted with pressure gauges and sealed with epoxy.

In order to determine the ampere-hour stability of the plate,

a regime designed to promote negative plate fading was employed. The regime was as follows:

Temperature: Room ambient

Charge: 400 mA for 16 hours

Discharge: 4.0A to 1.0 Volt

Rest: 7 hours

5 cycles per week

Cycling was continued until the discharge capacities of the cells stabilized. This required 16-18 cycles.

The oxygen recombination ability of the negative plate was determined by observing the steady state pressures in the cells at various rates of continuous overcharge. The overcharge rates employed were 400 mA (C/10), 500 mA (C/8), and 800 mA (C/5). The C/5 overcharge rate is the upper threshold for continuous overcharge of standard sealed cells without recombination electrodes and was employed in this test in order to increase the amount of data available for use in selecting a suitable plate lot.

2.3.2 Results and Discussion

The capacity versus cycle data for the three lots evaluated are presented in Figure 24. As can be seen, two lots, 6939 and 6979, behaved essentially the same. The third lot,

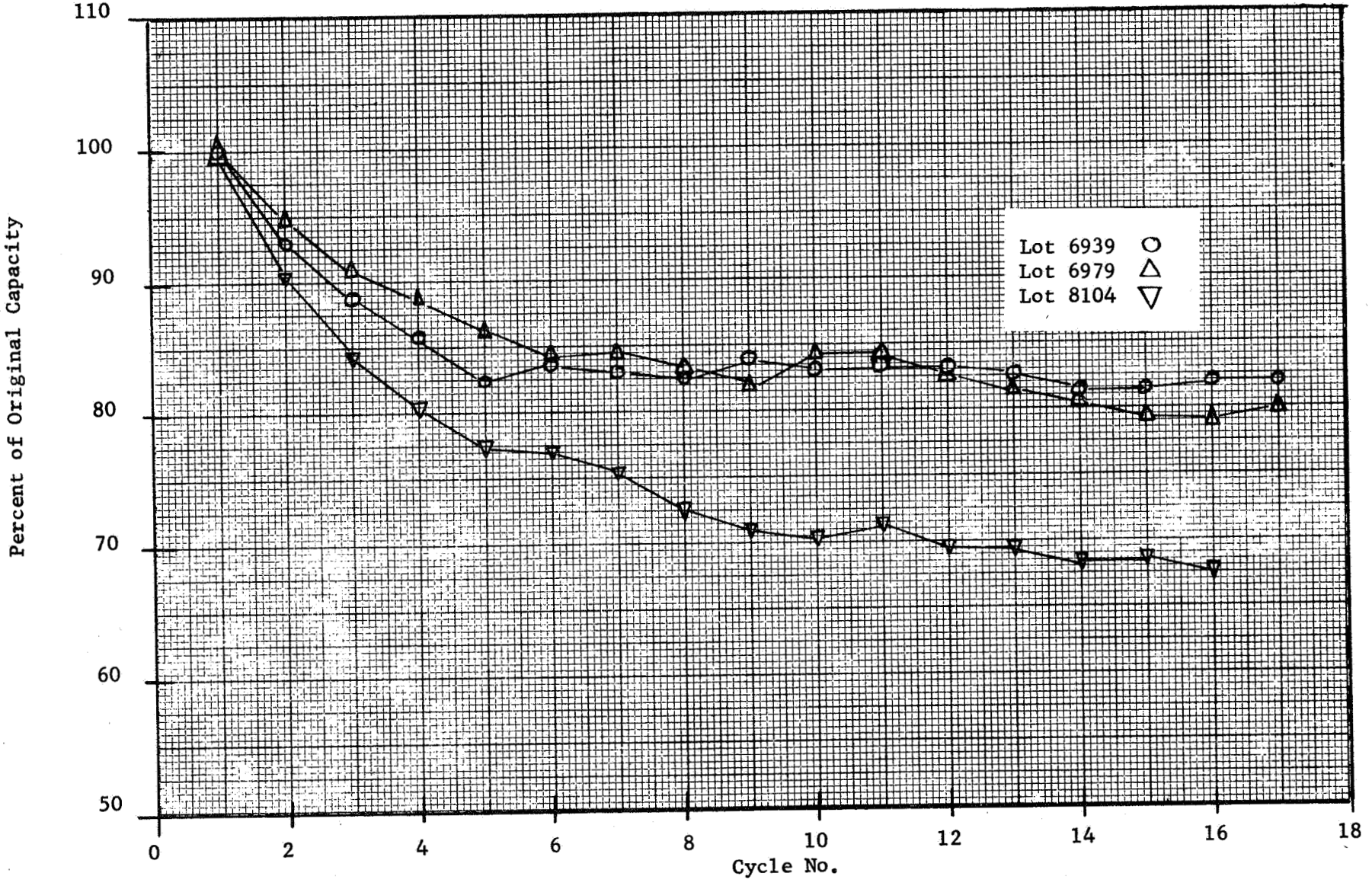

Figure 24 Ampere - Hour Stability of Negative Plates

8104, faded to a greater extent.

In addition to the cycling regime, the extent to which negative plates fade is related to the state-of-charge of the plate at the time of cell assembly. As no special precautions were taken in this test to insure uniform states-of-charge on all the negatives tested, the differences observed may be due to differences in the original state-of-charge of the plates.

The pressures developed in the cells during the continuous overcharge tests were in the range normally observed when charging at the rates employed. The pressures developed in the cells made with lot 6979 plate were, however, somewhat lower than the others.

Negative plate from lot 6979 exhibited the best balance of properties -- low fading and low continuous overcharge pressures -- and so was retained and used in prototype and final cells.

2.4 Task IV - Prototype Cell Design

2.4.1 Cell Design

Prototype cells were designed with a plate pack consisting

of 11 negative plates, 10 positive plates, and non-woven nylon separator. The recombination electrode consisted of two pieces, each 1.5 x 5.0 cm. located along the narrow edges of the pack, with electrical connection made to the can. The signal electrode of 9.8 cm^2 area was located on one broad face of the pack, the electrical connection being made through a special terminal located on the cover. This electrode configuration allowed for the variation of the resistances between the negative plates and both of the auxiliary electrodes.

In order to test the mechanical feasibility of the proposed design, one pre-prototype cell was constructed. The plate pack for this cell was made up with 10 negative and 9 positive plates. Dummies were added to bring the pack to proper thickness. A recombination electrode of 15 cm^2 area and identical to those used in the final prototypes was included, and a signal electrode, of 9.8 cm^2 area, was installed.

After assembly, the cell was subjected to a number of manual and automatic charge-discharge cycles in order to confirm its electrical performance. Results of these

tests, presented in the following section, were satisfactory, and the remainder of the prototype cells were assembled according to this proposed design.

2.4.2 Preliminary Tests

The cell described above was subjected to a number of tests in order to characterize its performance under a variety of operating conditions. The cell was cycled at ambient temperatures of -20°C, 25°C and 40°C, and at 25%, 50%, and 75% depth-of-discharge on a 60-30 orbit. Since the cell was constructed with only 90% of the required plates, the discharge rates were reduced to 90% of the nominal values for a 6 A-Hr. cell as shown in the table below:

Depth of Discharge	Rate, Amperes	90% Rate
25%	3.0	2.7
50%	6.0	5.4
75%	9.0	8.1

The cell was overcharged on each cycle beyond the optimum recharge in order to determine the ability of the oxygen recombination electrode to maintain low pressures under these adverse conditions. Charge coefficients (charge input divided by capacity delivered) in the range 1.30 to 1.92 were employed. Following the charge, the cell was dis-

charged to 1.0V in order to determine capacity. Residual capacity was drained by shorting the cell through a one ohm resistor for 16 hours so that the capacity determined on any cycle was independent of the previous cycle.

A summary of the cycles is presented in Table VI. In Figures 25, 26, and 27 are shown the cell performance parameters for 5.4 A (50% DOD) cycles at 40°C, 25°C, and -20°C, respectively. Also indicated are optimum cut-off points for each temperature, representing overcharges of 40%, 20% and 5% for the three test temperatures.

While the end-of-charge pressures may appear high, it must be remembered that the cells were overcharged far in excess of what is required. At -20°C, for instance, an overcharge of 5-10% should be adequate to fully recharge the cell; overcharges of 47-50% were used in these tests. Had the charge been terminated by a control electrode signal at the proper point, the high pressures would not have been obtained. This can readily be seen by reference to Figure 27.

In all cycles at 25°C and 40°C the pressure and signal both dropped to near zero within the first 30 minutes of discharge. At -20°C the decline was, of course, slower due

to the decreased activity of the recombination electrode and decreased O_2 recombination on the negative plates. In addition, the pressures developed during the -20°C cycles were much higher than normal due to the great excess of charge beyond that needed to fully recharge the cell. Had the charge been terminated after only 5% of overcharge (instead of the 50% employed) such high pressures would not have developed, and the recombination rates would have been sufficient to bring the cell to a low pressure during subsequent discharge.

In Figure 28 are shown the performance parameters for the cell during manual cycling on a 60-30 minute orbit to 25% DOD. The charge was terminated when the control electrode signal reached 100 mV, and the cell rested at open circuit for the remainder of the charge period. The reproducibility of the cell performance over a number of such cycles demonstrated the electrical feasibility of the proposed design.

2.5 Task V - Prototype Cell Tests

2.5.1 Test Cells and Equipment

Twenty seven prototype cells of 6 A-Hr nominal capacity were constructed for cycle testing. Cells were constructed according to the design outlined in Section 2.4.1. Cells

TABLE VI

SUMMARY OF PRE-PROTOTYPE CELL CYCLES

CYCLE	AMB. TEMP °C	RATE (1)	CHARGE				DISCHARGE	CHG. COEF.	REMARKS
			A-HRS	ECV	PRESS PSIA	SIG. (2)	CAP. to 1.0V		
1	25	2.7	13.5	1.43	12.5	271	7.0	1.92	25° NOT MAINTAINED
2	25	2.7	10.8	1.45	29	305	6.8	1.59	
3	25	5.4	9.5	1.50	41	320	6.7	1.42	see Figure 26
4	25	5.4	10.0	1.50	43	320	6.8	1.47	
5	25	8.1	9.3	1.55	52	290	6.8	1.37	
6	25	8.1	8.9	1.54	54	330	6.5	1.37	
7	25	2.7	9.2	1.51	47	308	7.1	1.30	3-A
8	25	2.7	10.8	1.48	43	325	6.9	1.56	3-B
9	25	2.7	10.4	1.51	61	400	7.0	1.48	3-C
10	-20	2.7	8.1	1.67	59	45	5.4	1.50	
11	-20	5.4	7.2	1.75	91	69	4.9	1.47	see Figure 27
12	-20	8.1	6.8	1.78	96	65	4.6	1.48	
13	25	5.4	9.9	1.54	40	235	7.2	1.38	
14	40	2.7	9.4	1.41	24	260	6.8	1.38	
15	40	5.4	9.9	1.46	40	305	6.6	1.50	see Figure 25
16	40	8.1	10.1	1.51	52	320	6.9	1.46	
17	25	5.4	9.9	1.54	52	245	7.0	1.41	

NOTES:

1. SAME RATE FOR BOTH CHARGE AND DISCHARGE
2. CONTROL ELECTRODE SIGNAL, mV ACROSS 10Ω RESISTOR BETWEEN CONTROL ELECTRODE AND NEGATIVE PLATE.
3. RECOMBINATION ELECTRODE TIED TO NEGATIVE BY 0.010Ω, EXCEPT AS NOTED:
   - A- NOT CONNECTED
   - B- 0.375 OHM
   - C- DIODE

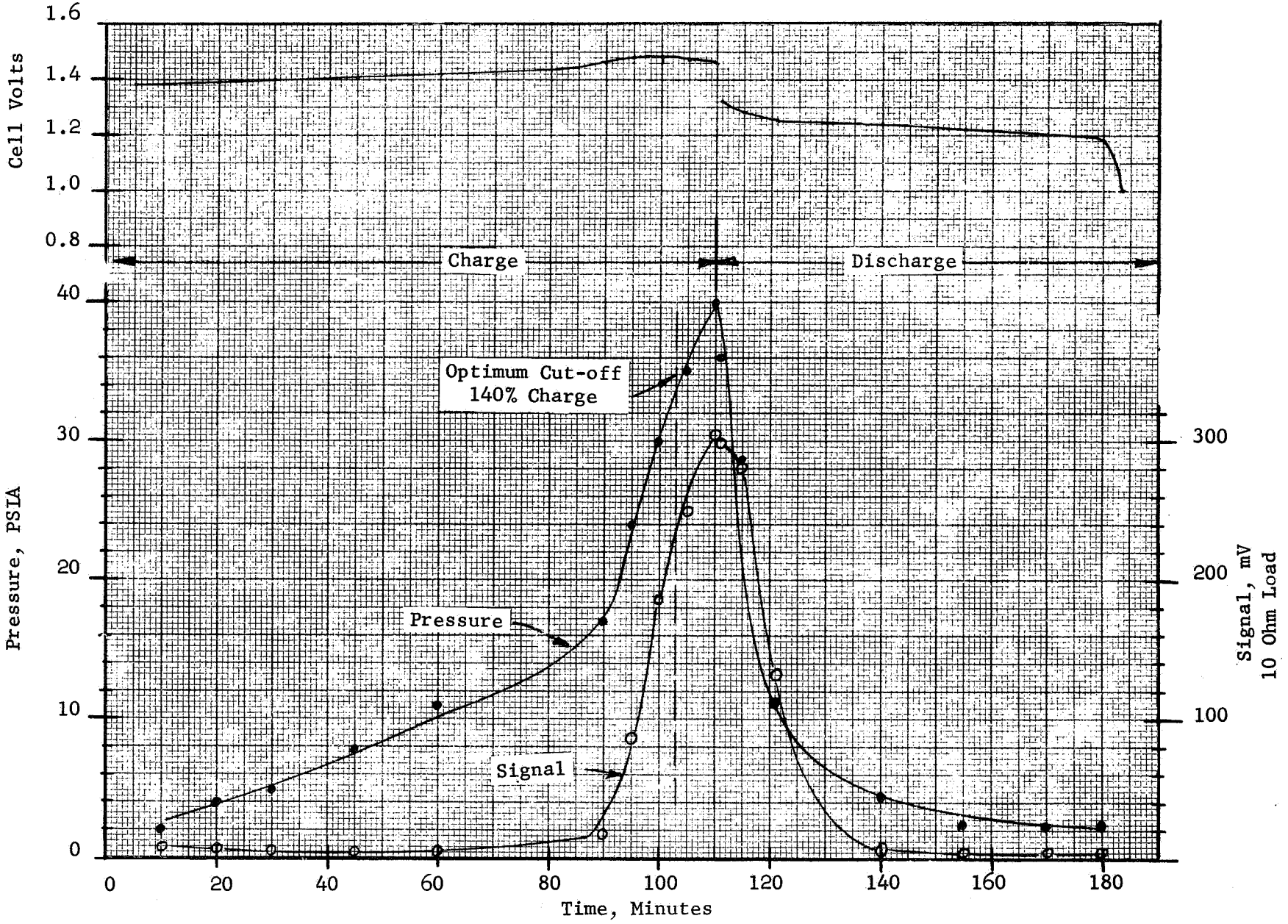

Figure 25 5.4A Cycle, 40°C

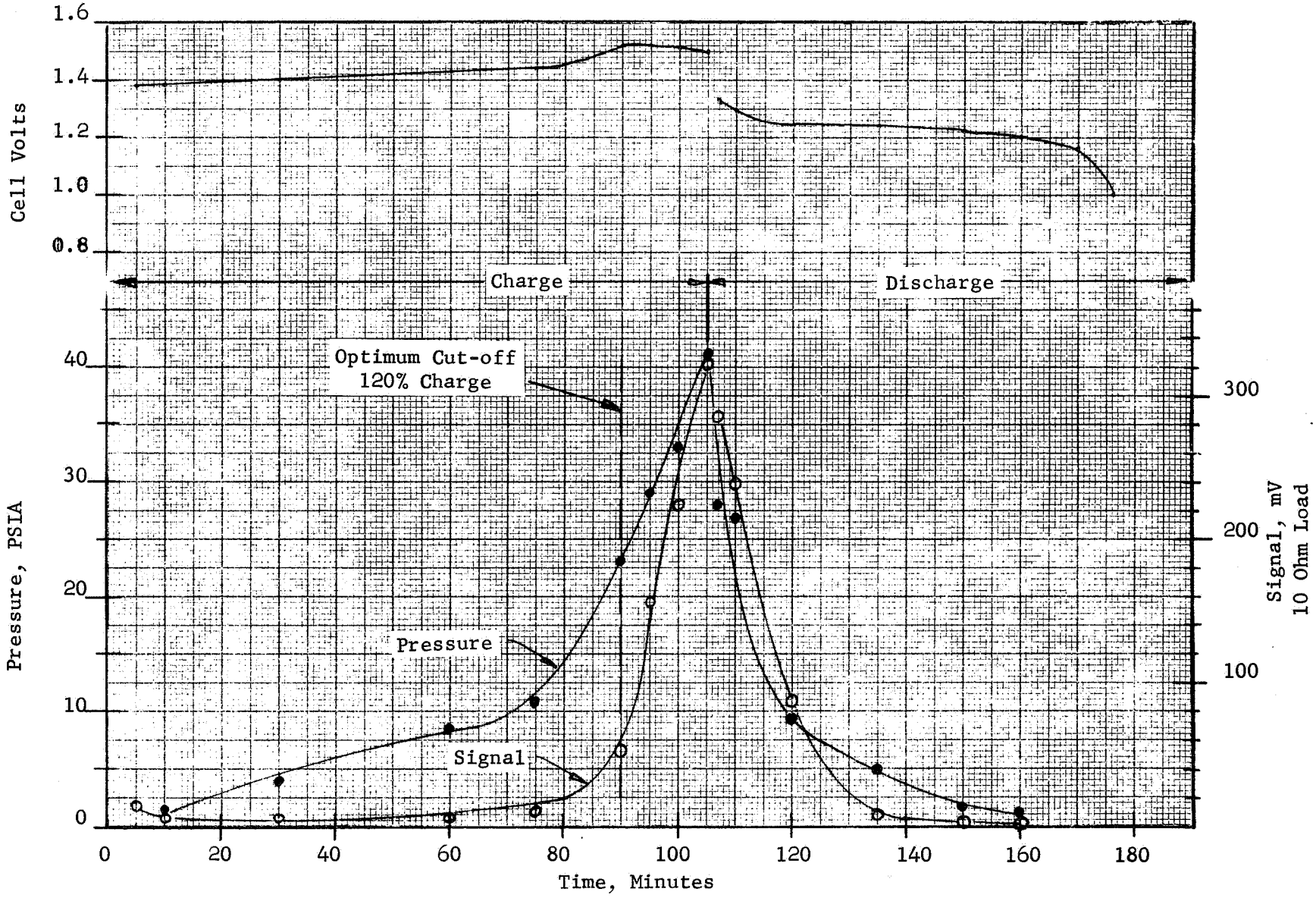

Figure 26 5.4A Cycle, 25°C

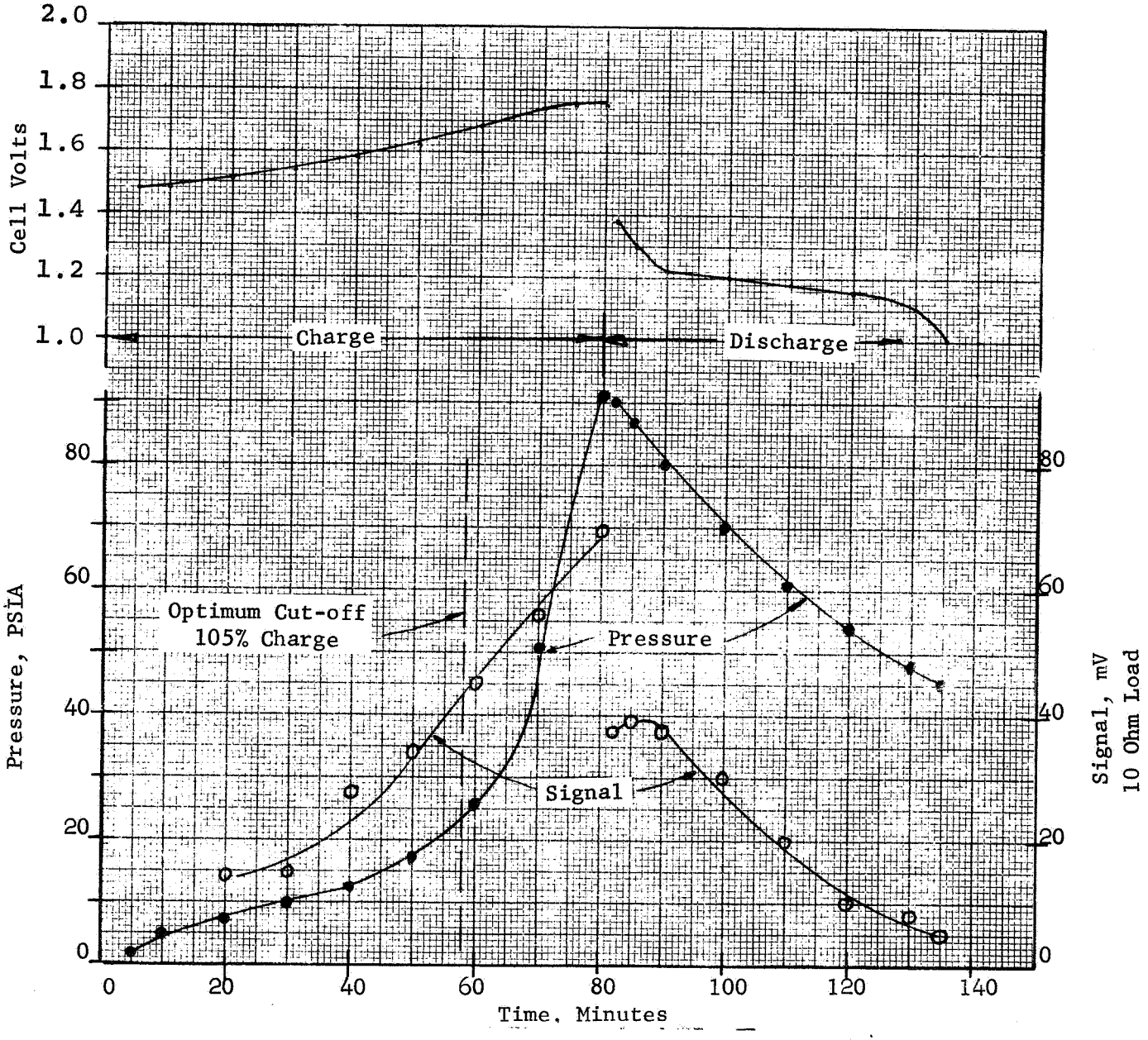

Figure 27 5.4A Cycle, -20°C

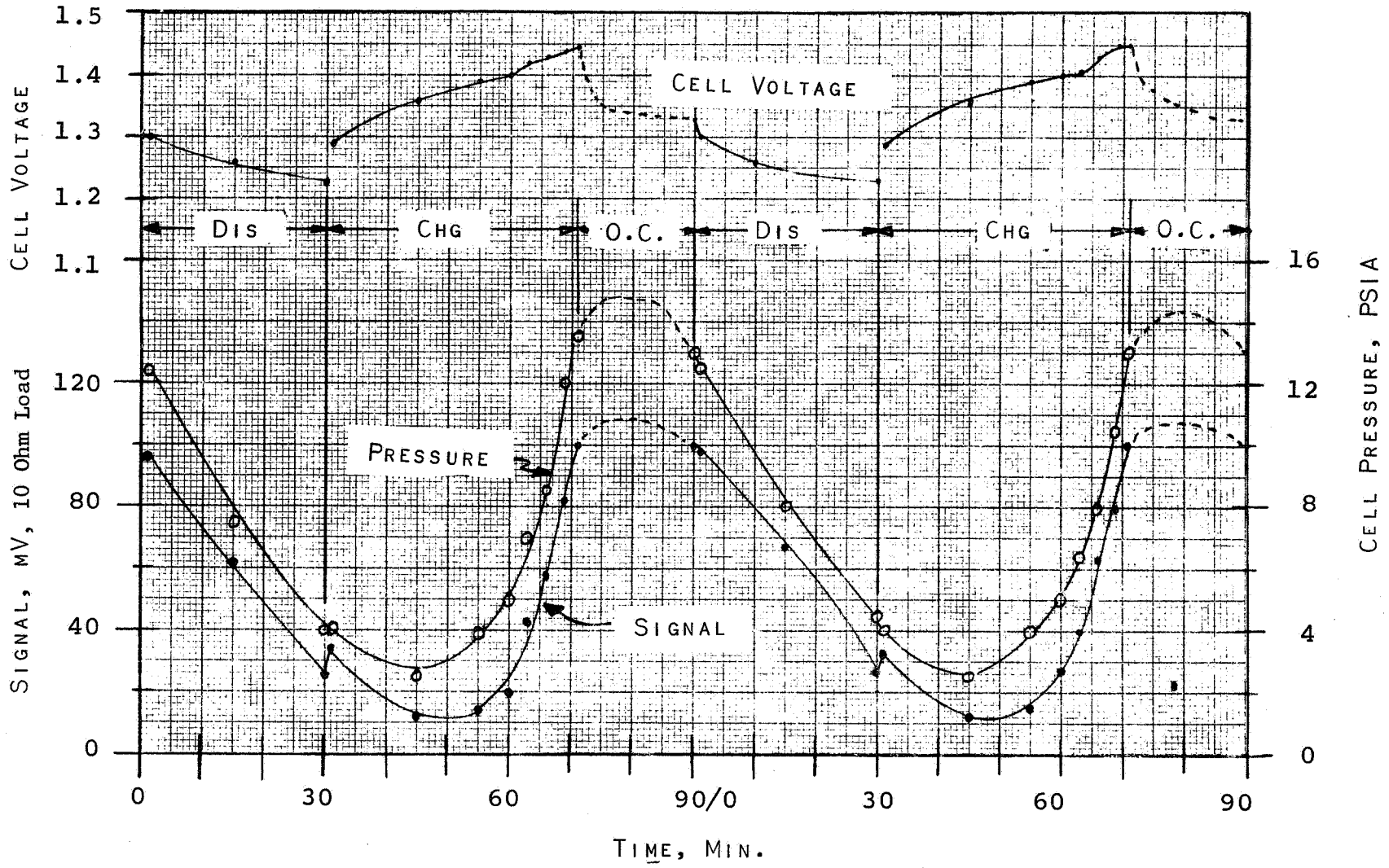

Figure 28

PERFORMANCE OF 4-ELECTRODE CELL AT 25% DOD, 25°C

were fitted with pressure gauges and thermocouples.

Capacity of the test cells was determined by charging at C/10 (600 mA) for 24 hours and discharging at C/2 (3.0A) to 1.0 volt. Capacities were in the range of 6.5 to 7.3 A-Hr. Following the capacity determination, the cells were put on cycle tests, according to the following schedule:

Test I:

All cells at room temperature

All cells at 25% DOD.

Test II:

Three cells at each regime:

	Temperature		
DOD	-20°C	25°C	40°C
25%	X	X	X
50%	X	X	X
75%		X	

A block diagram of the automatic cycling equipment is shown in Figure 29. Three such units are required, one for each rate. A photograph of the control panel and cell monitoring equipment is presented in Figure 30.

The charge control circuit can be used to terminate the charge with a signal of from 30mV. Tests of the

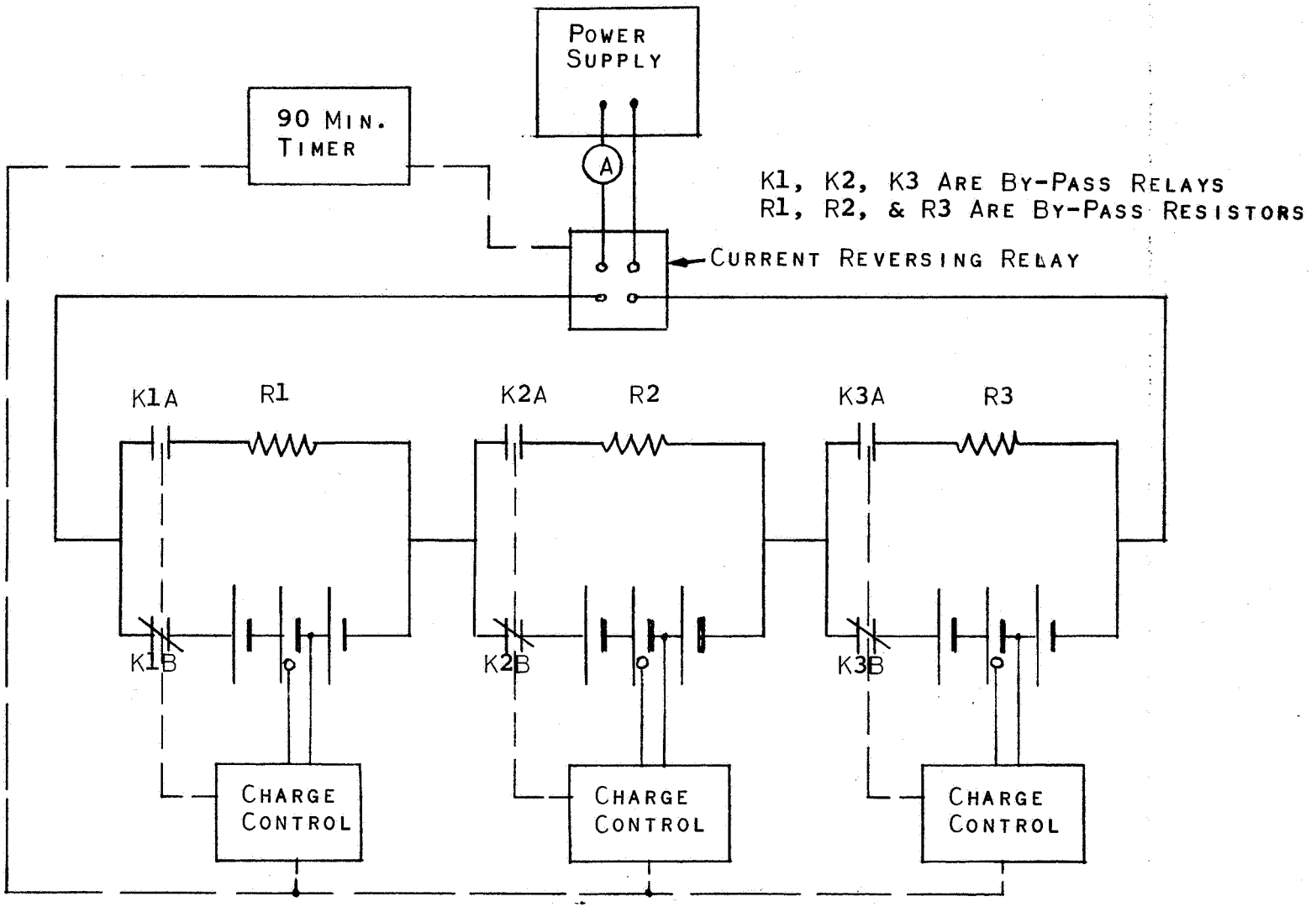

Figure 29

BLOCK DIAGRAM OF AUTOMATIC CYCLE EQUIPMENT

AT BATTERY BUSINESS SECTION

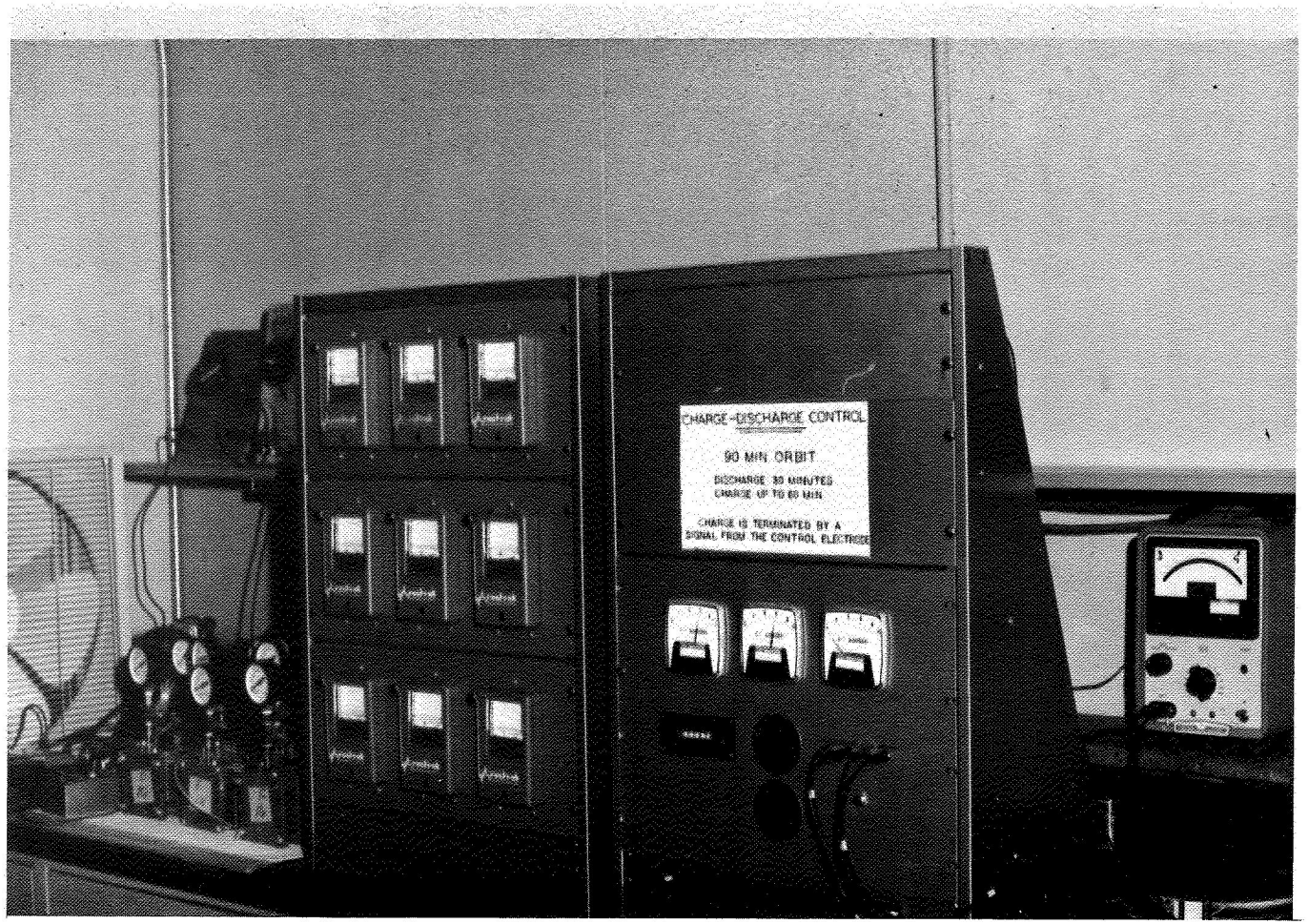

Figure 30

PHOTOGRAPH OF CONTROL PANEL

circuitry were carried out, prior to cycling the prototype cells, by cycling the pre-prototype cell, described previously, on a 60-30 orbit to 50% DOD, charging and discharging at 6A. Approximately 100 cycles were completed before this checking-out was terminated.

During these cycles the charge was reproducibly terminated by signals of 50 mV and 236 mV. The cycle-to-cycle reproducibility of the controller can be seen in Figure 31 which shows the signal response during four consecutive cycles. Also indicated on the figure are the duration of the charge, open circuit, and discharge portions of the cycle. The cell received about 25% overcharge during these cycles, and the pressure at the end of charge was about 25 PSIA.

2.5.2 Electrode Circuitry and Control Settings

The impedance between the recombination electrode and the negatives must be selected so as to limit the recombination current to a fraction of the charge current. Thus all the oxygen generated before the cell is fully charged will be recombined at a low pressure. When the positive electrodes go into overcharge the rate of oxygen evolution exceeds the rate of recombination, and the cell pressure rises.

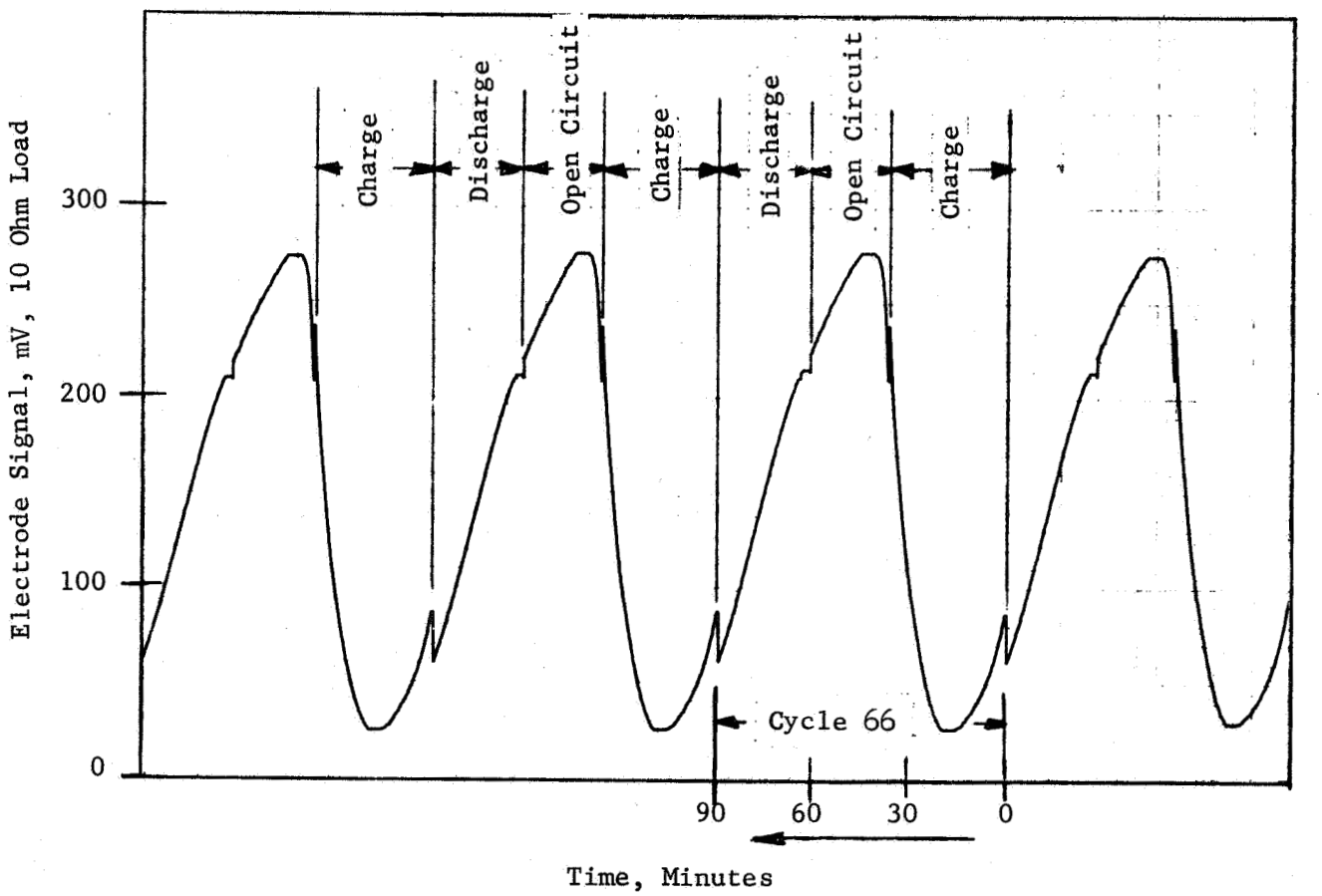

Figure 31

RESPONSE OF SIGNAL ELECTRODE
DURING REPETATIVE CYCLING
OF FOUR-ELECTRODE CELL

The control electrode senses this pressure rise and responds in proportion to it.

The recombination electrode load impedances originally selected were in the range 0.01 to 0.25 ohm. At these low values the recombination of oxygen was too effective, and the cell pressures did not rise high enough to obtain adequate signals from the control electrode. Impedances in the range 0.50 to 3.0 ohms were found to effectively limit the recombination current, depending upon charge rate and temperature, and result in adequate pressure rises for control purposes.

At very low rates, i.e., C/6, at moderate temperatures, the higher impedances must be used (see Section 2.1.4). At rates higher than C lower impedance values, 0.5 ohm, may be used and still have an adequate pressure rise. Load impedances of 1.0 ohm were found to give adequate, but not excessive, pressure rises in cells over the entire -20°C to +40°C temperature range for charge rates between C/2 and 1.5 C, and so were used for cycling the prototype cells, 2.5.3.

Selection of the proper control electrode signal to be used

for terminating the charge is, of course, necessary to insure proper cycling.

Results obtained during the signal electrode evaluation, Section 2.1.4, demonstrated that these electrodes could be used to reproducibly terminate the charge when the cell pressure reached a predetermined value. It was observed, however, that the percentage recharge accomplished by charging to an arbitrarily selected pressure was different from cell to cell. For example, when the charge was terminated at 20 PSIA oxygen pressure, the percentage recharge varied, on different cells, from 110 to 135%.

In order to charge a cell to a specified percent overcharge, using a control electrode signal, it is necessary to determine the signal corresponding to the desired overcharge, under the same conditions of cycling to which the cell will be subjected. The controller is then set to terminate the charge at this signal. This was the procedure followed in the prototype cell tests.

2.5.3 Results of Cycle Tests

Test I: All cells were conditioned by cycling at 25% DOD at room temperature. As in all cycle tests, the cells were charged and discharged at the same rate - 3.0A in this test -

and the charge was terminated by a signal from the control electrode. The test lasted one week (82 cycles) as this was sufficient time to determine that the cells and control equipment were performing in a satisfactory manner.

Typical cell performance parameters observed during this test are illustrated in Figure 32. Neither cell pressures nor control electrode voltages were monitored during this test, but the constancy of the percent recharge is evidence of stable and reproducible performance.

Test II: The performance of the prototype cells was investigated over the -20°C to +40°C temperature range by cycling according to the schedule presented in Section 2.5.1. A summary of the cycles completed is presented in Table VII.

Low Temperature (-20°C)Cycling: Two batteries, B and C, were subjected to uninterrupted cycling at -20° for about seven weeks, completing 775 and 777 cycles to 50% and 25% DOD respectively. Performance of the cells during typical cycles is shown in Figures 33 and 34.

Cell pressures and control electrode voltages were monitored periodically during the cycling, and the results

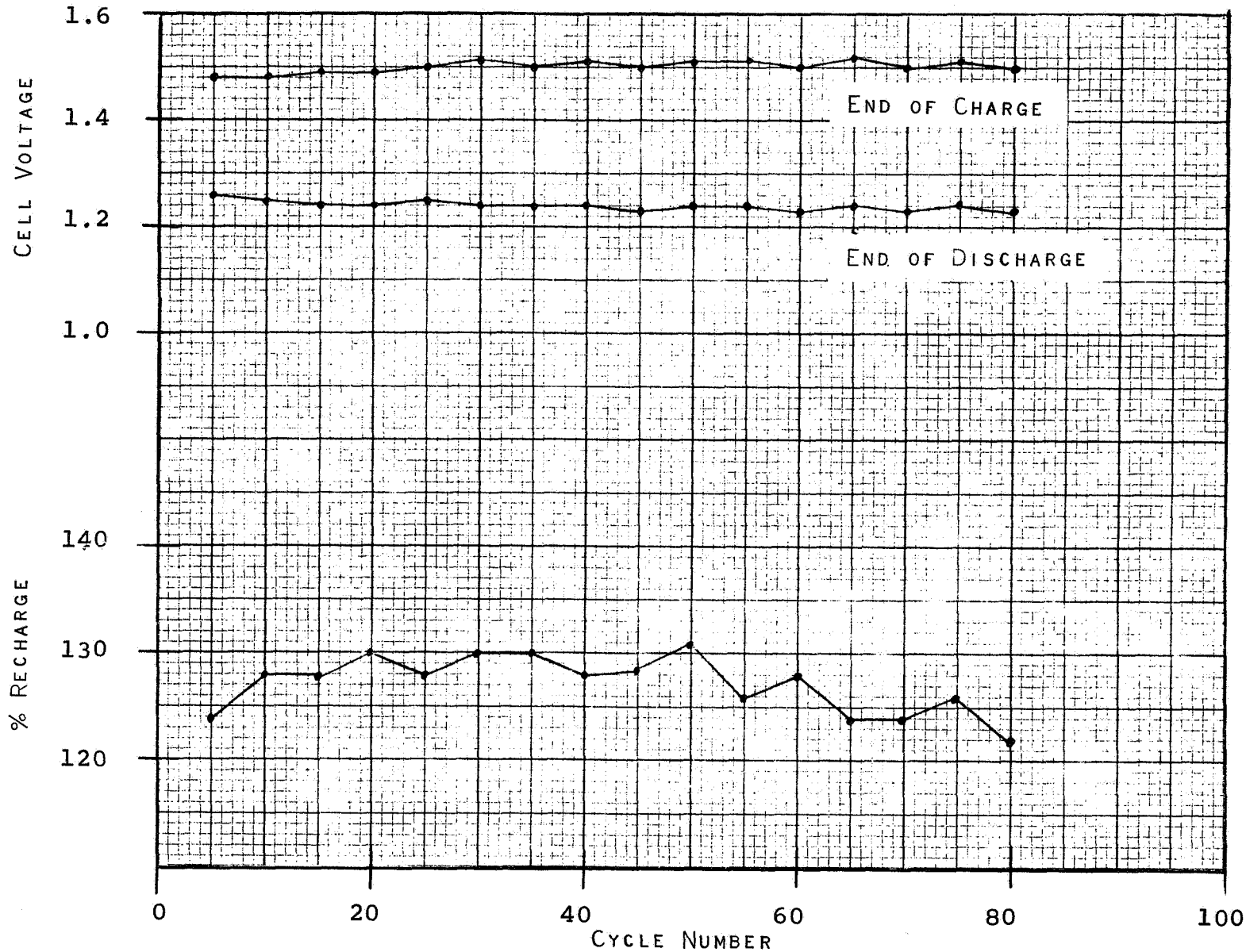

Figure 32

TYPICAL CELL PERFORMANCE DURING 25% DOD, 25°C CYCLING

TABLE VII

SUMMARY OF CYCLE TESTS ON

PROTOTYPE CELLS

BATTERY DESIGNATION	TEMPERATURE °C	% DOD	CYCLES COMPLETED
B	-20	50	775
C	-20	25	777
D	25	75	380[2]
E	25	50	280[3]
F	25	25	818
H	40	50	150[2]
J	40	25	175[3]

NOTES:

1. EACH BATTERY CONSISTS OF THREE CELLS
2. CELLS RECEIVED SPECIAL PROCESSING
3. CYCLE TESTS DISCONTINUED DUE TO FALLING END-OF-DISCHARGE VOLTAGES

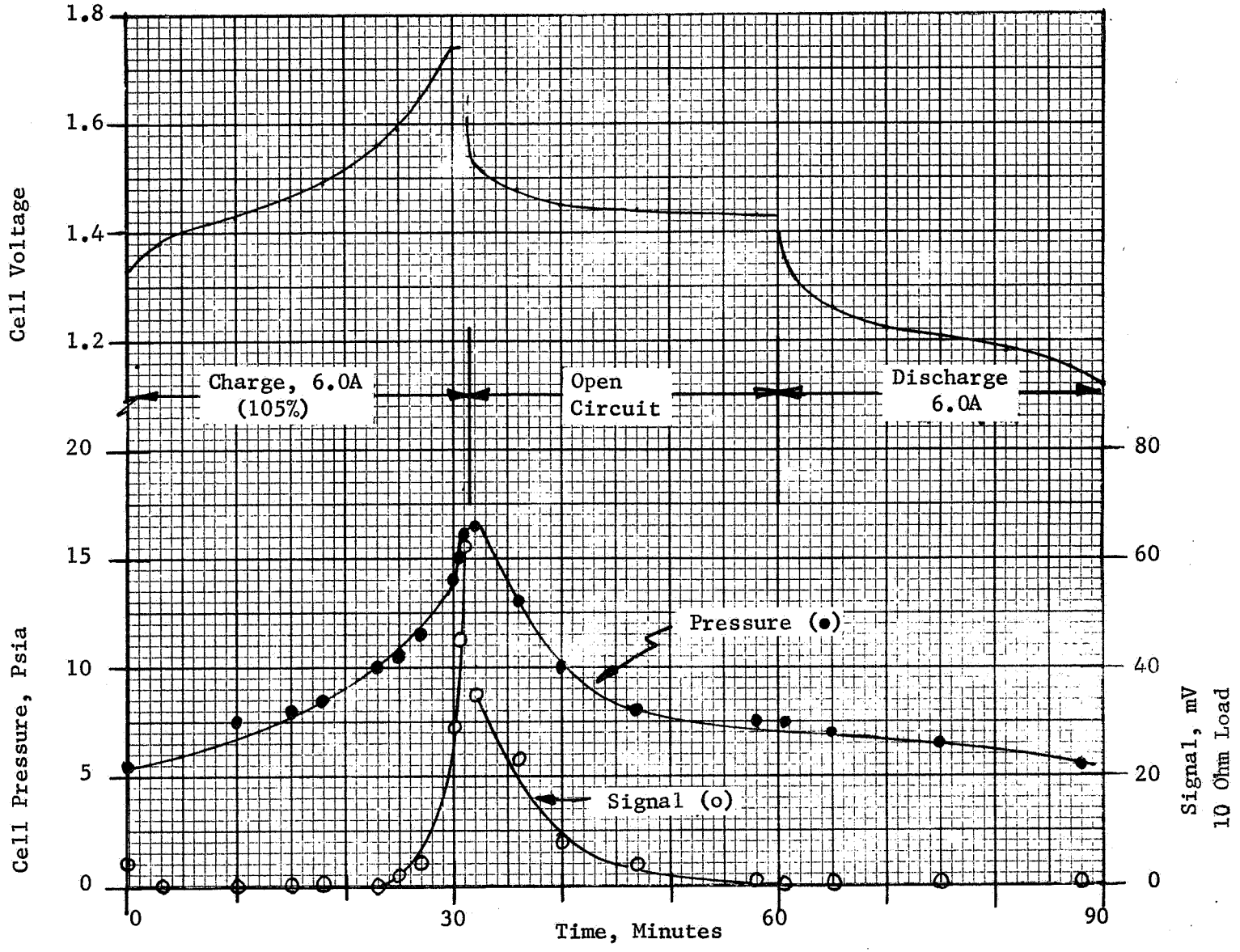

Figure 33 Performance of Cell Cycling at -20°C to 50% DOD
Battery B

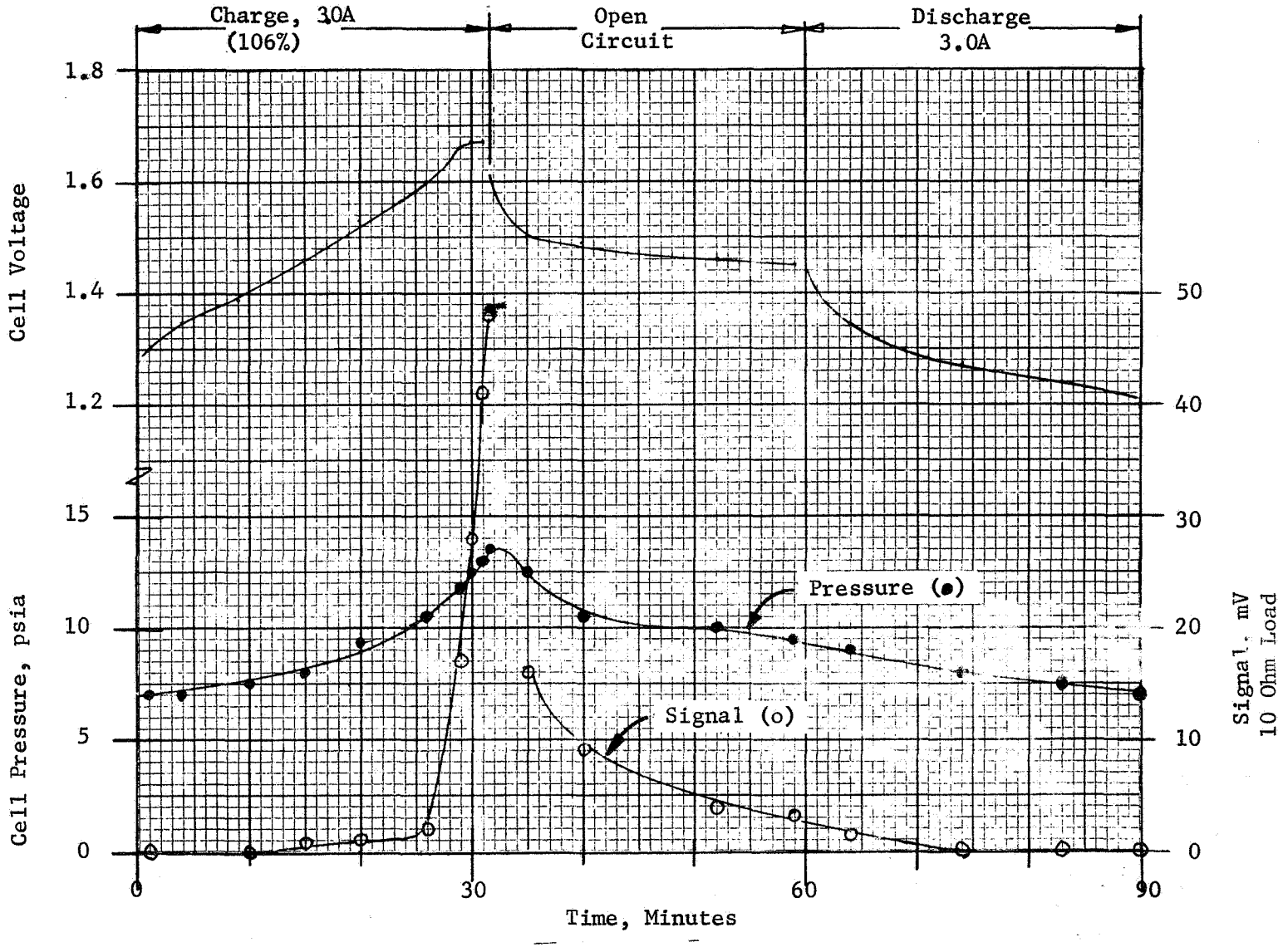

Figure 34 Performance of Cell Cycling at -20°C to 25% DOD
Battery C

were essentially constant. End-of-charge pressures for battery B, for example, were in the range of 15-18 PSIA, and with the trip level set at 60 mV, the charge returned was 105-109% of the capacity delivered. The constancy of these results show that there were no changes in the characteristics of either the recombination or control electrodes as a result of this low temperature cycling.

Ambient Temperature (25°C) Cycling: Ambient temperature cycling was carried out at three depths-of-discharge, 25%, 50%, and 75%. Typical performance of a cell cycling to 25% DOD is presented in Figure 35.

The performance of the cells cycled to 25% DOD at 25°C was essentially constant for the duration of the test, which was continued for over 800 cycles. End-of-charge pressures were in the range of 12-16 PSIA, and with the control electrode trip level set at 150 mV, the recharge was between 120% and 125%.

A downward trend was observed, however, in the end-of-discharge voltages of the cells cycled to 50% and 75% DOD, as shown in Figure 36. Such trends have been observed previously in Ni-Cd cells without auxiliary electrodes subjected to cycling at deep discharges and/or elevated temperatures.

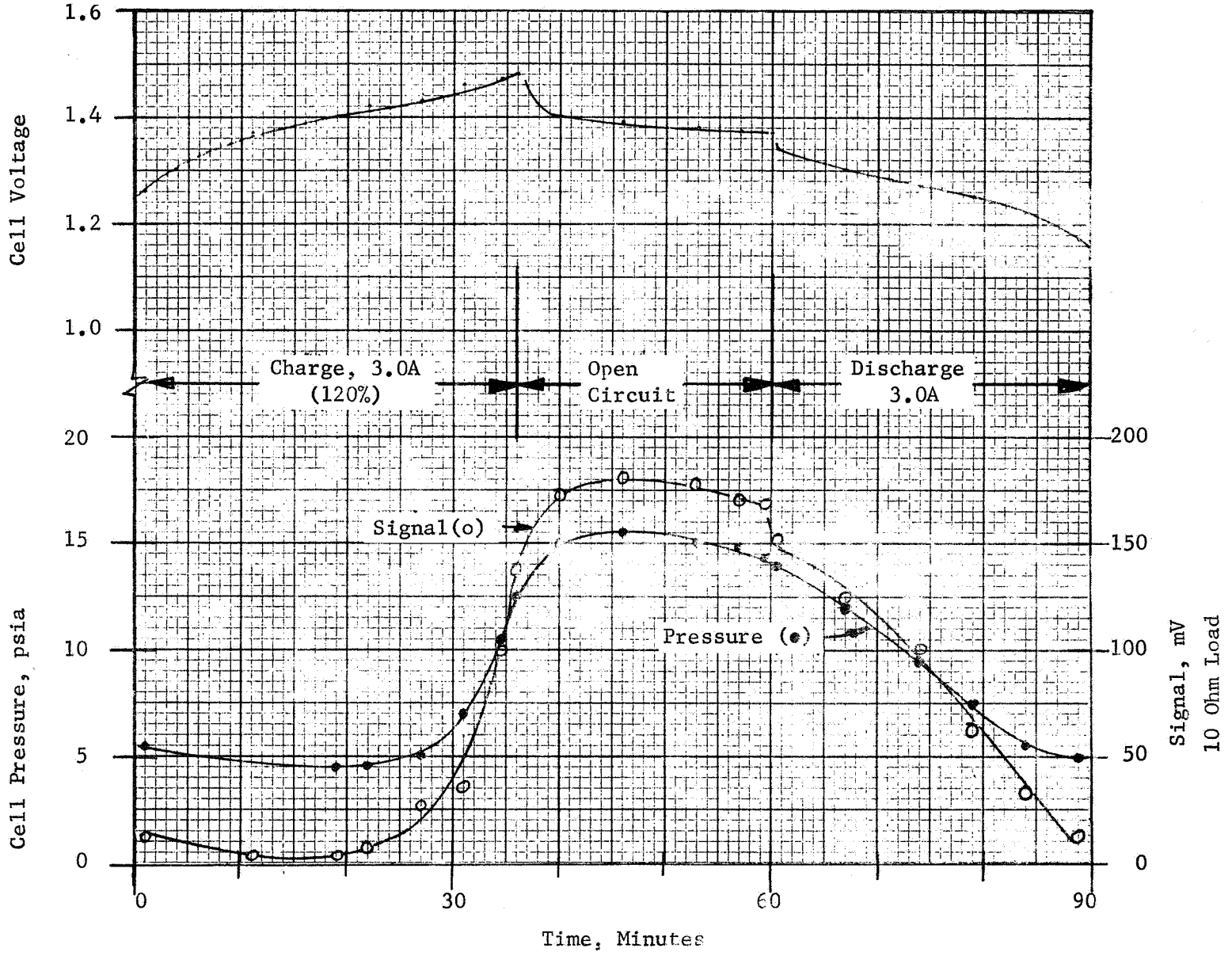

Figure 35 Performance of Cell Cycling at 25°C to 25% DOD

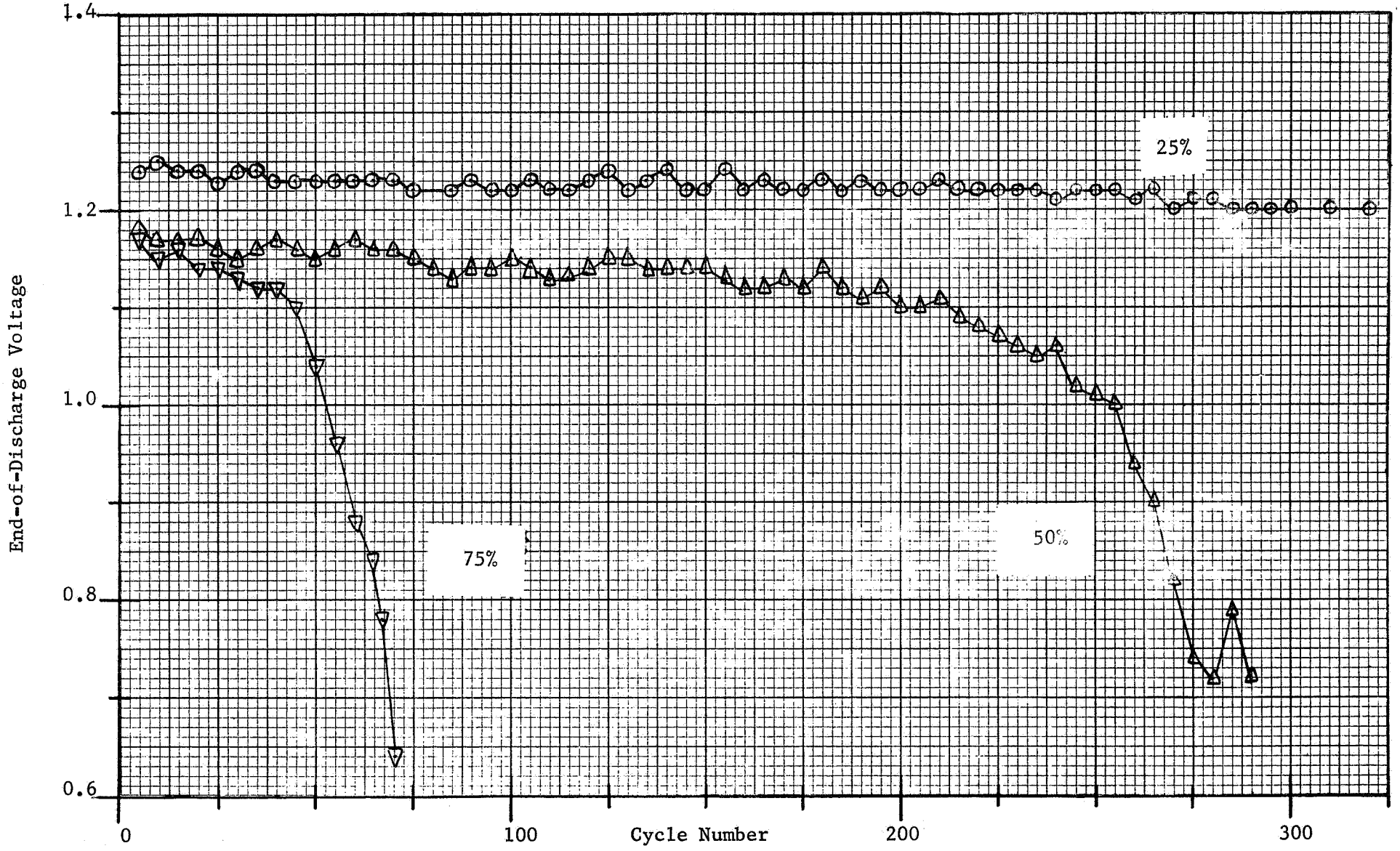

Figure 36 End-of-Discharge Voltages for Cells Cycled at 25°C

These trends have been associated with changes occurring in the negative plates. It is possible, however, to minimize these changes by suitably adjusting the state-of-charge of the negative plates prior to cycling.

The negative plates in a cell can be discharged a specified amount by adding the ampere-hour equivalent of oxygen. Similarly, the negatives may be precharged by venting the proper amount of oxygen from a cell during overcharge. The state-of-charge adjustments employed in this work involved this general precharge method, and the differences were in the extent of precharge and in certain of the details in the process, such as temperature, charge rate, etc.

The efficiency of this treatment can be seen by reference to Figure 37 in which are presented the end-of-discharge voltages of cells cycled to 75% DOD at 25°C before and after precharge of the negative plates. It is seen that this treatment increased the cycle capability of the cells by a factor of eight, and the cells were still cycling satisfactorily when the tests were discontinued. Although the cells which had been cycled to 50% DOD at 25°C also exhibited a downward trend in end-of-discharge voltage,

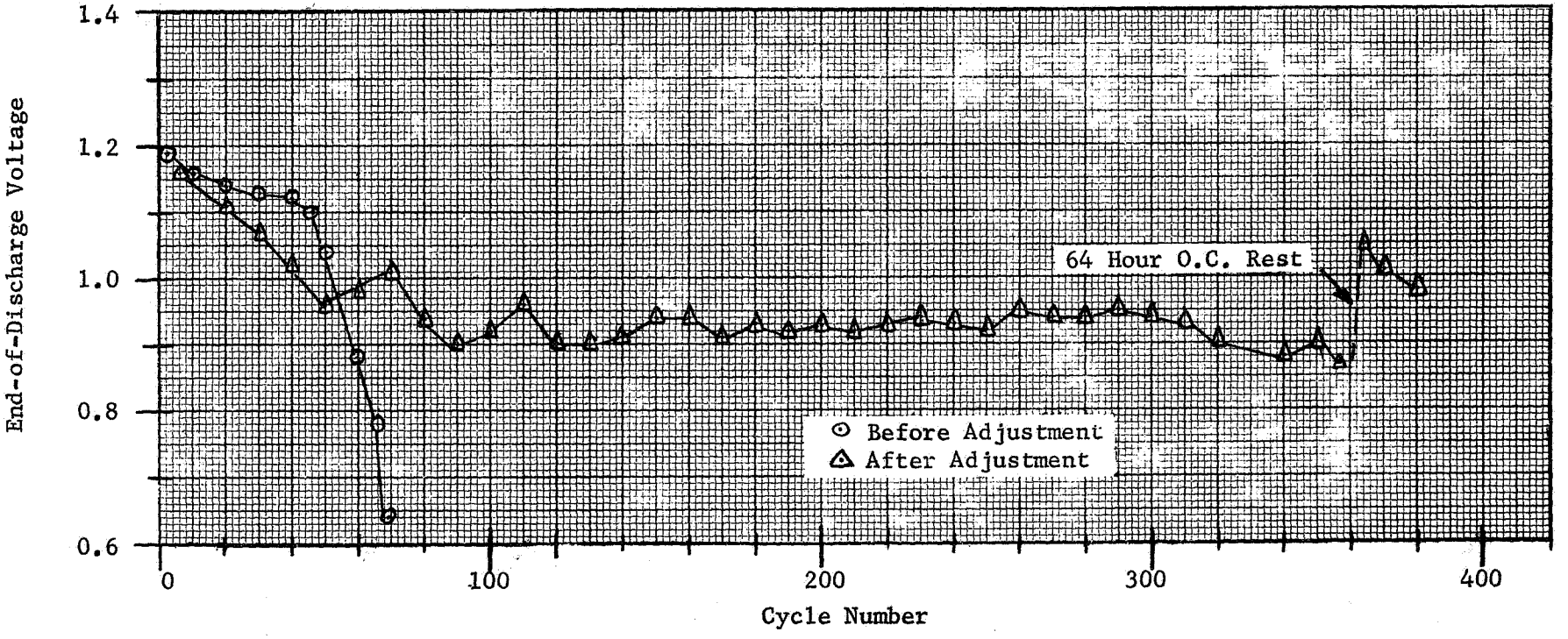

Figure 37 Effect of Adjusting Negative State-of-Charge on Cycle Life at 25°C, 75% DOD

they were not subjected to this additional treatment. From the results observed with the 75% DOD cells, however, it seems justified to assume that this treatment would also have benefited these cells.

High Temperature (40°C) Cycling: Cells were cycled to 25% and 50% DOD at 40°C. Cells were originally subjected to cycling without precharging the negative plates, and their cycle capabilities were limited. Cells cycled to 25% DOD were operated for only 175 cycles before they were removed due to falling end-of-discharge voltages. Cells cycled to 50% DOD lasted only 19 cycles before they were removed; the end-of-discharge voltages at this time were about 0.70 V.

The cells which had been cycled to 50% DOD were then subjected to negative precharge. The results were again very encouraging. After treating, the cells cycled to 50% at 40°C for about 100 cycles with the end-of-discharge voltages stable between 1.10 and 1.15 V. Typical performance during this cycling is shown in Figure 38. Following these cycles, one cell, after being charged at 6.0 A at 40°C, was taken to 25°C and discharged to 75% DOD. Cycling at 25°C to 75% DOD

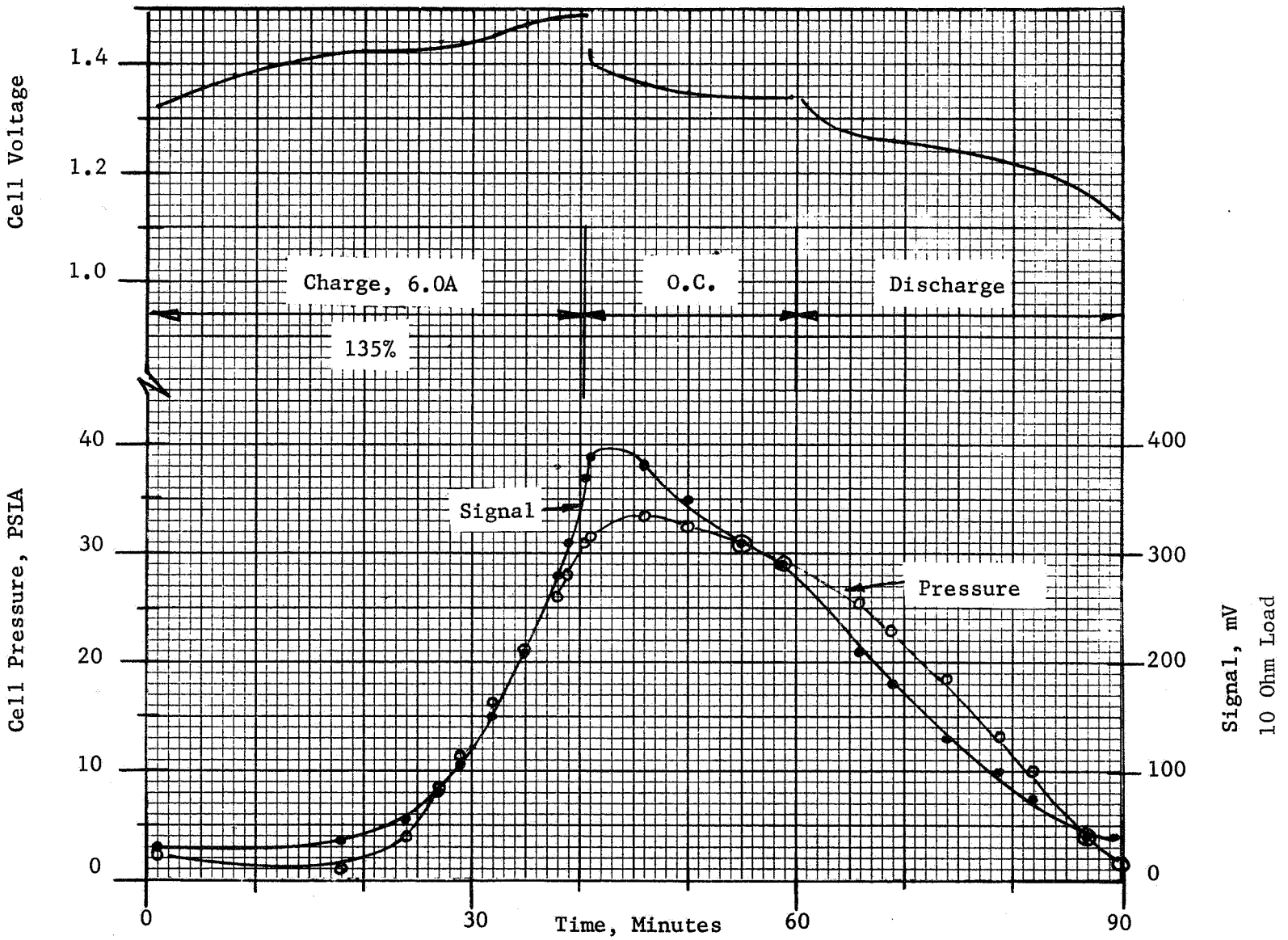

Figure 38 Performance of Cell Cycling to 50% DOD at 40°C

was continued for an additional 56 cycles, with the end-of-discharge voltage of the cell being stable between 1.07 and 1.14 V. The cell was then subjected to 60 cycles to 50% DOD at -20°C, with the end-of-discharge voltages in the range 1.10 to 1.15 V. It should be noted that the above changes in cycle regime were accomplished without interruptions for cell reconditioning, etc.

Two groups of cells were subjected to negative precharge, and in both cases the cycle capabilities were significantly increased. Both groups of cells were precharged in essentially the same manner, although there were minor variations in the conditions under which the precharge was accomplished. In order to further confirm the improved performance obtained by precharging the negative plates, and also to determine the best method of accomplishing the precharge, an additional series of tests was conducted. These tests are outlined in Table VIII.

Results of the tests were as follows:

Test A: After completing the precharge, the extent of precharge accomplished was determined by fully discharging the

TABLE VIII

SUMMARY OF CELL PROCESSING EXPERIMENTS

TEST A

PURPOSE: Determine the best technique for state-of-charge adjustment.

SAMPLE SIZE: 9 cells; 3 per technique.

PROCEDURE:

1. Recondition cells by applying 1Ω short for 16 hours.
2. Adjust negative plate state-of-chagre, using three techniques:
   a) Flood cells. Charge at C/6, -20°C, with vent open for 16 hours. Remove excess electrolyte.
   b) Charge at C/6, -20°C, with vent open for 16 hours.
   c) Charge at C/5, 25°C, with vent closed. Periodically vent cell until desired A-Hr equivalent of oxygen has been vented.
3. Determine the amount of adjustment accomplished by each technique.

TEST B

PURPOSE: Confirm improved performance.

SAMPLE SIZE: 4 cells.

PROCEDURE:

1. Recondition cells, as in A-1.
2. Adjust negative plates using the best technique of Test A.
3. Cycle two cells at each regime:
   a) 75% DOD at 25°C
   b) 50% DOD at 40°C

cells and then observing the quantity of oxygen required to discharge the residual negative capacity. It was found that method "C" resulted in not only the largest extent of precharge, but also yielded the most reproducible results. This method was then applied to the cells of Test B.

Test B: All cells were subjected to negative precharge, per method "C". The cells were then subjected to cycling at both 25°C to 75% DOD and 40°C to 50% DOD. These regimes were chosen for this evaluation as the efficiency of the treatment can be determined after relatively few cycles. The treated cells were operated for about 100 cycles at both regimes, and the end-of-discharge voltages were in the ranges observed previously, around 1.10 V for those at 40°C and 50% DOD, and 1.05 V for those at 25°C and 75% DOD.

3.0 CONCLUSIONS

The results presented in this report demonstrate that the cells developed under this contract represent a significant advance in the state-of-the-art. They have demonstrated their ability to cycle under conditions which cannot be met by cells of conventional design. Prototype cells have cycled for prolonged periods over the entire -20°C to +40°C temperature range to depths-of-discharge of 50% (to 75% at 25°C) on 90 minute orbits. In addition, it was possible to change from a 50% DOD regime to one at 75% DOD without reconditioning of cells. This indicates that the memory affect observed in the past has been greatly reduced.

This extension in cycle capability is the result of two interacting factors: the recombination electrode and the adjustment of the state-of-charge of the negative plates.

The recombination electrode has as its primary function the maintenance of safe pressure levels within the cell by recombining the oxygen generated by the positive plates during charge. It also returns the pressure to a low value during the open circuit and the discharge portions of the cycle. This insures that the subsequent charge will not

be terminated by a premature signal from the oxygen-sensing control electrode on account of residual oxygen pressure. These electrodes possess another feature, however, which has heretofore been overlooked. They provide a catalyst which can promote the reaction between hydrogen and oxygen. In this manner, they also prevent excessive pressure build-up due to an accumulation of hydrogen in the cell.

As cells can be built with a mechanism for the safe removal of any hydrogen generated, they can be constructed with a larger percentage of their excess negative capacity in the charged state. Cells so constructed have only one limiting electrode, the positive, and so the problems associated with the negative plates are minimized.

4.0 RECOMMENDATIONS FOR FUTURE WORK

While significant extensions in cycle capability of cells have been demonstrated, the full extent of the improvements achieved are not yet known. In order to further extend the new technology developed in this contract and to extend the usefulness of auxiliary electrode cells, developments which have made these advances possible should be investigated in more detail. These are the recombination electrode and negative plate state-of-charge adjustment.

Recombination electrodes have been used for some time in sealed nickel-cadmium cells in order to prevent excessive oxygen pressure build-up during charge. The limited cycle capability of certain of these cells at elevated temperatures and deep discharges have sometimes been associated with the operation of this electrode. Results presented in this report, however, show that cells containing recombination electrodes are capable of prolonged cycling under these conditions, if the cells are constructed with properly adjusted negative plates.

There are, however, certain aspects of the operation of recombination electrodes which should be investigated. The first of these is the long-term behavior and stability of the electrode itself. Any loss in recombination ability with time would result in higher cell

pressures. In addition, the loss of catalytic activity would effect the electrode's ability to combine hydrogen and oxygen. The extent, if any, of the migration of the catalytic agents from the electrode to other areas of the cell should also be investigated. The effect of the recombination electrode current on the nickel-cadmium cell pack should also be evaluated.

While the effects of adjusting the state-of-charge of the negative plates on the cycle capability of recombination electrode cells have been shown, the results can only be considered as preliminary. The tests were not of sufficient duration to determine the full extent of the improved cycle capability obtained. In addition, the extent and method of accomplishing the adjustment were not fully investigated. A study aimed at investigating these parameters should be carried out in order to optimize the process and receive the maximum benefit from it.

The positive plates, now the limiting factor in cell performance, should also be investigated. Work should be directed at improving their high temperature capability especially. In addition, the chemistry and distribution of the electrolyte should also be scrutinized.

Tests to evaluate the various parameters outlined above should be carried out over a wide range of temperatures and cycle regimes.

Suitable controls should also be included in the test program. In this manner all the factors affecting cell performance can be determined.

The results of such a comprehensive program should be a further extension in the state-of-the-art. The criteria for building auxiliary electrode cells with prolonged cycle capability would be well defined. In addition, the optimum cycle conditions for such cells could be determined. The sum total would be to further extend the usefulness of such cells for spacecraft applications. By increasing the deep cycle capability of cells, it should be possible to use cells with less reserve capacity and, hence, attain greater utilization of watt-hr/lb capability.

5.0 NEW TECHNOLOGY

The work done under this contract has resulted in several significant advances in the state-of-the-art. The significant new developments are:

a) control electrodes, which when connected through a suitable resistance to the negative plate, generate signals which are approximately linear with oxygen pressure;

b) recombination electrodes suitable for improving the utility of the control electrode, and protecting the cell from over-pressure during sustained over-charge, and which are operable over the temperature range of -20°C to +40°C;

c) methods for building cells, incorporating recombination and control electrodes, which possess superior cycle capability at deep discharge and/or elevated temperatures.

A C K N O W L E D G E M E N T

The authors wish to thank the Project Officer, Mr. Floyd E. Ford, NASA/Goddard Space Flight Center, for his valuable suggestions and discussions during the course of this work.

NASA/Goddard Space Flight Center

OFFICIAL DISTRIBUTION LIST FOR BATTERY REPORTS

May 1, 1967

National Aeronautics & Space Admin.
Scientific and Technical Information Facility
College Park, Maryland 20740
Attn: NASA Representative
Send 2 copies plus 1 reproducible

National Aeronautics & Space Admin.
Washington, D.C. 20546
Attn: RNW/E. M. Cohn

National Aeronautics & Space Admin.
Washington, D.C. 20546
Attn: FC/A. M. Greg Andrus

National Aeronautics & Space Admin.
Goddard Space Flight Center
Greenbelt, Maryland 20771
Attn: Gerald Halpert, Code 735

National Aeronautics & Space Admin.
Goddard Space Flight Center
Greenbelt, Maryland 20771
Attn: Thomas Hennigan, Code 716.2
Send 3 copies

National Aeronautics & Space Admin.
Goddard Space Flight Center
Greenbelt, Maryland 20771
Attn: Joseph Sherfey, Code 735

National Aeronautics & Space Admin.
Langley Research Center
Instrument Research Division
Hampton, Virginia 23365
Attn: John L. Patterson, MS-234

National Aeronautics & Space Admin.
Langley Research Center
Instrument Research Division
Hampton, Virginia 23365
Attn: M. B. Seyffert, MS 112

National Aeronautics & Space Admin.
Lewis Research Center
21000 Brookpark Road
Cleveland, Ohio 44135
Attn: N. D. Sanders, MS 302-1

National Aeronautics & Space Admin.
Lewis Research Center
21000 Brookpark Road
Cleveland, Ohio 44135
Attn: M. J. Saari, MS 500-202

National Aeronautics & Space Admin.
Lewis Research Center
21000 Brookpark Road
Cleveland, Ohio 44135
Attn: R. R. Miller, MS 500-202

National Aeronautics & Space Admin.
Geo. C. Marshall Space Flight Center
Huntsville, Alabama 35812
Attn: Philip Youngblood

National Aeronautics & Space Admin.
Geo. C. Marshall Space Flight Center
Huntsville, Alabama 35812
Attn: Richard Boehme
Bldg. 4487-BB

National Aeronautics & Space Admin.
Manned Spacecraft Center
Houston, Texas 77058
Attn: William R. Dusenbury
Propulsion & Energy Systems Branch
Bldg. 16, Site 1

National Aeronautics & Space Admin.
Manned Spacecraft Center
Houston, Texas 77058
Attn: Richard Ferguson (EP-5)

National Aeronautics & Space Admin.
Manned Spacecraft Center
Houston, Texas 77058
Attn: Mr. Barry Trout

National Aeronautics & Space Admin.
Manned Spacecraft Center
Houston, Texas 77058
Attn: Forrest E. Eastman (EE-4)

National Aeronautics & Space Admin.
Washington, D.C. 20546
Attn: Office of Technology
Utilization

National Aeronautics & Space Admin.
Ames Research Center
Pioneer Project
Moffett Field, California 94035
Attn: Arthur Wilbur/A. S. Hertzog

National Aeronautics & Space Admin.
Ames Research Center
Moffett Field, California 94035
Attn: Jon Rubenzer
Biosatellite Project

National Aeronautics & Space Admin.
Electronics Research Center
575 Technology Square
Cambridge, Mass. 02139
Attn: Dr. Sol Gilman

Jet Propulsion Laboratory
4800 Oak Grove Drive
Pasadena, California 91103
Attn: Mr. Aiji Uchiyama

Department of the Army

U. S. Army Engineer R&D Labs.
Fort Belvoir, Virginia 22060
Electrical Power Branch
Energy Conversion Research Lab.

Commanding General
U. S. Army Weapons Command
Attn: AMSWE-RDR, Mr. G. Reinsmith
Rock Island Arsenal
Rock Island, Illinois 61201

U. S. Army Natick Laboratories
Clothing and Organic Materials Div.
Natick, Massachusetts 01760
Attn: G. A. Spano

Commanding Officer
U. S. Army Electronics R&D Labs.
Power Sources Division
Fort Monmouth, New Jersey 07003
Attn: Code SELRA/PS

Harry Diamond Laboratories
Room 300, Building 92
Conn. Ave. & Van Ness Street, N. W.
Washington, D.C. 20438
Attn: Nathan Kaplan

Department of the Navy

Office of Naval Research
Washington, D.C. 20360
Attn: Head, Power Branch, Code 429

Naval Research Laboratory
Washington, D.C. 20390
Attn: Dr. J. C. White, Code 6160

U. S. Navy
Special Projects Division
Marine Engineering Laboratory
Annapolis, Maryland 21402
Attn: J. H. Harrison

Naval Air Systems Command
Department of the Navy
Washington, D.C. 20360
Attn: Milton Knight (Code AIR-340C)

Commanding Officer
(Code QEWE, E. Bruess/H. Schultz)
U. S. Naval Ammunition Depot
Crane, Indiana 47522

Naval Ordnance Laboratory
Department of the Navy
Corona, California 91720
Attn: William C. Spindler (Code 441)

Naval Ordnance Laboratory
Silver Spring, Maryland 20910
Attn: Philip B. Cole (Code 232)

Commander, Naval Ship Sys. Command
Department of the Navy
Washington, D.C. 20360
Attn: C. F. Viglotti (Code 66605)

Commander, Naval Ship Sys. Command
Department of the Navy
Washington, D.C. 20360
Attn: Bernard B. Rosenbaum
(Code 03422)

Department of the Air Force

Flight Vehicle Power Branch
Aero Propulsion Laboratory
Wright-Patterson AFB, Ohio 45433
Attn: James E. Cooper

AF Cambridge Research Lab.
Attn: CRE
L. G. Hanscom Field
Bedford, Massachusetts 01731
Attn: Francis X. Doherty
Edward Raskind (Wing F)

Rome Air Development Center, ESD
Attn: Frank J. Mollura (RASSM)
Griffis AFB, New York 13442

Other Government Agencies

National Bureau of Standards
Washington, D.C. 20234
Attn: Dr. W. J. Hamer

National Bureau of Standards
Washington, D.C. 20234
Attn: Dr. A. Brenner

Office, Sea Warfare System
The Pentagon
Washington, D.C. 20310
Attn: G. B. Wareham

Mr. Donald A. Hoatson
Army Reactors, DRD
U. S. Atomic Energy Commission
Washington, D.C. 20545

Bureau of Mines
4800 Forbes Avenue
Pittsburgh, Pennsylvania 15213
Attn: Dr. Irving Wender

Private Organizations

Aerojet-General Corporation
Chemical Products Division
Azusa, California 91702
Attn: William H. Johnson

Aeronutronic Division of Philco Corp.
Technical Information Services
Ford Road
Newport Beach, California 92663

Aerospace Corporation
P. O. Box 95085
Los Angeles, California 90045
Attn: Library Acquisition Group

Allis-Chalmers Mfg. Co.
1100 South 70th Street
Milwaukee, Wisconsin 53201
Attn: Dr. P. Joyner

A. M. F.
Attn: Dr. Lloyd H. Shaffer
689 Hope Street
Springdale, Connecticut 06879

American University
Mass. & Nebraska Avenue, N. W.
Washington, D.C. 20016
Attn: Dr. R. T. Foley,
Chemistry Department

Arthur D. Little, Inc.
Acorn Park
Cambridge, Massachusetts 02140
Attn: Dr. Ellery W. Stone

Atomics International Division
North American Aviation, Inc.
8900 De Sota Avenue
Canoga Park, California 91304
Attn: Dr. H. L. Recht

Battelle Memorial Institute
505 King Avenue
Columbus, Ohio 43201
Attn: Dr. C. L. Faust

Bell Laboratories
Murray Hill, New Jersey 07971
Attn: U. B. Thomas

Bell Telephone Laboratories, Inc.
Whippany, N. J. 07981
Attn: D. O. Feder, Room 3B-294

The Boeing Company
P. O. Box 3868
Seattle, Washington 98124
Attn: Sid Gross, MS 85-86

Borden Chemical Company
Central Research Lab.
P. O. Box 9524
Philadelphia, Pennsylvania 19124

Burgess Battery Company
Foot of Exchange Street
Freeport, Illinois 61033
Attn: Dr. Howard J. Strauss

C & D Batteries
Division of Electric Autolite Co.
Conshohocken, Pennsylvania 19428
Attn: Dr. Eugene Willihnganz

Calvin College
Grand Rapid, Michigan 49506
Attn: Prof. T. P. Dirkse

Catalyst Research Corporation
6101 Falls Road
Baltimore, Maryland 21209
Attn: H. Goldsmith

ChemCell Inc.
150 Dey Road
Wayne, New Jersey 07470
Attn: Peter D. Richman

G. & W. H. Corson, Inc.
Plymouth Meeting
Pennsylvania 19462
Attn: Dr. L. J. Minnick

Cubic Corporation
9233 Balboa Avenue
San Diego, California 92123
Attn: Librarian
Mrs. Judy Kalak

Delco Remy Division
General Motors Corporation
2401 Columbus Avenue
Anderson, Indiana 46011
Attn: Dr. J. J. Lander

Douglas Aircraft Company, Inc.
Astropower Laboratory
2121 Campus Drive
Newport Beach, California 92663
Attn: Dr. George Moe

Dynatech Corporation
17 Tudor Street
Cambridge, Massachusetts 02139
Attn: R. L. Wentworth

E. I. DuPont De Nemours & Co.
Explosives Department
Repauno Development Laboratory
Gibbstown, New Jersey 08027
Attn: Mr. R. W. Prugh
(Contract NASw-1233)

Eagle-Picher Company
Post Office Box 47
Joplin, Missouri 64801
Attn: E. P. Broglio

Electric Storage Battery Co.
Missile Battery Division
2510 Louisburg Rd.
Raleigh, North Carolina 27604
Attn: A. Chreitzberg

Electric Storage Battery Co.
Carl F. Norberg Research Center
19 West College Avenue
Yardley, Pennsylvania 19067
Attn: Dr. R. A. Schaefer

Electrochimica Corporation
1140 O'Brien Drive
Menlo Park, California 94025
Attn: Dr. Morris Eisenberg

Electro-Optical Systems, Inc.
300 North Halstead
Pasadena, California 91107
Attn: Martin Klein

Emhart Corp
Box 1620
Hartford, Connecticut 06102
Attn: Dr. W. P. Cadogan

Engelhard Industries, Inc.
497 DeLancy Street
Newark, New Jersey 07105
Attn: Dr. J. G. Cohn

Dr. Arthur Fleischer
466 South Center Street
Orange, New Jersey 07050

General Electric Company
Schenectady, New York 12301
Attn: Dr. R. C. Osthoff/Dr. W. Carson
Advanced Technology Lab.

General Electric Company
Missile & Space Division
Spacecraft Department
P. O. Box 8555
Philadelphia, Pennsylvania 19101
Attn: E. W. Kipp, Room U-2307

General Electric Company
Battery Products Section
P. O. Box 114
Gainsville, Florida 32601
Attn: W. H. Roberts

General Electric Company
Research and Development Center
P. O. Box 8
Schenectady, New York 12301
Attn: Dr. H. Liebhafsky

General Motors-Defense Research Labs.
6767 Hollister Street
Santa Barbara, California 93105
Attn: Dr. J. S. Smatko/Dr. C. R. Russell

Globe-Union, Incorporated
P. O. Box 591
Milwaukee, Wisconsin 53201
Attn: Mr. J. D. Onderdonk
V. P. Marketing

Gould-National Batteries, Inc.
Engineering & Research Center
(Dr. D. Douglas)
2630 University Avenue, S. E.
Minneapolis, Minnesota 55418

Gulton Industries
Alkaline Battery Division
212 Durham Avenue
Metuchen, New Jersey 08840
Attn: Dr. Robert Shair

Gulton Industries
Alkaline Battery Division
212 Durham Avenue
Metuchen, New Jersey 08840
Attn: H. N. Seiger
Contract NAS W-12,300 only

Hughes Aircraft Corporation
Centinda Ave. & Teale Street
Culver City, California 90230
Attn: T. V. Carvey

Hughes Aircraft Corporation
Bldg. 366, M. S. 524
El Segundo, California 90245
Attn: P. C. Ricks

IIT Research Institute
10 West 35th Street
Chicago, Illinois 60616
Attn: Dr. H. T. Francis

Institute for Defense Analyses
R&E Support Division
400 Army-Navy Drive
Arlington, Virginia 22202
Attn: Mr. R. Hamilton

Institute for Defense Analyses
R&E Support Division
400 Army-Navy Drive
Arlington, Virginia 22202
Attn: Dr. G. Szego

Idaho State University
Department of Chemistry
Pocatello, Idaho 83201
Attn: Dr. G. Myron Arcand

Institute of Gas Technology
State and 34th Street
Chicago, Illinois 60616
Attn: B. S. Baker

International Nickel Co.
1000-16th Street, N. W.
Washington, D.C. 20036
Attn: Wm. C. Mearns

Johns Hopkins University
Applied Physics Laboratory
8621 Georgia Avenue
Silver Spring, Maryland 20910
Attn: Richard E. Evans

Johns Hopkins University
Applied Physics Laboratory
8621 Georgia Avenue
Silver Spring, Maryland 20910
Attn: Mr. Louis Wilson

Leesona Moos Laboratories
Lake Success Park, Community Drive
Great Neck, New York 11021
Attn: Dr. H. Oswin

Livingston Electronic Corporation
Route 309
Montgomeryville, Pa. 18936
Attn: William F. Meyers

Lockheed Missiles & Space Company
Technical Information Center
3251 Hanover Street
Palo Alto, California 93404

Mallory Battery Company
Broadway & Sunnyside Lane
North Tarrytown, New York 10591
Attn: R. R. Clune

P. R. Mallory & Co., Inc.
Northwest Industrial Park
Burlington, Massachusetts 01803
Attn: Dr. Per Bro

P. R. Mallory & Co., Inc.
3029 E. Washington Street
Indianapolis, Indiana 46206
Attn: Technical Librarian

Martin Company
Denver Division
(P1001, Mr. R. C. Wildman)
Mail No. P-6700-1
Denver, Colorado 80201

Martin Company
Electronics Research Department
P. O. Box #179
Denver, Colorado 80201
Attn: William B. Collins, MS 1620

Mauchly Systems, Inc.
Fort Washington Industrial Park
Fort Washington, Pennsylvania
Attn: John H. Waite

Melpar
Technical Information Center
7700 Arlington Blvd.
Falls Church, Virginia 22046

Metals and Controls Division
Texas Instruments, Inc.
34 Forrest Street
Attleboro, Massachusetts 02703
Attn: Dr. E. M. Joe

Midwest Research Institute
425 Volker Boulevard
Kansas City, Missouri 64110
Attn: Physical Science Laboratory

Monsanto Research Corporation
Everett, Massachusetts 02149
Attn: Dr. J. O. Smith

North American Aviation Co.
S & ID Division
Downey, California 90241
Attn: Dr. James Nash

Oklahoma State University
Stillwater, Oklahoma 74075
Attn: Prof. William L. Hughes
School of Electrical Engineering

Paul Howard Associates Inc.
Centerville, Maryland 21617

Power Information Center
University of Pennsylvania
3401 Market St., Rm. 2107
Philadelphia, Pennsylvania 19104

Power Sources Division
Whittaker Corporation
9601 Canoga Avenue
Chatsworth, California 91311
Attn: Dr. M. Shaw

Prime Battery Corp.
15600 Cornet Street
Santa Fe Springs, California 90670
Attn: David Roller

RAI Research Corp.
36-40 37th Street
Long Island City, N. Y. 11101

Radio Corporation of America
Astro Corporation
P. O. Box 800
Hightstown, New Jersey 08540
Attn: Seymour Winkler

Radio Corporation of America
AED
P. O. Box 800
Princeton, New Jersey 08540
Attn: I. Schulman

Radio Corporation of America
415 South Fifth Street
Harrison, New Jersey 07029
Attn: Dr. G. S. Lozier
Bldg. 18-2

Southwest Research Institute
8500 Culebra Road
San Antonio, Texas 78206
Attn: Library

Sonotone Corporation
Saw Mill River Road
Elmsford, New York 10523
Attn: A. Mundel

Texas Instruments, Inc.
P. O. Box 5936
Dallas, Texas 75222
Attn: Dr. Isaac Trachtenberg

TRW Systems, Inc.
One Space Park
Redondo Beach, California 90278
Attn: Dr. A. Krausz, Bldg. 60, Rm. 147

TRW Systems, Inc.
One Space Park
Redondo Beach, California 90278
Attn: Dr. Herbert P. Silverman

TRW, Inc.
23555 Euclid Avenue
Cleveland, Ohio 44117
Attn: Librarian

Tyco Laboratories, Inc.
Bear Hill
Hickory Drive
Waltham, Massachusetts 02154
Attn: Dr. A. C. Makrides

Unified Sciences Associates, Inc.
826 S. Arroyo Parkway
Pasadena, California 91105
Attn: Dr. S. Naiditch

Union Carbide Corporation
Development Laboratory Library
P. O. Box 5056
Cleveland, Ohio 44101

Electromite Corporation
Attn: R. H. Sparks
General Manager
562 Meyer Lane
Redondo Beach, California 90278

Union Carbide Corporation
Parma Laboratory
Parma, Ohio 44130
Attn: Dr. Robert Powers

University of Pennsylvania
Electrochemistry Laboratory
Philadelphia, Pennsylvania 19104
Attn: Prof. John O'M. Bockris

Westinghouse Electric Corporation
Research and Development Center
Churchill Borough
Pittsburgh, Pennsylvania 15235

Whittaker Corporation
3850 Olive Street
Denver, Colorado 80237
Attn: J. W. Reiter

Whittaker Corporation
Narmco R&D Division
3540 Aero Court
San Diego, California 92123
Attn: Dr. M. Shaw

Yardney Electric Corporation
40 Leonard Street
New York, New York 10013
Attn: Dr. Geo. Dalin